POLITECNICO
MILANO 1863

SCUOLA DI INGEGNERIA INDUSTRIALE
E DELL'INFORMAZIONE

Design and Validation of a Radio Frequency Interference Prediction Tool for the SMOS Mission

Tesi di Laurea Magistrale in
Space Engineering - Ingegneria Spaziale

Author: **Teodoro Bonariol**

Student ID: 941028
Advisor: Prof. Pierluigi Di Lizia
Academic Year: 2021-22

Abstract

In the last few years, the number of satellites launched has been increasing, in particular those of private companies for Earth observation purposes. Polar orbits are exploited for these satellites and consequently high latitude ground stations have become even more fundamental in order to down link and acquire the payload data in near real time. However, the transmission frequency bands over these stations have become overcrowded, leading to an increase of Radio Frequency Interference events. This causes partial and even total loss of transmitted data. The Soil Moisture and Ocean Salinity mission of the European Space Agency Earth Explorer programme is affected by this problem, in particular during the passes over the Svalbard ground station. Therefore, the aim of this work is the implementation and validation of a prediction tool able to predict in advance the list of future passes that might be affected by an interference from other adjacent satellites. The tool development consists in collecting a list of potentially conflicting commercial and military satellites, in retrieving their corresponding TLEs for the time range of interest and in propagating their orbital state, using the SPICE Toolkit functions. This model is validated comparing the predicted results with the reported events of past interference, identifying the responsible satellites. Then, an analysis for potential patterns on the data of these confirmed events is made; this leads to the identification of four parameters (time of the day at which the RFI happens, minimum angular distance, elevation and azimuth values at maximum interference), which shows meaningful patterns related to each family of responsible satellites. Therefore, these patterns are used inside the prediction model in order to compute the probability of a new event: this is based on the computation of the Mahalanobis distance of this predicted event with respect to the available dataset and then on the computation of the corresponding probability value. To conclude, the prediction model shows very good accordance between predicted and reported events.

Keywords: Mahalanobis Distance, Radio Frequency Interference, SMOS, SPICE, Software Validation

Abstract in lingua italiana

Negli ultimi anni, il numero di satelliti lanciati in orbita è aumentato, in particolare satelliti di aziende private dedicati all'osservazione della Terra. Orbite polari sono sfruttate per questi satelliti e di conseguenza le stazioni di terra ad alte latitudini sono diventate sempre più fondamentali per scaricare e acquisire in tempo reale i dati degli strumenti di bordo. Le bande di trasmissione sopra queste stazioni sono però diventate sovraffollate, con il conseguente aumento di eventi di interferenza radio. Questa situazione comporta una parziale e a volte totale perdita dei dati trasmessi. La missione Soil Moisture and Ocean Salinity del programma Earth Explorer dell'European Space Agency è anch'essa interessata da questo problema, in particolare durante i passaggi sulla stazione di terra localizzata a Svalbard. Lo scopo di questo lavoro è quindi l'implementazione e la validazione di un tool predittivo capace di prevedere la lista dei passaggi futuri di SMOS che potrebbero essere interessati da interferenze da parte di altri satelliti vicini. Lo sviluppo del tool consiste nel realizzare una lista di satelliti commerciali e militari potenzialmente in conflitto, nel recuperare le loro corrispondenti TLE per il periodo di tempo di interesse e nel propagare il loro stato orbitale, usando le funzioni dello SPICE Toolkit. Questo modello è validato confrontando i risultati predetti con gli eventi riportati di interferenze passate, identificando i satelliti responsabili. Successivamente, viene eseguita un'analisi su potenziali schemi nei dati di questi eventi confermati; questo studio conduce all'identificazione di quattro parametri (orario del giorno a cui l'RFI avviene, minima distanza angolare, valori di elevazione e azimut in corrispondenza della massima interferenza), che mostrano schemi significativi associati a ciascuna famiglia dei satelliti responsabili. Questi schemi sono usati all'interno del modello predittivo per calcolare la probabilità di un nuovo evento: questa probabilità è basata sul calcolo della distanza di Mahalanobis dell'evento predetto rispetto ai dati disponibili e, in seguito, sul calcolo del corrispondente valore di probabilità. In conclusione, il modello predittivo mostra una buona concordanza tra gli eventi predetti e quelli riportati.

Parole chiave: Distanza di Mahalanobis, Interferenza Radio, SMOS, SPICE, Validazione di Software

Contents

1 | Introduction

In the following chapter, an introduction to the topics addressed in this thesis work is presented. The description of the Soil Moisture and Ocean Salinity (SMOS) mission, of its ground segment and of the data transmission to ground are performed, alongside the background motivations of this thesis. Subsequently, the objective of this work is presented, also considering the requirements for the software development. Then, the current State of the Art is addressed and finally the outline of this thesis work in described.

1.1. SMOS mission

The Soil Moisture and Ocean Salinity mission is the second mission launched as part of the Earth Explorer programme of the European Space Agency Earth Observation directory. It is the first space mission to get data about Ocean Salinity and Soil Moisture. In fact, the mission goal is to create global maps of Ocean Salinity and of Soil Moisture, which are key variables in the *Water Cycle* and, in particular, in the exchange processes between Earth's surfaces and the atmosphere. Soil moisture changes due to water interchanges among ground, oceans and atmosphere, it regulates the energy interchange between the ground and the atmosphere, therefore it is a critical variable for the improvement of meteorological and hydrological modelling and forecasting, of water resource management and of monitoring of plant growth in agriculture. While salinity and temperature define the sea and ocean density, which therefore is an important factor driving sea and ocean currents. The salinity is related with evaporation and precipitation and is a key variable to characterize global ocean circulation and its seasonal and annual variability in order to improve ocean and atmosphere models. Beyond Soil Moisture and Ocean Salinity maps, SMOS is also able to track hurricanes, thanks to the detection of microwave emissions from wind-generated foam, allowing hurricane-force wind speeds to be measured from space. Moreover, it is able to study ice thickness and its evolution across the years, to produce vegetation maps and to analyze the rain water transport contributing to the *Water Cycle*.

The physical principle on which the science mission is based is the fact that the amount of

energy radiated by a body depends on its electric properties, in particular on the emissivity, which is the measure of the effective amount of radiation that an object can emit. The emissivity depends on different parameters: electrical properties of the material, direction of observation, roughness of the surface, polarisation and frequency. In particular, the principle on which SMOS is able to measure soil moisture and ocean salinity is related to the fact that both modify the dielectric properties of the materials, decreasing the emissivity values of both the ground and seas, respectively. These changes are well seen in the L-band spectrum, around a frequency of 1.4 GHz, corresponding to a wavelength of 21 cm. Moreover L-band measurements are not affected by vegetation, weather and atmospheric conditions.

In principle, for these measurements, a single-dish, large antenna measuring tens of meters would be required to achieve adequate coverage and spatial resolution. However, this would not be feasible due to cost and spacecraft weight, therefore SMOS uses a L-band interferometric radiometer, which allows measurements with a higher number of smaller antennae. This is achieved by the payload MIRAS (Microwave Imaging Radiometer using Aperture Synthesis), designed and built by Airbus Spain. This technique is based on the cross-correlation of observations from all possible combinations of receiver pairs. A two-dimensional hexagon-like image of about 1000 km is taken every 1.2 seconds.

In particular, MIRAS is the only payload mounted on board SMOS, has a mass of 335 kg and a circular cross section of 8 meters. It has 69 antennae called LICEF (LIght-weight Cost EFfective), each with a mass of 190 g, a diameter of 165 mm and a height of 19 mm. MIRAS has a Y-shaped antenna, consisting of a central structure with 3 deployable arms, each consisting of 3 segments, as it can be seen in Figure 1.1. The 69 LICEF antennae are equally distributed over the three arms and the central structure. Payload calibration is needed because the LICEF receivers are sensitive to temperature and ageing. Therefore, they need to be calibrated in flight in order to ensure that the accuracy requirements of the measurement can be met. The payload is calibrated in different ways, in particular using the sky, because the working frequency corresponds to the one of neutral atomic hydrogen. Biweekly calibrations are scheduled with SMOS pointing toward the sky. This has produced a L-band sky map, used by astronomers and also employed in order to subtract the galaxy reflection on Earth during data processing.

Figure 1.1: Artist's view of SMOS flight configuration

SMOS is in a quasi-circular dusk-dawn Sun synchronous orbit, whose orbital parameters are reported in Table 1.1, with ascending node of 6:00 UTC. This allows for 14 orbits per day and a revisit period of 3 days. Due to the nature of the selected orbit, it experiences eclipses around the winter solstice.

Orbital parameters	Value
Semi major axis [km]	7137.482
Eccentricity [-]	0.00012770
Inclination [deg]	98.4431
Right ascension of the ascending node [deg]	255.7592
Argument of perigee [deg]	84.0180

Table 1.1: SMOS current orbital parameters

SMOS was launched on board a Rockot rocket from Plesetzk Cosmodrome (Russia) on November 2^{nd}, 2009. The spacecraft platform is the PROTEUS one, developed by CNES and built by Thales Alenia Space France, and also used in other space missions, like Calipso, COROT and Jason 1 and 2. It has a mass of 262 kg and a volume of 1 m^3. SMOS features a constant attitude in which the boresight of the payload is forward tilted by 32.5° with respect to nadir, except during the calibration maneuvers. This configuration enables measurements at line-of-sight angles between 0° and 50°.

As far as the ground segment is concerned, SMOS employs two different communication bands: the S-band in order to transmit and receive telecommands and housekeeping telemetry (from the platform and the payload); this is received by CNES stations and

then sent to the FOS (Flight Operation Segment) team. CNES is responsible for platform operations, S-band ground stations and flight dynamics including orbital maintenance; the mission control center is located in Toulouse, France.

SMOS also has an X-band antenna to transmit the MIRAS science and housekeeping telemetry to two ground antennae: one located directly at the European Science Astronomy Center in Villafranca, Spain, and the second at Svalbard, in Norway (operated by KSAT), for acquisition of near real-time data products. The antenna located at ESAC is a 3.5 m dish dedicated completely to the acquisition from SMOS. It experiences 3 to 4 passes per day, usually in early morning and late afternoon, due to the nature of SMOS dusk-dawn orbit. Moreover, SMOS has also a dedicated antenna in Svalbard, which provides communication in 10 out of the 14 orbits per day when the antenna located at ESAC is not able to acquire in real-time due to its geographical location.

The two X-band antennae are located at:

	Svalbard	**ESAC**
Longitude [deg]	15.4116	-3.9516
Latitude [deg]	78.2316	40.4426
Elevation [m]	458.1092	655.8510

Table 1.2: X-band antennae locations

The Flight Operation Segment is located at ESAC, along with the DPGS (Data Processing Ground Segment) and the CEC (Calibration Engineering Centre) teams. The FOS is responsible for payload real-time operations and telemetry monitoring, mission and payload planning and operations on-call support, while the DPGS team performs daily data processing and distribution, IT maintenance, daily routine antenna operations and mitigation of Radio Frequency Interferences. The CEC team is responsible for data quality checks, anomaly detection and instrument calibration support.

Moreover, SMOS is the first satellite to observe Earth in the L-band spectrum, which corresponds, as previously said, to the frequency of neutral atomic hydrogen: this frequency is protected by international law from man-made emissions, however some Radio Frequency Interference sources have been identified and attempted to be terminated by the DPGS.

Regarding the X-band data transmission, SMOS employs a central frequency of 8150 MHz, with a bandwidth from 8141 MHz to 8159 MHz, which is inside the X-band Earth

observation band provided by the International Telecommunication Union. The useful downlink data rate is 16.8 Mbps, with a CCSDS packet size of 476 Bytes. Moreover, the transmitter uses a 8PSK modulation with Trellis coding and Reed Solomon encoding, while the antenna has a field of view of 130°, from -65° to +65° off-nadir, which corresponds to the maximum gain in the main polarization.

The antenna matrix of direction cosines is reported in Table 1.3, where X_{sat}, Y_{sat} and Z_{sat} are the axes defining the body reference frame of the satellite and X_{Ant}, Y_{Ant} and Z_{Ant} the axes defining the reference frame of the antenna. The antenna main radioelectric axis in along the Z_{Ant} axis. The Local Vertical Local Horizontal, body and antenna frames are shown in Figure 1.2: it can be noted that SMOS body frame differs from the LVLH one and therefore this is taken into account when performing the attitude computation and the rotation between the two frames.

	$\mathbf{X}_{sat}$	$\mathbf{Y}_{sat}$	$\mathbf{Z}_{sat}$
$\mathbf{X}_{Ant}$	-0.243691	-0.229065	0.942414
$\mathbf{Y}_{Ant}$	-0.484467	-0.813038	-0.322893
$\mathbf{Z}_{Ant}$	0.840182	-0.535255	0.087156

Table 1.3: Antenna direction cosine matrix

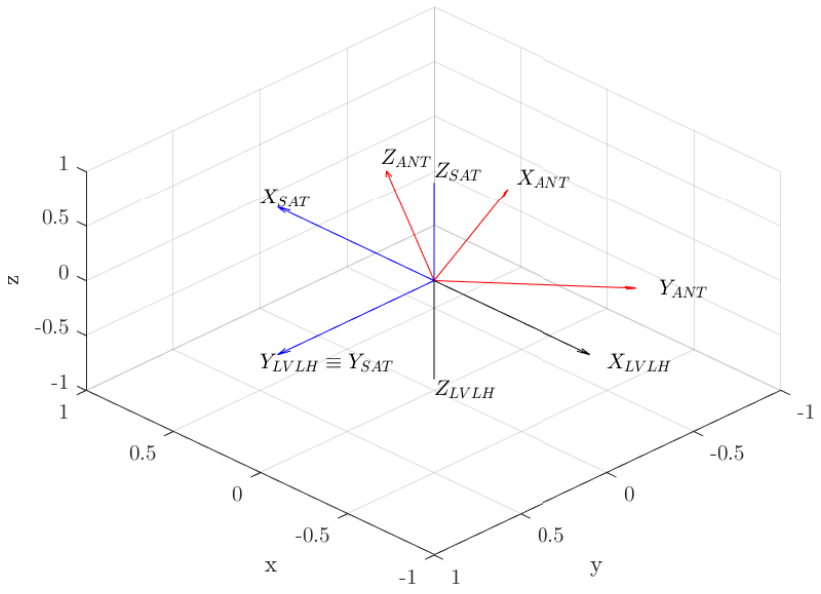

Figure 1.2: LVLH, body and antenna frames

1.2. Background

In the last few years, the number of satellites launched has been increasing strongly, with almost a 50% increase in 2021 with respect to 2020 [38]. In addition to traditional space agencies and governmental organizations, commercial companies are now also operating or planning to operate an increasing number of satellites for Earth observation purposes. In fact, Earth observation represents the second satellite main purpose of existence, after the communication one [33].

The best orbit to perform Earth remote sensing is a Sun-synchronous one, because the satellite passes over any given point of the planet's surface at the same local mean solar time. A Sun-synchronous orbit is useful for imaging, reconnaissance satellite and weather satellites, because every time that the satellite is overhead, the surface illumination angle on the planet underneath will be nearly the same. Therefore, more and more satellites utilise this orbit and they also need to transmit their acquired data to the ground: given their polar orbits, the high latitude ground stations are the ones most optimally located because they can communicate with LEO polar orbiting satellite on every revolution.

Among the many polar stations, the one of interest for this thesis work is the Svalbard Satellite Station, which is located on Platåberget near Longyearbyen in Svalbard, Norway, because, as previously described, it is part of SMOS ground stations. It is operated by Kongsberg Satellite Services (KSAT), a joint venture between Kongsberg Defence & Aerospace and the Norwegian Space Centre (NSC). Due to its unique location at 78° N, it is recognized as one of the most optimally located ground station in the world for the aforementioned reason [15].

Therefore, there is an overcrowding of the transmission frequency bands near the high latitude ground stations. The problem of Radio Frequency Interference among two or more satellites during transmission to a ground station is affecting even more the space sector. In fact, Radio Frequency Interference represents the single largest impact to robust satellite operation performance. Interference issues result in significant costs for the satellite operator due to loss of data and therefore of income, when the signal is interrupted. According to a survey by the Satellite Interference Reduction Group, 93% of satellite operator respondents suffer from satellite interference at least once a year. More than half experience interference at least once per month, while 17% see interference continuously in their day-to-day operations [22].

Furthermore, frequency bands are allocated by the ITU to the different services either worldwide or regionally. Band allocations are set out in the Table of Frequency Alloca-

tions. Each band may be allocated to one or more services [10]. The 8.025-8.400 GHz X-band is allocated to Earth Exploration Satellites for Space to Earth communication [9]. This is the frequency band in which SMOS is allocated for MIRAS data downlink. However, the use of this band by Earth observation satellites for payload data downlink operations is increasing and is resulting in harmful interference between these operators. A victim satellite transmitting on a downlink to an Earth station and one or several other satellites transmitting to either a different antenna at the same ground location or to a separate location but with a line-of-sight connection to the victim Earth station could lead to a RFI between these satellites. This is partly due to the growing number of satellites and partly also due to significantly higher data rates required in order to down link the higher amount of data [16]. In fact, this is one the reasons such that more and more satellites are using the X-band spectrum: higher transmission frequency means higher allowable data rate.

1.3. Thesis objective

As described in Section 1.1, the FOS is responsible for payload mission planning: among all these duties, one week in advance, it computes the X-band passes of the corresponding planning week above the two ground stations in ESAC and Svalbard. However, due to the reasons explained in Section 1.2, the SMOS X-band telemetry and science data can get partially or totally lost during passes over the Svalbard ground station. In these circumstances, sometimes the source of the problem cannot be easily determined since the root reason is not well and quickly identified (i.e. ground segment, space segment or Radio Frequency Interference by another satellite). Therefore, by analyzing previous events, the objective of the thesis is the implementation of a prediction model and tool able to predict in advance the list of future passes that might be affected by an RFI from other satellite, considering the mission planning performed by FOS. The output should contain the predicted responsible satellite, the timings and a probability of interference.

The previous events, collected by the DPGS, are reported in Table A.1, Table A.2 and Table A.3, while the events reported during the course of this work are shown in Table A.4. The tables report the affected pass time, the number of packets lost and, in some cases, a remark provided either by KSAT or by the DPGS team. These events will be used to perform the validation of the tool.

During the course of this work, the requirements for the FOS SMOS X-band RFI Prediction Tool (XRPT) have been issued: they are reported in Table A.5, Table A.6, Table A.7, Table A.8, Table A.9, Table A.10 and Table A.11.

1.4. State of the Art

As described in Section 1.2, the problem of Radio Frequency Interference is significantly increasing. However, it is affecting the sector since the beginning of space exploration and exploitation. Therefore, the prediction of possible interference events has been analyzed in order to find possible prediction tools. In fact, in the following, two methods to predict RFIs are presented, along with two different applications to satellite mission operations.

Since the 1960s NASA Space Tracking and Data Acquisition Network (STADAN) ground stations experienced RFIs caused by the appearance of two or more interfering satellites with overlapping 136 MHz emission spectrums, located simultaneously within view of a given GS antenna. Hence an automated prediction program was developed, based on the fact that satellites' orbits can be determined at least one-week in advance and therefore an a-priori RFI prediction can be made with the aim of re-scheduling the station operations during the periods affected by RFIs. The program was able to perform orbit computations and to calculate the received signal-to-interference power ratio for all visible satellites. A heuristic threshold for the interference condition was assumed when the signal-to-interference power ratio was below $+20\ dB$ and when the transmission frequencies were inside a certain bandwidth range with respect to their corresponding central frequencies. The accuracy of the program has been verified by comparing RFI predictions with STADAN station reported satellite interference and good agreement has been obtained [39]. The software to be developed presents some similarities: it should be able to predict in advance possible RFIs, based on orbital propagation and starting from a database of satellites, and it should be validated comparing the predicted and reported events. However, the proposed condition on the signal-to-interference power ratio cannot be employed given the fact that most of the required parameters are not available. Moreover, this program was developed to handle around 50 satellites, nowadays the number of satellites to be considered is much higher and it is not always possible to identify the required antenna characteristics.

The main problem concerns the downlink adjacent interference when two satellites operate in close proximity and share the same frequency. This has been analysed for the downlinks of all SARSAT (Search and Rescue Satellite Aided Tracking) LEO satellites, that use the same 1544.5 MHz frequency. In cases where the satellites are within the main lobe of the local user terminal antenna, transmissions from adjacent satellites act as interference to one another, effectively decreasing the signal-to-noise ratio of the desired downlink. This can result in missed distress beacon bursts or no stored solutions received at the Local User Terminals, consequently, no data is provided about a distress location. If the

transmitted EIRP from each satellite is similar, for two satellites close to each other, the two signals will act as interference to each other, severely degrading the received signal. The received carrier frequency provides a useful measure of the interference level: the relative velocity between the satellite and the LUT causes a Doppler shift in the received frequency and, as the orbital positions of the two satellites converge, so do their relative velocities to the LUT and Doppler curves. The implemented software enables prediction of Doppler curves, in fact when the difference in relative velocity and angular separation is minimal, the Doppler curves of the carrier frequency become almost identical. When receiver locks on the interfering signal, a jump in the received carrier frequency is seen. These interruptions in carrier lock result in loss of downlink capability and can visually show when interference has occurred. The similarity of predicted and real time recorded curves has been analysed, resulting in a good accordance [23]. The same problem concerns SMOS and this approach shows that the interference occurs when two satellites are in a conjunction with respect to the ground antenna. However, this software approach will not be used given that the real Doppler curves are not available.

Assessment and prediction of RFIs are present also in the Joint Polar Satellite System (JPSS) ground system ConOps. Inside the Mission Schedule, time-ordered events are reported. In particular, station visibilities for other spacecrafts are generated based on TLEs. This group of spacecrafts includes those which pose a potential RFI risk to the JPSS-managed and supported missions or are in contention for FCDAS (Fairbanks Command and Data Acquisition Station) 13-meter antenna resources. During this activity, the Mission Planning and Scheduling identifies potential RFI conjunctions and utilizes predicted visibility events to minimize the potential conflicts with other missions utilizing FCDAS. The CGS (Common Ground System) also performs Radio Frequency Interference analysis to support mission planning and scheduling, supplementing the analysis provided by the ground station service providers and providing RFI situational awareness. The CGS Predict Orbit Events activity propagates the orbit state of JPSS-supported satellites, TDRS spacecrafts and other satellites of potential RFI sources or station scheduling conflicts for 40 days and saves the results in an ephemeris file. Under nominal conditions, this propagation is performed on a weekly basis. This activity calculates the potential RFIs and generates the orbital events for predicted conjunctions, which are determined based on the predicted TLEs and RF characteristics of these satellites. This is used to generate the orbital events for JPSS-managed mission GS visibilities which are in conflict as determined using a user provided threshold value of maximum conjunction [19]. This approach is very similar to the one used inside the software, given that it starts from defining a database of potentially conflicting satellites, propagating their orbits for a cer-

tain amount of time and then searching for the potential RFI conjunctions over a selected ground station.

Furthermore, inside the European Space Agency, the GENEOS Flight Dynamics tool is used for all Earth observation missions: it is capable of predicting interference events among different satellites with respect to a GS during a selected planning week. It will be used to validate and compare the results of the software.

1.5. Thesis outline

Here a brief description of the thesis contents is performed. In Chapter 2, the theory at the basis of this work is analysed, highlighting all the theoretical topics dealt in this thesis. While, in Chapter 3, the steps followed in the implementation of the software, along with the description of the algorithms used inside the tool, are defined. In Chapter 4, the validation process of the different models employed for this thesis work and the results are shown, identifying the list of satellites responsible for the interference events. Moreover, in the same chapter, the results of the identification of possible patterns inside the data of previous RFIs and the consequent statistical analysis, with the aim of computing the Mahalanobis distance, are described. Finally, Chapter 5 reports the conclusion of this thesis work and presents a possible future development, including Machine Learning and Neural Networks.

2 | Theoretical background

In the following chapter, the theoretical bases of this thesis are described. First, the Sun-synchronous orbit, which is adopted for SMOS, is presented, along with its orbital characterization. Then, the attitude parameters employed are considered, with the description of the quaternion and of the Euler angles and of their direct transformations to the direction cosine matrix. Subsequently, the different types of reference frames used inside this work and how to obtain them are described: the topocentric horizon coordinate frames for the GS, the Local Vertical Local Horizontal in order to compute the attitude of SMOS. Moreover, the Two-Line Element set is characterized in the following, along with the Simplified General Perturbations orbit propagator. Then, the Radio Frequency Interference is described, focusing on the adjacent satellite interference. The mathematical characterization of the Mahalanobis distance and of the probability value is presented. At the end of this chapter, the SPICE Toolkit is introduced, with the description of its kernels, time standards, reference frames and functions used inside the algorithm.

2.1. Sun-synchronous orbit

As said in Section 1.1, SMOS is in a dawn-dusk Sun-synchronous orbit, that is a quasi-circular LEO polar orbit with a Local Time of Ascending Node of 6:00 UTC. This type of orbit allows to obtain the optimum scientific measurements, because the surface illumination angle on the planet will be nearly the same providing consistent lighting conditions, that is a useful characteristic for Earth observation satellites.

A dawn-dusk orbit, where the local mean solar time of passage (it is referred to local mean solar time, not to apparent solar time, because the Sun will not be in exactly the same position in the sky during the course of the year) for equatorial latitudes is around sunrise or sunset, is a special case of a Sun-synchronous orbit: it allows the satellite to ride on the terminator between day and night. This also means that the solar arrays are always illuminated, except for short eclipse periods during the winter season. It is also useful for some satellites with passive instruments that need to limit the Sun's influence on the measurements, as it is possible to always point the instruments towards the night side

of the Earth. Another particular case of a Sun-synchronous orbit is the noon-midnight orbit, where the local mean solar time of passage for equatorial latitudes is around noon or midnight.

Technically, a Sun-synchronous orbit is arranged so that it precesses through one complete revolution each year, in order to always maintain the same relationship with the Sun.

All planets, including Earth, do not have a spherical mass distribution, therefore they bulge out of the equator because of the centrifugal forces. This is called oblateness, which means that the equatorial radius is larger than the polar one. For the Earth oblateness, the dominant term is called J_2 and it is defined as [36]:

$$J_2 = \frac{R_E - R_P}{R_E} \tag{2.1}$$

Where R_E is the equatorial radius, R_P is the polar one and the former is 21 km larger than the latter one, for Earth; the J_2 term is equal to $1.08263 * 10^3$.

Oblateness causes the right ascension of the ascending node Ω and the argument of perigee ω to vary significantly with time. Focusing on the first parameter, the average rate of change is defined as [36]:

$$\dot{\Omega} = -\left[\frac{3}{2}\frac{\sqrt{\mu} \cdot J_2 \cdot R^2}{(1-e^2)^2 \cdot a^{7/2}}\right] \cdot cos(i) \tag{2.2}$$

With R and μ are respectively the radius and gravitational parameter of the Earth; a and e are the semi major axis and the eccentricity of the orbit, while i is the orbit's inclination. This effect is called nodal regression.

The effect of the orbit inclination on nodal regression is leveraged by Sun-synchronous orbits, whose orbital plane makes a constant angle α with respect to the Sun, as illustrated in Figure 2.1. In order for this to occur, the orbital plane must rotate in inertial space with the angular velocity of the Earth in its orbit around the Sun, which is 360° divided by 365.26 days, which results to be 0.9856° per day [25]. With the orbital plane precessing eastward at this rate, the ascending node will lie at a fixed mean local solar time. Considering Equation (2.2), in order to have an eastward precession, the orbit inclination should be between 90° and 180°, meaning that the orbit should be retrograde. Given that the $\dot{\Omega}$ term due to J_2 depends on both inclination and semi major axis, a typical LEO circular Sun-synchronous orbit should have an inclination of around 98° [36], which in fact corresponds to the value of SMOS.

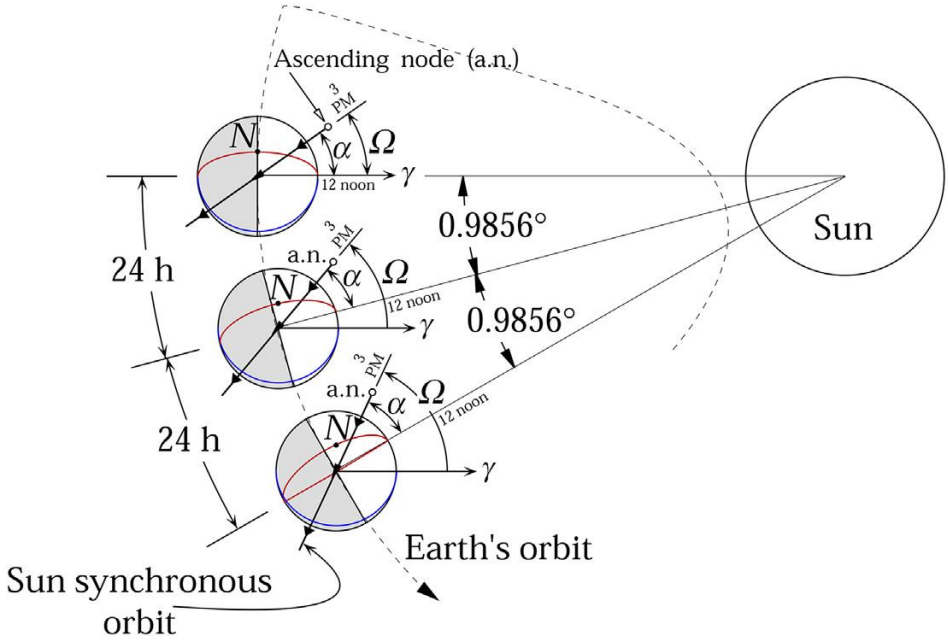

Figure 2.1: Sun-synchronous orbit representation [25]

2.2. Attitude parameters

It is always necessary to be able to switch from a reference frame to another reference frame, such as the case of representing the body frame as seen by an inertial frame or by a local vertical local horizontal frame. Therefore, attitude parameters have to be employed in order to build such rotation matrix [37].

In this section, first the direction cosine matrix is described, which will be used to define each rotation computed inside the software. Then, the Euler axis and angle are presented in order to be able to describe the quaternion vector. Inside the tool, the real quaternions are recovered from the spacecraft telemetry and used to define SMOS body frame with respect to the LVLH one. Finally, also the Euler angles are introduced: they are used in the Prediction model to define the direction cosine matrix imposing the SMOS constant 32.5° forward tilt angle. Furthermore, the direct transformation from either the quaternion and the Euler angles to the direction cosine matrix is described.

Each axis of a reference frame is defined in the current reference frame by the three components of its unit direction vector. Assembling the components of the three axes,

the direction cosines matrix is obtained, in which each row represents one axis:

$$A = \begin{bmatrix} u_1 & u_2 & u_3 \\ v_1 & v_2 & v_3 \\ w_1 & w_2 & w_3 \end{bmatrix}$$

A is the direction cosine matrix, which is an orthogonal rotation matrix, with the following properties:

$$AA^T = I, \qquad A^T = A^{-1} \tag{2.3}$$

Moreover, in order to compose a sequence of two or more rotations, it is sufficient to build the overall direction cosine matrix as the product of the individual rotations (so of the individual direction cosine matrix), taken in the reversed order compared to the sequence used.

Real, orthogonal matrices, like the direction cosine matrix, have one unit eigenvalue, to which it is associated the eigenvector **e**:

$$A\mathbf{e} = \mathbf{e}. \tag{2.4}$$

Therefore, vector **e** does not change due to the rotation represented by matrix A. This is possible only if the rotation occurs around axis **e**. This axis is called Euler axis and the rotation amplitude around this axis is called Euler angle.

A quaternion is a unit-norm vector of four parameters, linked to the Euler axis and angle through the following relation:

$$\begin{cases} q_1 = e_1 \cdot sin\left(\dfrac{\phi}{2}\right), \\ q_2 = e_2 \cdot sin\left(\dfrac{\phi}{2}\right), \\ q_3 = e_3 \cdot sin\left(\dfrac{\phi}{2}\right), \\ q_4 = cos\left(\dfrac{\phi}{2}\right). \end{cases} \tag{2.5}$$

In some cases, it is convenient to divide the quaternion into a vector part **q** and a scalar part q_4:

$$\mathbf{q} = \begin{bmatrix} q_1 \\ q_2 \\ q_3 \end{bmatrix}$$

The direct transformation from the quaternion to the direction cosine matrix A, leads to:

$$A = (q_4^2 - \mathbf{q}^T\mathbf{q})I + 2\mathbf{q}\mathbf{q}^T - 2q_4[q\wedge]). \tag{2.6}$$

where $[q\wedge] = \begin{bmatrix} 0 & -q_3 & q_2 \\ q_3 & 0 & -q_1 \\ -q_2 & q_1 & 0 \end{bmatrix}$

The attitude can be also represented by means of three Euler angles, which are a minimal representation and have a clear physical interpretation. The concept is based on the fact that it is always possible to make two orthogonal frames overlap by appropriate rotation of one of them three times around its reference axes. The direction cosine matrix can be written by adopting the rule of consecutive rotations. In fact, it is possible to combine the elementary rotation matrices since each rotation is around one of the coordinate axes. For example,

$$A_{313}(\phi, \theta, \psi) = A_3(\psi) \cdot A_1(\theta) \cdot A_3(\phi). \tag{2.7}$$

where

$$A_3(\psi) = \begin{bmatrix} cos(\psi) & sin(\psi) & 0 \\ -sin(\psi) & cos(\psi) & 0 \\ 0 & 0 & 1 \end{bmatrix}$$

$$A_1(\theta) = \begin{bmatrix} 1 & 0 & 0 \\ 0 & cos(\theta) & sin(\theta) \\ 0 & -sin(\theta) & cos(\theta) \end{bmatrix}$$

$$A_3(\phi) = \begin{bmatrix} cos(\phi) & sin(\phi) & 0 \\ -sin(\phi) & cos(\phi) & 0 \\ 0 & 0 & 1 \end{bmatrix}$$

2.3. Reference frames

Different reference frames are considered inside the software implementation and will be described in this section.

Communication to ground begins when the satellite is in the desired orbital position. Ground stations can communicate with LEO satellites only when the satellite is in their visibility region. For each observer's position on the Earth, a horizon plane can be defined: it is considered as the tangent plane to the surface of the Earth at the observer's location. For the ground stations, it corresponds to the location of the receiving or transmitting

antenna. The position of the satellite within its orbital path with respect to the ground station point of view can be defined by the Azimuth and Elevation angles. The azimuth (A) is the angle of the direction of the satellite, measured in the horizon plane from the geographical north in clockwise direction. The range of azimuth is 0° to 360°. While, the elevation, also called altitude (a), is the angle between the satellite and the observer's horizon plane. The range of elevation is between 0° and 90° [25].

This frame is called topocentric horizon reference frame. A topocentric coordinate system is one that is centered at the observer's location on the surface of the Earth. In particular, as shown in Figure 2.2, the horizon frame is centered at an observer's position O whose position vector is R. The xy plane is the local horizon, which is the plane tangent to the ellipsoid at point O. The z-axis is normal to this plane directed outward toward the local zenith. The x-axis is directed eastward and the y-axis points north [25]. The observer's position O can be retrieved knowing the longitude and latitude of the ground station.

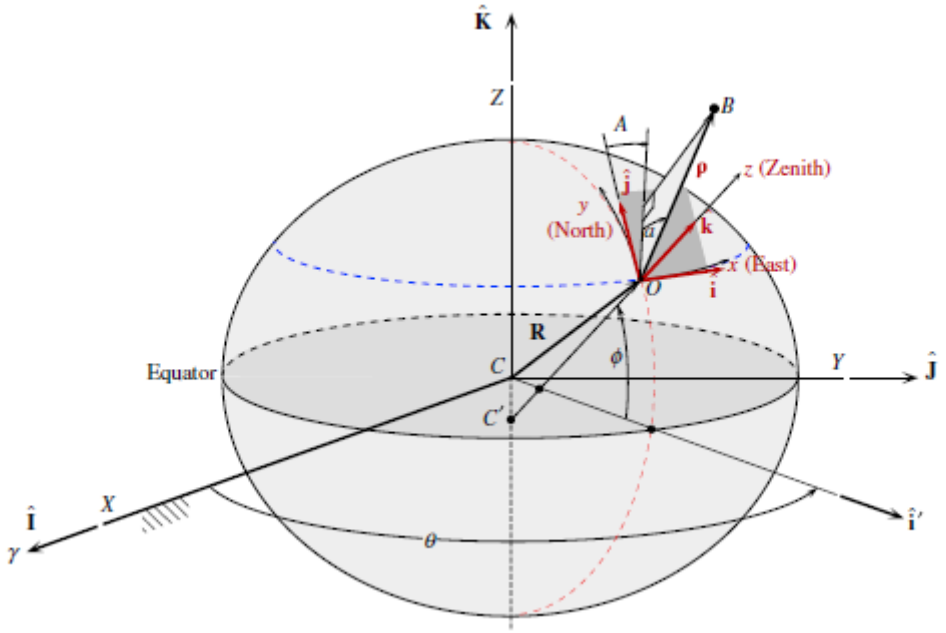

Figure 2.2: Topocentric horizon reference frame [25]

The range under the lowest elevation angle represents the worst link budget case, since that range represents the maximal possible distance between the ground station and the satellite. Therefore, this represents the position in which a satellite is more susceptible to interference [24].

The Local Vertical Local Horizontal (LVLH) frame, also known as Orbit frame, is another reference used in this work. It is centered in correspondence of the centre of mass of the

spacecraft. The x-axis is directed along the outward radial direction with respect to the centre of the Earth, while the z-axis is perpendicular to the orbital plane. The y-axis completes the right-hand triad: it is parallel to the orbital velocity vector only in case of circular orbits. Therefore, the xy plane coincides with the orbital plane. Being centered in correspondence of the satellite, this reference frame is moving along the orbit with the spacecraft, hence it is also called Co-moving frame [25].

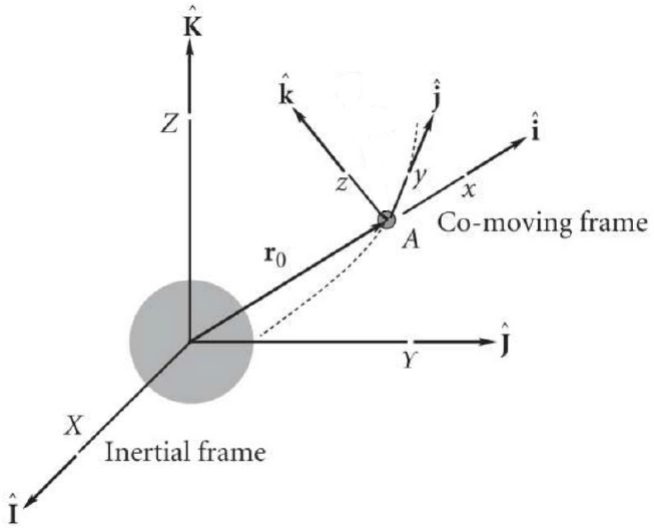

Figure 2.3: Local Vertical Local Horizontal frame

In Algorithm 2.1, the transformation from the spacecraft state to the orbital parameters is presented: this will be used inside the software in order to compute, at each timestep, the keplerian parameters. In fact, they are needed in order to rotate from the inertial reference frame to the LVLH one. As described previously in Section 2.2, the rotation matrix is defined as follows:

$$R_{313}(\omega + \theta, i, \Omega) = R_3(\omega + \theta) \cdot R_1(i) \cdot R_3(\Omega). \tag{2.8}$$

where

$$R_3(\omega+\theta) = \begin{bmatrix} cos(\omega+\theta) & sin(\omega+\theta) & 0 \\ -sin(\omega+\theta) & cos(\omega+\theta) & 0 \\ 0 & 0 & 1 \end{bmatrix}, \; R_1(i) = \begin{bmatrix} 1 & 0 & 0 \\ 0 & cos(i) & sin(i) \\ 0 & -sin(i) & cos(i) \end{bmatrix}$$

$$\text{and } R_3(\Omega) = \begin{bmatrix} cos(\Omega) & sin(\Omega) & 0 \\ -sin(\Omega) & cos(\Omega) & 0 \\ 0 & 0 & 1 \end{bmatrix}$$

Algorithm 2.1 State to Keplerian Elements Transformation Algorithm [25]

1: Retrieve SMOS state (**r**,**v**), compute the norms of **r** and **v**, compute radial component of the velocity (v_r).
2: Compute angular momentum vector **h** and its norm (h) as the cross product between **r** and **v**.
3: Compute inclination as

$$i = cos^{-1}\left(\frac{h_z}{h}\right) \tag{2.9}$$

4: Compute line of nodes direction (**N**) and its norm (N) as

$$\mathbf{N} = [0, 0, 1] \times \mathbf{h} \tag{2.10}$$

5: **if** $N_y \geq 0$ **then**
6: Compute right ascension of the ascending node as

$$\Omega = cos^{-1}\left(\frac{N_x}{N}\right) \tag{2.11}$$

7: **else**
8: Compute right ascension of the ascending node as

$$\Omega = 360^\circ - cos^{-1}\left(\frac{N_x}{N}\right) \tag{2.12}$$

9: **end if**
10: Compute eccentricity vector (**e**) and its norm (e).
11: **if** $e_z \geq 0$ **then**
12: Compute argument of perigee as

$$\omega = cos^{-1}\left(\frac{\boldsymbol{N} \cdot \boldsymbol{e}}{Ne}\right) \tag{2.13}$$

13: **else**
14: Compute argument of perigee as

$$\omega = 360^\circ - cos^{-1}\left(\frac{\boldsymbol{N} \cdot \boldsymbol{e}}{Ne}\right) \tag{2.14}$$

15: **end if**
16: **if** $v_r \geq 0$ **then**
17: Compute true anomaly as

$$\theta = cos^{-1}\left(\frac{\boldsymbol{r}}{r} \cdot \frac{\boldsymbol{e}}{e}\right) \tag{2.15}$$

18: **else**
19: Compute true anomaly as

$$\theta = 360^\circ - cos^{-1}\left(\frac{\boldsymbol{r}}{r} \cdot \frac{\boldsymbol{e}}{e}\right) \tag{2.16}$$

20: **end if**
21: Compute semi-major axis though computation of perigee and apogee radii as

$$a = 0.5 \cdot (r_{perigee} + r_{apogee}) \tag{2.17}$$

2.4. Two-Line Element

A NORAD (North American Aerospace Defense) Two-Line Element (TLE) set consists of two 69-character lines of data which can be used together with the SGP4/SDP4 orbital model to determine the position and velocity of the associated satellite. Each satellite has been assigned its corresponding NORAD Catalog Number. This is a unique identifier assigned by the United States Space Command in the order of launch or discovery for each Earth-orbiting artificial satellite in their Satellite Catalog. In fact, the United States Space Force tracks all detectable objects in Earth orbit, creating a corresponding TLE for each object. The TLE data representation is specific to the simplified perturbations models, so any algorithm using a TLE as a data source must implement one of these models to correctly compute the state at a time of interest. TLEs can describe only the trajectories of Earth-orbiting objects and are widely used as input for propagating future orbital tracks.

Data for each satellite consists of two lines in the format reported in Table 2.1 and Table 2.2 [29].

Line 1		
Field	**Column**	**Description**
1.1	01	Line Number of Element Data
1.2	03-07	Satellite Number
1.3	08	Classification
1.4	10-11	International Designator (last two digits of launch year)
1.5	12-14	International Designator (launch number of the year)
1.6	15-17	International Designator (piece of the launch)
1.7	19-20	Epoch Year (last two digits of year)
1.8	21-32	Epoch (day of the year and fractional portion of the day)
1.9	34-43	First Time Derivative of the Mean Motion
1.10	45-52	Second Time Derivative of Mean Motion (decimal point assumed)
1.11	54-61	B^* drag term (decimal point assumed)
1.12	63	Ephemeris type
1.13	65-68	Element number
1.14	69	Checksum (Modulo 10)

Table 2.1: Two-Line Element Set, Line 1

Line 2		
Field	**Column**	**Description**
2.1	01	Line Number of Element Data
2.2	03-07	Satellite Number
2.3	09-16	Inclination [Deg]
2.4	18-25	Right Ascension of the Ascending Node [Deg]
2.5	27-33	Eccentricity (decimal point assumed)
2.6	35-42	Argument of Perigee [Deg]
2.7	44-51	Mean Anomaly [Deg]
2.8	53-63	Mean Motion [Revolutions per day]
2.9	64-68	Revolution number at epoch
2.10	69	Checksum (Modulo 10)

Table 2.2: Two-Line Element Set, Line 2

Column 1 of each line of the Two-Line Element set indicates the line number (and hence the format) for that line. The next field on each line (1.2 and 2.2) indicates the satellite NORAD Catalog Number. For a valid Two-Line Element set, both 1.2 and 2.2 must be identical. Field 1.3 indicates the security classification of the data: all publicly available data have a U in this field to indicate unclassified data. The next three fields (1.4 through 1.6) define the International Designator of the object. It specifies the year of the launch (field 1.4), the launch of that year (field 1.5), and the piece of that launch (field 1.6) for each object. The next two fields (1.7 and 1.8) together define the reference time for the element set and are jointly referred to as the epoch. Field 1.7 is the two-digit year, while field 1.8 is the day of that year. The epoch defines the time to which all of the time-varying fields in the element set are referenced. Field 1.9 represents the first derivative of the mean motion divided by two, in units of revolutions per day^2, instead 1.10 represents the second derivative of the mean motion divided by six, in units of revolutions per day^3. Together, these two fields give a second-order picture of how the mean motion is changing with time. However, these two fields are used only by the simpler SGP model. Field 1.11 represents the so-called B^*, which is an SGP4-type drag coefficient. In aerodynamic theory, every object has a ballistic coefficient, B, that is the product of its coefficient of drag, C_D, and its cross-sectional area, A, divided by its mass, m.

$$B = \frac{C_D A}{m} \tag{2.18}$$

The ballistic coefficient represents how susceptible an object is to drag: the higher the number, the more susceptible it is. B^* is an adjusted value of B using the reference value of atmospheric density, ρ_o:

$$B^* = \frac{B\rho_o}{2} \tag{2.19}$$

B^* has units of (Earth radii)$^{-1}$. Field 1.12 represents the ephemeris type (i.e. orbital model) used to generate the data: all distributed element sets have a value of zero and are generated using the SGP4/SDP4 orbital model. Field 1.13 represents the element set number. Normally, this number is incremented each time a new element set is generated. The last column on each line (fields 1.14 and 2.10) represents a modulo-10 checksum of the data on that line. The checksums for each line are calculated by adding all numerical digits on that line, including the line number.

Line 2 consists primarily of mean elements calculated using the SGP4/SDP4 orbital model. Fields 2.3, 2.4, 2.6 and 2.7 all have units of degrees and can range from 0° up to 360°, except for field 2.3 (representing the inclination) which only goes up to 180°. The eccentricity (field 2.5) is a unitless value with an assumed leading decimal point. For example, a value of 1234567 corresponds to an eccentricity of 0.1234567. The mean motion (field 2.8) is measured in revolutions per day. The final field on line 2, prior to the checksum, is the revolution number [28].

Simplified General Perturbations models are a set of five mathematical models (SGP, SGP4, SDP4, SGP8 and SDP8) used to calculate orbital state vectors of Earth-orbiting objects relative to the Earth-centered inertial coordinate system. This set of models is often referred collectively as SGP4 (Simplified General Perturbations 4 orbit propagator) due to the frequency of use of this model with Two-Line Element sets produced by NORAD. In fact, these data are produced by fitting observations from the US Space Surveillance Network to produce Brouwer mean elements using the SGP4.

The NORAD element sets are *mean* values obtained by removing periodic variations in a particular way. In order to obtain good predictions, these periodic variations must be reconstructed by the prediction model in exactly the same way they were removed by NORAD. All space objects are classified by NORAD as near-Earth (orbital period less than 225 minutes) or deep-space (period greater than or equal 225 minutes). Depending on the period, the NORAD element sets are automatically generated with the near-Earth or deep-space model. Simplified General Perturbations models apply to near-Earth objects and predict the effect of perturbations caused by the Earth's shape, drag, radiation and gravitation effects from other bodies such as the Sun and Moon [27].

There are different ways to retrieve TLEs from internet: in this work, three different sources have been used and will be investigated in details in Section 3.2:

- CelesTrak
- n2yo.com
- SpaceTrack

2.5. Radio Frequency Interference

There are many factors that may cause data losses during a satellite pass over a ground station, in particular adverse weather conditions, Radio Frequency Interference, network outages and ground or satellite equipment failures. Energetic particles and radiation from the Sun, especially during solar storms, can also create periodic outages which may lead to loss of data. Among all these sources, a Radio Frequency Interference is an electromagnetic interference in the radio frequency spectrum. It is a disturbance generated by an external source, degrading the overall performance of the system and possibly leading to a total loss of data.

The interference is caused by unwanted signals that interrupt the reception of radio waves. It can be produced within the same satellite systems or from other satellites using the same or similar frequencies. Satellite interference can be categorized into specific groups including adjacent channel interference, cross polarization interference, deliberate interference and adjacent satellite interference. Adjacent channel interference is caused by unsolicited signals in an adjacent frequency channel, while cross-polarization interference is caused when the antenna is not peaked properly and/or the polarization is incorrectly set-up. Deliberate interference involves hostile attempts to disrupt the service. Finally, adjacent satellite interference (ASI) is an unintentional interference that may be degrading the received signal at the antenna during a pass when neighboring orbiting satellites sharing the same frequency are adjacent and interfere to each other [26].

ASI is the type of interference which occurs to SMOS during the reported events, therefore it will be analysed in detail. Adjacent satellite interference is categorized into downlink and uplink interference:

- Downlink ASI happens when two satellites sharing the same downlink frequency are located close to each other from the perspective of the receiving ground station antenna, which receives unwanted signals from the adjacent spacecraft. During these periods of interference, the downlink of the adjacent satellites may be severely

impaired. This interference causes issues with satellite service providers and may prevent the satellite terminal from working correctly, leading to a partial or a total loss of downlinked data.

- Uplink ASI occurs when adjacent satellites receive and re-broadcast strong uplink signals from ground antennae which are either too small and/or improperly pointed at the wrong satellite in orbit.

Figure 2.4 shows that potential RFI occurs when the victim receiver (on-board a satellite in the case of an uplink or at the ground station in the case of a downlink) simultaneously collect power from a desired signal source and other undesired interferers [34].

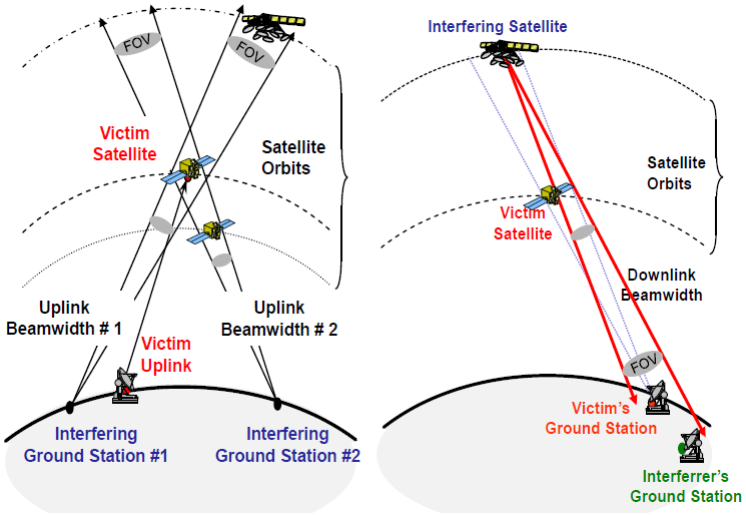

Figure 2.4: Adjacent satellite interference: on the left the uplink case, on the right the downlink one

The interference events reported for SMOS happen during Space to Earth transmission, so they are associated to the Downlink ASI.

As introduced in Section 1.1, since its launch, SMOS scientific data suffers from another type of RFI, which is associated to the fact that its radiometer works in the passive band 1400-1427 MHz and any man-made emissions in this band are prohibited by ITU Radio-Regulations. These are due to illegal emissions in this band, by adjacent band emissions having strong leakage, as well as by unwanted emissions caused by faulty equipment. In order to minimize the impact of RFIs and to improve scientific retrieval, several strategies has been initiated by the different SMOS teams. This requires the SMOS team to detect the RFI sources and to provide accurate and updated information on its location and indicative strength observed by the satellite to local authority in order to identify and possibly terminate the interference signal [12].

2.6. Mahalanobis distance and p-value

The Mahalanobis distance is a measure of the distance between a sample point and a distribution of data, characterised by a mean μ and a covariance matrix Σ. It is the multivariate equivalent of the Euclidean distance, introduced by Prof. Mahalanobis in 1936. It is based on the idea of measuring how many standard deviations away the sample point is from the mean of the distribution. The Mahalanobis distance is unitless, scale-invariant and takes into account the correlations of the data set, differently from the Eulerian distance which has some limitations for set of data with some degree of correlation [35].

The Mahalanobis distance D_M of an observation $\mathbf{x} = (x_1, x_2, x_3, \ldots, x_N)^T$ from a set of data with mean $\mu = (\mu_1, \mu_2, \mu_3, \ldots, \mu_N)^T$ and with a nonsingular covariance matrix Σ is defined as [20]:

$$D_M(\mathbf{x}) = \sqrt{(\mathbf{x} - \mu)^\mathsf{T} \Sigma^{-1} (\mathbf{x} - \mu)} \tag{2.20}$$

With Σ defined as the symmetrical Variance-Covariance matrix:

$$\Sigma = \begin{bmatrix} var(x_1) & cov(x_1, x_2) & \ldots & cov(x_1, x_N) \\ cov(x_2, x_1) & var(x_2) & \ldots & cov(x_2, x_N) \\ \ldots & \ldots & \ldots & \ldots \\ cov(x_N, x_1) & cov(x_N, x_2) & \ldots & var(x_N) \end{bmatrix}$$

The effect of dividing by the covariance is of main importance: if the variables in the dataset are strongly correlated, then, the covariance will be high. Dividing by a large covariance, it will effectively reduce the distance. Likewise, if the data are not correlated, then the covariance is not high and the distance is not reduced much. So effectively, it addresses the problems of scale as well as the correlation of the variables that affects the Eulerian distance [35].

The Mahalanobis distance is then used to find outliers in statistical analyses. To determine if any of the distances are statistically significant, the probability value of the corresponding observation is calculated, as the p-value that corresponds to the χ-square distribution of the square Mahalanobis distance with k degrees of freedom, where k is the number of variables [20]:

$$p\_value(\mathbf{x}) = 1 - cdf(D_M^2, k) \tag{2.21}$$

where *cdf* represents the cumulative distribution function of the χ-square distribution. The critical p-value to determine if an observation could be considered an outlier with respect to the available data is assumed as 0.001. This will be better defined in Section 4.5.

2.7. SPICE Toolkit

SPICE (Spacecraft Planets Instrument C- matrix Events) is a set of software routines and a suite of data formats, consisting of observation geometry data and time conversion functions to plan, for example, scientific observations from a space vehicle, to analyze the science data gathered from those observation or to find events during the mission.

SPICE was developed and is maintained by the Navigation and Ancillary Information Facility (NAIF) team of the Jet Propulsion Laboratory.

SPICE performs all kinds of geometrical and time calculations involving spacecraft, payloads, Solar System bodies and ground stations: for example, SPICE helps retrieving the state of a spacecraft at one particular moment in the desired reference frame [31].

2.7.1. SPICE kernels

SPICE stores geometry and time data in files called kernels. These are the core of the system, since they provide:

- information about the different reference frames used to describe the position and motion of Solar System bodies;
- ephemeris information for spacecrafts, solar system bodies and ground stations;
- attitude information, with respect to a selected reference frame;
- information about the spacecraft clock and how to convert from it to ephemeris time and/or UTC and the other way around;
- mounting alignment and field-of-view geometry for the spacecraft's instruments and antennae.

Each kernel is a separated file whose extension identifies its type, as well as whether it is a binary or text kernel (for a binary kernel, the extension starts with a *b* and for a text kernel it starts with a *t*). A kernel stores information which can be read by any application that uses the SPICE Toolkit [31].

2.7.2. Types of kernels

A SPICE kernel can have one of the following types [31]:

- **SPK Spacecraft and Planetary ephemeris**
  SPK kernels store ephemeris information for planets, other Solar System bodies and

spacecrafts. They are binary kernels and their file names have extension *bsp*.

- **PCK Planetary Constants**
  PCK kernels store information about planets and other bodies of the Solar System. Information stored in a PCK kernel can be, for instance, the mass of a planet or how it rotates as a function of time. They can be binary (extension *bpc*) or text (extension *tpc*) files.

- **IK Instrument**
  IK kernels contain information about instrument parameters, like field of view of a camera or the number of pixels of a CCD. They are text kernels, with extension *ti*.

- **CK Pointing**
  C-kernels are binary kernels with extension *bc* which store information about the orientation of the spacecraft or of any of its components.

- **EK Events**
  Events like the science plan are stored in these kernels.

- **FK Reference Frame specifications**
  In this type of text kernel (with extension tf) information about different reference frames used in a mission and how to transform vectors from one reference system to another can be found.

- **SCLK Spacecraft Clock correlation data**
  This text kernel (with extension *tsc*) allows the SPICE system to translate from the spacecraft clock coefficients to UTC or other time systems and vice-versa.

- **LSK Leapseconds**
  A leapseconds kernel (text kernel with extension *tls*) stores information about the leapseconds that have occurred.

2.7.3. Kernels used in the algorithm

Here the list of the kernels used inside the software:

- *naif0012.tls* and *latest_leapseconds.tls*
  These are two leapseconds kernel files.

- *de414.bsp*
  It is a SPK kernel, containing ephemeris information for all the planets of the Solar System and for the Moon, relative to the Solar System barycenter.

- *pck0010.tpc*
  This kernel contains orientation and size/shape data for planets, natural satellites, the Sun and selected asteroids. Orientation data provided in this file are used by the SPICE Toolkit to evaluate the orientation of body-fixed, body-centered reference frames with respect to the J2000 frame. The orientation models express the direction of the pole and location of the prime meridian of a body as a function of time. The size/shape models represent all bodies as ellipsoids, using two equatorial radii and a polar radius.

- *estrack_V04.bsp*
  SPK kernel that stores information about the position of the ESTRACK stations with respect to the center of the Earth.

- *estrack_V04.tf*
  This is a frame kernel defining a topocentric horizon reference frame for the ESA ground stations, as defined in Section 2.3.

  The rotation defined in this file transforms vectors from the previously defined topocentric frame to an Earth-fixed frame. This is a 3-2-3 rotation with angles defined as the negative of the site longitude, the negative of the site colatitude and 180 degrees.

- *earthfixeditrf93.tf*
  This kernel associates the ITRF93 frame with the EARTH_FIXED reference frame. Loading this kernel together with a kernel whose data are relative to the EARTH_FIXED frame (for example, a topocentric frame kernel for ground stations) allows the SPICE system to treat that kernel's data as though they are relative to the ITRF93 frame. This kernel normally should be loaded together with a binary PCK file providing Earth rotation data, like *earth_latest_high_prec.bpc*.

- *earth_latest_high_prec.bpc*
  A binary high-precision Earth PCK file used to convert the station location from terrestrial to inertial coordinates and vice versa (in particular, it represents the orientation of the Earth ITRF93 body-fixed reference frame relative to the J2000). This kernel provides Earth orientation data taking into account precession, nutation, nutation corrections, UT1-TAI difference and polar motion. This kernel uses each new release of the reconstructed Earth Orientation Parameters file by JPL, which covers well into the past and approximately two months into the future beyond the production date; in fact, the accuracy of the future data degrades rapidly. Inside the software, this kernel is updated daily in order to always have the highest accuracy

as possible [21].

2.7.4. Time standards

There are two widely used types of time standards in SPICE: those related to the rotation of the Earth and those related with the frequency of atomic oscillations (like ET and UTC). The latter are the closest approximations to a uniform time [31].

SPICE supports several time systems, namely:

- UTC, Coordinated Universal Time
- ET, Ephemeris Time
- SCLK, Spacecraft Clock Time.

The first two are used inside the tool.

2.7.5. UTC

The basis for the UTC is the International Atomic Time (TAI). It is based on the atomic second as defined by the oscillation of the undisturbed cesium atom. Atomic time is a count of the number of atomic seconds that have occurred since the astronomically determined instant of January 1, 1958 00:00:00, at the Royal Observatory in Greenwich.

UTC can be represented in several ways in SPICE, two of the most used are:

- **YYYY-MM-DDThh:mm:ss.fff**
  The time is represented as year, month, day of month, hours, minutes, seconds and fraction of second. For example, 2022-02-12T12:50:55.103. This type is the one used inside the software in order to represent the computed times.
- **YYYY-DDDThh:mm:ss.fff**
  The time is represented as year, day of year, hours, minutes, seconds and fraction of second. For example, 2022-138T00:00:00.000.

Ideally, every UTC day at 00:00:00 should correspond with midnight at Greenwich, as observed astronomically. This time is called UT1. It assumes that the time between two consecutive passes of the Sun above Greenwich is 24 hours. However, the rotation of the Earth is not uniform, which means that there is a difference between UTC midnight and UT1. To keep the difference from being too large, UTC is occasionally adjusted so that it never exceeds 0.9 seconds.

When Greenwich UT1 midnight lags behind midnight UTC by more than 0.7 seconds, a leapsecond will be added to the collection of UTC names. This leapsecond has traditionally been added after the last *normal* UTC name of December 31 or June 30. When a leapsecond is added at the end of a year, UTC time progresses in the following way:

December 31 23:59:58, December 31 23:59:59, December 31 23:59:60, January 1 00:00:00

If Greenwich UT1 midnight runs ahead of UTC midnight by more than 0.7 seconds, a negative leapsecond will be added. In this case, the progression will be:

December 31 23:59:57, December 31 23:59:58, January 1 00:00:00.

Therefore, leapseconds kernels must be added to the pool in order to store this information.

2.7.6. ET

There are two forms of ephemeris time: Barycentric Dynamical Time (TDB) and Terrestrial Dynamical Time (TDT). Barycentric Dynamical Time is used when describing the motion of bodies with respect to the Solar System barycenter, while Terrestrial Dynamical Time is used when describing motions of objects near the Earth.

When ephemeris time is called by the Toolkit routines, TDB is the implied time system. This time is called Ephemeris Time (ET). Ephemeris time is given in terms of seconds past a reference epoch. The reference epoch used throughout the Toolkit is the epoch J2000 (roughly noon on January 1, 2000).

2.7.7. SCLK

Most spacecrafts have an on-board clock, that controls the times at which various actions are performed by the spacecraft and its science instruments. This clock is not a normal one, but rather a counter, which counts instants of time. The duration of each instant of time and how it is represented by the clock depends on the particular spacecraft. A spacecraft clock can be made up of several counters, each one increasing its value in steps of one when the previous one reaches its maximum value.

2.7.8. Reference frames

Several reference frames are built into the SPICE routine [31]:

- inertial frames such as J2000;
- body-fixed frames provided in text PCK files, such as the body-fixed rotating frame

and body-fixed frames based on high precision Earth rotation models.

All other frames are not built into SPICE. Instead, these frames have to be specified via a set of parameters in an FK kernel file. This is the case of the Svalbard and ESAC topocentric horizon frames, which are specified via the *estrack_ V04.tf*.

The main reference frame used in the calculations for the Solar System bodies is the J2000 reference frame. This is a cartesian frame with origin in the center of the Earth, whose +Z axis is perpendicular to the mean equatorial plane of the J2000 epoch and the +X axis contains the point where the Sun crosses the equatorial plane from South to North, also at the J2000 epoch. For instance, the J2000 reference frame is a inertial frame, because it is not attached to the rotating Earth [31].

The Earth body-fixed rotating frame used in this work is the International Terrestrial Reference Frame (ITRF), corresponding to a set of points with their three-dimensional Cartesian coordinates which realize an ideal reference system, the International Terrestrial Reference System (ITRS), as defined by the International Earth Rotation Service (IERS). The ITRS definition fulfills the following conditions:

- it is geocentric, which means that the center of mass is defined for the whole Earth, including oceans and atmosphere;
- the unit of length is the meter, using the SI system of measurement;
- its orientation was initially given by the Bureau International de l'Heure orientation at 1984;
- the time evolution of the orientation is ensured by using a no-net-rotation condition with regards to horizontal tectonic motions over the whole Earth.

The ITRS is realized by estimates of the coordinates and velocities of a set of Earth stations [17].

Currently only the ITRF93 frame is supported within SPICE. It is a high accuracy Earth rotation model, that takes into account:

- Precession, according to the 1976 IAU model due to Lieske;
- Nutation, as defined by the 1980 IAU model, with IERS corrections due to Herring;
- True sidereal time using accurate values of the difference between TAI and UT1;
- Polar motion.

High accuracy determination of surface locations relative to an inertial frame involves

motions in addition to Earth rotation, including tectonic plate motion, tidal effects and relativistic effects. This is provided by the *earth_latest_high_prec.bpc* kernel [21].

2.7.9. SPICE functions

Hereafter the list of the SPICE functions used inside the code is presented, along with their required inputs and outputs.

- *furnsh(file)*
  It loads one or more SPICE kernels into a program. *file* is the name of a SPICE kernel file, either binary or text. If the file is a binary SPICE kernel, it will be loaded into the appropriate SPICE subsystem. If *file* is a SPICE text kernel, it will be loaded into the kernel pool. If *file* is a SPICE meta-kernel containing initialization instructions, the files specified in those variables will be loaded into the appropriate SPICE subsystem: this is the case used inside the software.

- *getelm*
  getelm parses a Two-Line Element set and returns the orbital elements properly scaled and in units suitable for use by other SPICE functions. As input, it requires the year of earliest representable Two-line Elements; the length of strings in *lines* array and the pair of *lines* containing the Two-Line Elements, which should be the same as they are presented in the Two-Line Element files available.

  The outputs are:

  - The epoch of the elements in seconds past J2000;
  - The Two-Line Element data converted in SPICE units to be used in *ev2lin*:
    1 = XNDT2O in radians/minute^2
    2 = XNDD6O in radians/minute^3
    3 = BSTAR
    4 = XINCL in radians
    5 = XNODEO in radians
    6 = EO
    7 = OMEGAO in radians
    8 = XMO in radians
    9 = XNO in radians/minute
    10 = EPOCH of the elements in seconds past ephemeris epoch J2000.

- *ev2lin*
  ev2lin routine evaluates NORAD Two-Line Element data for near-Earth orbiting

spacecrafts (i.e. spacecraft with orbital periods less than 225 minutes, therefore using the SGP4 model, as explained in Section 2.4). The inputs are the array containing Two-Line Element data converted in SPICE units from *getelm*, the ephemeris seconds past J2000 at which a state should be produced from the input elements and the $CONSTS$ array.

The $CONSTS$ represents the constants needed inside the function:

$1.082616 * 10^{-3}$ = J2 gravitational harmonic for Earth [-]

$-2.53881 * 10^{-6}$ = J3 gravitational harmonic for Earth [-]

-1.65597*10^{-6} = J4 gravitational harmonic for Earth [-]

7.43669161*10^{-2} = Square root of the gravitational parameter for Earth which is expressed in Earth radii cubed per minutes squared

120 = Low altitude bound for atmospheric model in km

78 = High altitude bound for atmospheric model in km

6378.1363 = Equatorial radius of the Earth in km

1 = Distance units/Earth radius, which normally is equal to 1 [-]

The output is the state produced at the input epoch. Units are km and km/s.

- *pxform*
  $pxform$ returns the matrix that transforms position vectors from one specified frame to another at a specified epoch. In fact, it needs the original and final reference frames and the ephemeris seconds past J2000 at which the rotation matrix should be produced. The output is the required rotation matrix.

- *eul2m*
  This function constructs a rotation matrix from a set of Euler angles. The rotation angles about third, second and first rotation axes (in radians) and the corresponding axis numbers of third, second and first rotation axes are the inputs. They are, respectively, a set of three angles and three coordinate axis numbers; each pair angle and axis specify a coordinate transformation consisting of a rotation by the indicated angle about the indicated coordinate axis. The output is the rotation matrix representing the composition of the rotations defined by the input angle-axis pairs. That is the result of performing the rotations about the axes in the indicated order.

- *et2utc*
  et2utc function converts an input time from ephemeris seconds past J2000 to Calendar, Day-of-Year or Julian Date format, UTC. It requires the input epoch, in ephemeris seconds past J2000, the format of the output time string and the number of digits of precision to which fractional seconds (for Calendar and Day-of-Year formats) or days (for Julian Date format) are to be computed. As output, the time string equivalent to the input epoch, in the specified format, is provided.

  The format of the output time string may be any of the following:

  C Calendar format, UTC;

  D Day-of-Year format, UTC;

  J Julian Date format, UTC;

$ISOC$ ISO Calendar format, UTC;

$ISOD$ ISO Day-of-Year format, UTC;

- *utc2et*
  utc2et function converts an input time from Calendar or Julian Date format, UTC, to ephemeris seconds past J2000, providing the inverse transformation of *et2utc*. As input, it requires the input time string, containing a Calendar or Julian Date, UTC, while, as output, the time in ephemeris seconds past J2000 is computed.

- *recrad*
  It converts rectangular coordinates of a point to range, right ascension and declination: the range is the distance of the point from the origin in the same unit of the input; the right ascension and declination are computed in radians, whose ranges are 0 to 2π and $-\pi/2$ to $\pi/2$, respectively.

- *recgeo*
  recgeo converts from rectangular coordinates to geodetic coordinates. The inputs are the rectangular coordinates of a point in km, the equatorial radius of a reference spheroid, equal to 6378.1363 km for Earth and the flattening coefficient, equal to $3.352 * 10^{-3}$. As output, it provides the geodetic longitude in radians [-π, π], the geodetic latitude also in radians [$-\pi/2$, $\pi/2$] and the altitude of the input point above the reference spheroid in km.

- *kclear*
  The function unloads all kernels, clears the kernel pool and reinitializes the subsystem.

3 | XRPT implementation

The steps followed for the design of the model are presented in this chapter. First, a database of satellites in polar orbit with transmission frequency inside the X-band frequency range of SMOS is obtained. Then, the algorithm to retrieve the TLEs for each satellite inside the database is shown, with the main objective that the recovered set should be as near as possible to the considered time range. The TLE sources are also described along with their corresponding retrieval methodology. Moreover, the Main algorithm is presented, considering each step in the computation and the assumptions used inside the model. The two different models are then described in detail: the Past RFI model is used for the previous events, where it is possible to recover the real attitude of SMOS from the telemetry data, while the Prediction model assumes a constant attitude for SMOS and it is employed inside the X-band RFI Prediction Tool to predict possible future interference events. Moreover, other algorithms are presented in order to fulfill the software requirements: in particular, the computation of the visibility windows over a selected GS and the computation of a probability of a predicted event based on the Mahalanobis distance.

3.1. Database

The first step in the tool implementation consists in making a database of satellites with transmission frequency inside the X-band frequency band of SMOS. The database aim is to have a list of satellites, each to be checked during the algorithm loop.

Therefore, two different strategies have been employed: for commercial satellites, the Space Network List (SNL) of the ITU have been consulted, while for the military ones, the list has been retrieved from *n2yo.com*. Subsequently, for the military satellites, just the ones in polar orbit have been considered and added to the database, because their respective transmission frequencies are not available.

The Space Network List contains basic information concerning planned or existing space stations, Earth stations and radio astronomy stations. It includes sections on Advanced

Publication Information, coordination requests, notifications, plans information and their related processing backlog [7]. In particular, it is possible to search inside the SNL by frequency and position of the satellite. Different data can be inserted: frequency band in MHz, Emission or Reception or both services, Space or Earth station, Geostationary or Non-geostationary space station and Longitude range for the Geostationary ones. For the required search, the frequency band of SMOS (from 8141 MHz to 8159 MHz) has been used, with the choice of Non-geostationary space stations. From this list, the active satellites already in orbit have been selected.

The *n2yo.com* website has different categories, among these it has a list of all currently tracked military satellites: the ones in LEO have been retrieved.

Then, given that the ground station on which this work is focused is Svalbard, it mainly tracks satellites in LEO polar orbit, as explained in Section 1.2. Therefore, from the preliminary list, only the satellites in this kind of orbit have been considered: from each satellite's current TLE, the orbital inclination has been computed. A threshold of inclination equal to 90° has been set, hence only the satellites with higher inclination have been selected. However, the satellites in retrograde non-polar orbits have been discarded (e.g. the Israeli Ofeq family of reconnaissance satellites which have an inclination of 141°).

The final database list is reported in Table B.1, Table B.2, Table B.3, Table B.4 and Table B.5, with the satellite organization, its name and importantly its NORAD number, from which, in the next step of the algorithm, the TLEs can be recovered.

3.2. TLE retrieval

TLEs are employed in order to propagate the orbital states of SMOS and of the other satellites in the database. As previously presented in Section 2.4, different internet sources are taken into account in order to retrieve the TLE of the corresponding satellite. This retrieval is done with the aim of recovering the nearest available set to the considered date. In fact, *CelesTrak* and *n2yo.com* are used to retrieve the current TLEs, which are used for the computation of current day passes or future ones: in some cases, especially for military satellites, *CelesTrak* does not have their TLEs, so these are retrieved from *n2yo.com*. Instead, *SpaceTrack* is able to recover past TLEs, given the desired time range, so these sets are used for all past passes.

The software implementation of these retrievals consists in an API query for *CelesTrak* and *n2yo.com*, while the *spacetrack* Python module is used in order to recover the TLEs from SpaceTrack.

For *CelesTrak*, the queries take the following form [30]:

https://celestrak.com/NORAD/elements/gp.php?{QUERY}=VALUE[&FORMAT=VALUE]

where *{QUERY}* can be:

- CATNR: Catalog Number (1 to 9 digits). It allows return of data for a single catalog number.
- INTDES: International Designator. It allows return of data for all objects associated with a particular launch.
- GROUP: Groups of satellites provided on the *CelesTrak* Current Data page.
- NAME: Satellite Name. It allows searching for satellites by parts of their name.
- SPECIAL: Special data sets for the GEO Protected Zone (GPZ) or GPZ Plus.

While the allowed formats can be:

- TLE or 3LE: Three-line element sets.
- 2LE: Two-line element sets (with no name).
- XML: OMM XML format including all mandatory elements.
- KVN: OMM KVN format including all mandatory elements.
- JSON: OMM keywords for all TLE elements in JSON format.
- JSON-PRETTY: OMM keywords for all TLE elements in JSON pretty-print format.
- CSV: OMM keywords for all TLE elements in CSV format.

Inside the software, the *CATNR* is used in order to retrieve the TLE searching each satellite NORAD number, while the format is set to *TLE*.

For *n2yo.com*, the REST API v1 is used. For all request, the base URL is *https://api.n2yo.com/rest/v1/satellite/* and an API key must be appended at the end of the URL as *&apiKey={your API key}*. Then the TLEs are retrieved according to the NORAD number. The API request is presented as follows [11]:

https://api.n2yo.com/rest/v1/satellite/tle/{NORAD ID}&apiKey={your API key}

Regarding the *spacetrack* Python module, the queries consist in first choosing the time range (*drange*) in which to make the TLE search and then in retrieving the set (*data*) for the corresponding satellite (identified by its NORAD number) inside the selected range in the desired format [13]. The time range is chosen as two days starting from the date of

the pass to be simulated, because the TLEs are not updated daily. The command used inside the software are presented in the following:

$$drange = op.inclusive\_range(start\ time,\ end\ time)$$
$$data = st.tle(norad\_cat\_id,\ epoch{=}drange,\ orderby{=}'TLE\_LINE1',\ format{=}'tle')$$

Considering SMOS TLEs, beside the retrieval from internet, two other sources are employed in the algorithm, due to the XRPT requirements. The first one consists in recovering the TLEs from the *smos_tle.txt* file present inside the FTP server: this file contains a set of SMOS TLE, which is updated once per week, on Monday morning, so it should only be used when computing passes near the current week. The second source consists in a local file present inside the software: this text file contains all SMOS available TLEs from the launch up to the last update. In fact, this file is automatically updated every time the software is run and is able to retrieve the latest available sets which are not already been saved. Moreover, according to the pass which is currently simulated, the nearest TLE set is retrieved automatically; in the case the simulated pass is beyond the latest available TLE set, this set is retrieved by the software and used in the computation.

Therefore, the user has three different options, when selecting the source from which SMOS TLE are retrieved, while for all other satellites the corresponding sets are recovered from internet. However, it is possible that, given the selected time range, the TLEs are not available. In the case of SMOS, this would stop the computation, hence the user should select another source. While, if any of the satellites in the database list does not have available TLEs, it is passed. For example, this can happen because for the considered time range, the satellite has not been launched yet.

The complete algorithm employed to retrieve the TLE for each satellite is presented in Algorithm 3.1.

Algorithm 3.1 TLE Retrieve Algorithm

```
Retrieve list of satellite, pass date and selected TLE source
if satellite is SMOS then
    if TLE source = FTP server then
        Retrieve smos_tle.txt file from FTP server and retrieve TLE
    else if TLE source = local file then
        if pass date ≤ latest available TLE date then
            Retrieve TLE from corresponding date
        else
            Retrieve latest available TLE
        else if TLE source = internet then
            if date ≥ today then
                Retrieve TLE from CelesTrak
                if TLE from CelesTrak is not available then
                    Retrieve TLE from n2yo.com
                end if
            else
                Retrieve TLE from SpaceTrack
            end if
        end if
    end if
    if TLE is not available then
        Break: cannot compute this pass
    end if
else
    for each satellite in the list do
        if date ≥ today then
            Retrieve TLE from CelesTrak
            if TLE from CelesTrak is not available then
                Retrieve TLE from n2yo.com
            end if
        else
            Retrieve TLE from SpaceTrack
        end if
        if TLE is not available then
            Skip this satellite
        end if
    end for
end if
```

3.3. Model implementation

The main algorithm used for the Past RFI and the Prediction models is described in Algorithm 3.2. However, some differences in the input selection are present: for the Past RFI model, the variables to select are the number of timesteps for the orbital propagation and the angular range. The ground station is already known due to the report of the event, like the AOS and LOS times, while the only TLE source that can be chosen is *SpaceTrack* in order to retrieve the nearest past available set. Moreover, during the identification of the responsible satellite, all spacecrafts inside the Database are considered for the simulation. While, for the Prediction model and therefore the XRPT, the user has to select all the needed variables to run the simulation: these consist in the selection of the ground station between the one in Svalbard and the one located at ESAC, in the selection of the TLE source among internet, FTP server and local file as explained previously, the time (choosing among current week, week number or time period), the Database (selecting among Previous RFI, Commercial, Military or All), the number of timesteps and the angular range. A more detailed description of the variables and of the user interface is presented in Section 4.6.

First, the SPICE kernels are loaded with the *furnsh* function. The algorithm simulates each pass: this could be the unique pass to be investigated for the Past RFI model or the many passes over the selected GS during a planning week for the Prediction model. It repeats the procedure for each satellite inside the selected database. For each spacecraft, it searches and retrieves its TLE through Algorithm 3.1: if the TLEs are not available, the satellite is skipped and an information will be passed to the output display to inform the user; if SMOS does not have any available set, the simulation is stopped with a warning. After the retrieval of the TLEs, they are converted to elements readable by SPICE thanks to the *getelm* function, then the state at the first timestep is computed with *ev2lin*: here only the satellites in the northern hemisphere are considered in order to fasten the simulation, hence there is an *if* condition on the Y component of the position vector.

Then, only for the satellites that meet the previous condition, the state is propagated in the *J2000* frame with *ev2lin* function for each timestep, along with the GS position; then the position with respect to the GS is obtained thanks to the difference between the spacecraft position vector and the GS position vector. This vector is rotated into the GS topocentric horizon reference frame with the rotation matrix computed by *pxform* and provided by the *estrack_V04.tf* and *estrack_V04.bsp* kernels; then the declination and azimuth with respect to the station are computed. For each timestep, the declination is

checked: only when the satellite is visible from the selected GS (assuming a value larger than 0°), the computation will continue.

Therefore, the rotation matrix between inertial to body frames is computed, according to Algorithm 3.3 for the Past RFI model or to Algorithm 3.4 for the Prediction model. Here a distinction is made: for SMOS, the direction between the spacecraft and the GS, which corresponds to the negative of the position vector, is rotated into SMOS body frame and the angle between this direction and the main direction of the X-band antenna (which corresponds to the Z direction, as indicated in Section 1.1) is computed: this is repeated for each timestep and these values, along with the ones of the position vector, declination and azimuth are saved. While, for all other satellites, the direction between the spacecraft and SMOS is computed as the difference between the satellite position vector and SMOS position vector, with respect to the GS. This is then rotated into SMOS body frame, where the angle between this direction and the main direction of the X-band antenna is computed. This is done in order to perform a check if both the GS and the satellite are within the field of view of the X-band antenna, which ranges from -65° to +65°: hence the angles previously computed are checked if they are both below 65° at the same timestep. This means that an interference could happen and the angular distance between SMOS and the satellite with respect to the station is computed: if it is inside the selected angular range, the parameters related to the current timestep are saved. If this condition is verified for more than one timestep, the values associated to this satellite conjunction are saved.

In this case, all the parameters related to the events are saved for the output file: they include satellite name, start and end times, duration, elevation and azimuth at maximum interference, number of packets lost (computed thanks to Equation (4.1)), minimum angular distance in degree and the time at which occurs and the probability (only for the Prediction model). In fact, then the computation of the Mahalanobis distance and of the p-value is performed, according to Algorithm 3.6.

Algorithm 3.2 Main Algorithm

```
Retrieve selected variables, retrieve satellite list from Database, load SPICE kernels.
for Each pass do
  for Each satellite in list do
    Retrieve TLE through Algorithm 3.1, get elements readable by SPICE, get state at first timestep
    if Y component of the position vector at first timestep > 0 then
      for Each timestep do
        Compute state and GS position in inertial frame, compute position with respect to the GS and rotate it in the GS topocentric horizon reference frame, compute declination and azimuth with respect to the GS
        if Declination at current timestep > 0 then
          Compute rotation matrix from inertial to body frame (Algorithm 3.3 or 3.4)
          if Satellite is SMOS then
            Compute GS - SMOS direction and rotated it into SMOS body frame, compute angle between antenna main direction and the latter direction (called angle_SMOS_GS), save values associated to SMOS
          else
            Compute satellite - SMOS direction and rotated it into SMOS body frame, compute angle between antenna main direction and the latter direction (called angle_SMOS_satellite)
            if both angle_SMOS_GS and angle_SMOS_satellite < 65° then
              Compute angle between SMOS and satellite with respect to the GS
              if angular distance is inside selected angular range then
                Save parameters related to current timestep
              end if
            end if
          end if
        end if
      end for
      if Number of timesteps for which the previous condition is verified is > 1 then
        Save all values related to this satellite conjunction
      end if
    end if
  end for
end for
```

3.4. Past RFI model

The Past RFI model deals with all events that have already happened, therefore the real attitude experienced by SMOS can be recovered through the down linked telemetry. This is done thanks to Algorithm 3.3, which is based on the quaternions available from the telemetry. After retrieving SMOS state, the orbital elements are computed through Algorithm 2.1, from which then the inertial to LVLH rotation matrix is computed, according to Equation (2.8). Instead from the quaternions, SMOS body direction cosines matrix can be obtained through Equation (2.6), introducing an orthonormalization step to preserve its structure and taking into account the particular body frame associated to SMOS, as described in Section 1.1. Finally, by multiplying the two matrices, the final inertial to body frame rotation matrix is computed. This is the matrix used inside Algorithm 3.2.

Algorithm 3.3 SMOS Real Attitude Retrieval Algorithm

1: Retrieve quaternions from the telemetry
2: Retrieve state at current timestep
3: From state compute keplerian elements through Algorithm 2.1
4: Compute inertial to LVLH frame rotation matrix by multiplying the three rotation matrices
5: From quaternions compute SMOS body matrix, orthonormalize the matrix
6: Compute inertial to body frame rotation matrix by multiplying the inertial to LVLH and the body rotation matrices, orthonormalize the matrix.

3.5. Prediction model

Regarding the attitude retrieval of SMOS used inside the Prediction model, the same steps presented in Algorithm 3.3 are employed. However, the attitude of SMOS cannot be recovered from the real quaternions given the fact that they are not available for future passes. Nevertheless, it is possible to exploit the fact that SMOS maintains a constant flight attitude, as explained in Section 1.1. Therefore, this feature is used inside the algorithm in order to compute the body rotation matrix: the direction cosine matrix is computed through Equation (2.7), imposing a Euler angle equal to the 32.5° forward tilt angle and the others as 0°. Finally, the inertial to body frame rotation matrix is computed, by multiplying the two matrices previously obtained.

However, given the fact that for the Prediction model a constant attitude is used, which differs from the real attitude experienced by SMOS due to attitude perturbations, the output results could be different from the ones obtained with the Past RFI model: this

should be taken into account when running the XRPT and therefore a larger angular range should be selected. Moreover, this is also discussed in Section 4.3.

Algorithm 3.4 SMOS Constant Attitude Retrieval Algorithm

1: Retrieve state at current timestep
2: From state compute keplerian elements through Algorithm 2.1
3: Compute inertial to LVLH frame rotation matrix by multiplying the three rotation matrices
4: Compute Euler angles imposing constant attitude, then compute SMOS body rotation matrix
5: Compute inertial to body frame rotation matrix by multiplying the inertial to LVLH and the body rotation matrices, orthonormalize the matrix.

For the Prediction model, the passes to be simulated are retrieved from the FOS planning week: each week, one week in advance, FOS makes the scheduling; in particular, the X-band passes with respect to either Svalbard or ESAC are computed. These passes are retrieved by the software and their corresponding AOS and LOS are used inside the model.

However, according to the XRPT requirements, the tool shall be able to retrieve the visibility windows of SMOS with respect to the selected ground station, when a selected time period is inserted. This is accomplished through Algorithm 3.5. It consists in first retrieving the selected variables and checking if SMOS TLEs are available for the selected time range thanks to Algorithm 3.1. If a set is present, it is converted to SPICE elements, from which SMOS orbital states are obtained for each timestep thanks to the *ev2lin* function and subsequently the corresponding declination values are computed. A inferior threshold is imposed: SMOS is considered visible from the GS when its declination is above 5°. However, the output of this algorithm should be the list of passes, hence the list of all the AOS and LOS times inside the selected time range, to be used inside the Main Algorithm. Therefore, an additional *if* cycle has to be performed: a timestep is considered AOS if at the current step SMOS is visible but at the previous one its declination is lower than 5°; also the first overall timestep can be AOS if it has a declination larger or equal to 5°. While, a timestep is LOS if it is above the visibility limit, but the following one is not. The last timestep can be a LOS if its declination is above 5°. The results of this algorithm have been validated, comparing them with the FOS planning week: a good accordance has been found.

Algorithm 3.5 SMOS GS Visibility Windows Retrieval Algorithm

```
Retrieve start and end times, retrieve TLE source, retrieve selected GS
Retrieve SMOS TLE with Algorithm 3.1
if TLE is available then
    Get elements readable by SPICE
    for Each timestep do
        Compute declination of SMOS with respect to the selected GS
        if Declination at current timestep ≥ 5° then
            SMOS is visible from the GS
            if Declination at previous timestep < 5° then
                Current timestep corresponds to AOS
            else if Current timestep is the first timestep then
                Current timestep corresponds to AOS
            else if Declination at next timestep < 5° then
                Current timestep corresponds to LOS
            else if Current timestep is the last timestep then
                Current timestep corresponds to LOS
            end if
        end if
    end for
end if
Collect all AOS and LOS times
```

In order to compute the probability of a predicted event to generate an interference, the Mahalanobis distance of the current prediction with respect to the dataset of the corresponding family is computed. These data come from the previously confirmed RFIs and correspond to the time of the day at which the RFI happened, the minimum angular distance and the elevation and azimuth values at maximum interference. Subsequently, from the Mahalanobis distance, it is possible to apply the χ square test to compute the probability value of the new event. A typical threshold of 0.001 is considered in order to understand if the predicted event is statistically significant: if the p-value is lower than the imposed threshold, the event is considered as an outlier with respect to the available data set, therefore a *Low* probability is assigned; otherwise a *High* probability is considered.

However, in order to get meaningful results, a number of past RFIs larger than 3 is required. Therefore, for the families or for the satellites with a small amount of previous confirmed events, the covariance matrix is computed from the complete data set, where the

values have been normalized with respect to the mean of the corresponding parameter of the respective family. This covariance matrix is then used with the normalized parameters of the current prediction. Instead, if a satellite has not been responsible for past RFIs, a probability cannot be assigned.

Algorithm 3.6 Mahalanobis Distance and p-value Computation Algorithm

```
Retrieve current prediction parameters
Retrieve corresponding satellite or family data of previous confirmed events
if Past events are more than 3 then
    Compute Mahalanobis distance and then the p-value
    if p-value ≥ 0.001 then
        Probability is High
    else
        Probability is Low
    end if
else if Past events are less than 3 then
    Normalize current prediction data with respect to the mean values of the corresponding satellite or family
    Compute covariance matrix from all data normalized with respect to the mean values of the corresponding family
    Compute Mahalanobis distance of this normalized data and then the p-value
    if p-value ≥ 0.001 then
        Probability is High
    else
        Probability is Low
    end if
else if No past events then
    Probability cannot be computed
end if
```

4 | XRPT validation and results

In this chapter, the results of the validation process of the model used inside the X-band RFI Prediction Tool is presented. The validation is performed first analysing the previous events and then the new events reported during the course of this work. Subsequently, an identification of patterns inside the results has been made, leading to a statistical analysis of the collected data. Moreover, the final version of the software is shown, along with the user interface description and the requirements' fulfillment.

4.1. Past RFI model results

After the implementation of the model, it must be validated before being used inside the software. The validation has been conducted running the model for each of the previous events, reported in Table A.1, Table A.2 and Table A.3. Given that these are past cases, the real attitude is available, therefore the model with the real attitude is used: the quaternions have been recovered from the spacecraft telemetry for each event.

The satellites that the model initially predicts to be the responsible are presented in Table 4.1. While the complete results are shown in Table 4.3 and Table 4.4. These tables describe the main parameters for each of the predicted RFI: its start and end times, its duration in seconds, its position, the values of elevation and azimuth with respect to the Svalbard GS at minimum angular separation, the estimated packets lost and the minimum angular distance in degree and the time at which it occurs.

The position parameter represents the location of SMOS during the corresponding visibility window: a distinction between the ascending phase (i.e. the minimum angular distance is reached before the elevation maximum value) and descending phase (i.e. it is reached after the time of maximum elevation).

The estimated duration and the number of packets lost are linked through the X-band antenna datarate: in fact, it is possible to reconstruct the number of packets lost from the duration and vice versa with the following formula:

$$Duration = \frac{Packets \cdot 476}{\frac{16.8}{8 \cdot 10^6}} \tag{4.1}$$

where 476 Bytes represents the CCSDS standard packet size, 16.8 Mbps (Megabit per second) is the useful downlink datarate and $8 \cdot 10^6$ transforms the Mbps in Bps (Byte per second). This formula can be also applied to the reported events in order to compute its estimated duration: this is shown in Table 4.2.

As it can be noted from the results in Table 4.1, there are some events that do not have any predicted satellite: this could be due to the fact that the real responsible satellite is not in the database or more probably that these events are not associated with a RFI due to aN adjacent satellite, but due to other reasons (e.g. GS problems, tracking problems, etc). While, in other cases, two or more satellites are predicted to be responsible for an event: for *event 15*, it is not possible to identify the real guilty satellite due to the lack of other data or of patterns related to the same spacecrafts. In the other cases, the time at which the RFI happened is reported, therefore it is possible to find the responsible satellite comparing the reported timing with the complete results:

- Event 19: for this event, the RFI has been reported to have happened at 13:55:46 UTC, which is consistent with the computed time of minimum angular separation, which is 13:55:45.75 UTC. So the responsible satellite is SUPERVIEW-1 03.
- Event 28: ICESAT-2 is predicted to have a maximum interference at 23:09:05.31 UTC, which is consistent with the reported time of 23:09:05 UTC. While COSMO SKYMED-2 has a minimum angular distance predicted at 23:09:07.62, which is not consistent. Moreover, the computed minimum angular distance of ICESAT-2 is close to 0°, while the one of COSMO SKYMED-2 is large, confirming ICESAT-2 as the responsible satellite.
- Event 29: in this case, the duration of the RFI is known; it happened between 23:02:22 and 23:02:57. The predicted duration for COSMO SKYMED-1 is between 23:02:20 and 23:02:55, which is consistent to the reported one, so this satellite is considered to be the real responsible.
- Event 30: this reported RFI happened at 13:31:35 UTC, which is consistent with the values predicted for SUPERVIEW-1 04, while the other predicted satellites have timings which are not coherent with the reported time.

Moreover, even if data about these events were not available, a reasoning concerning

the patterns associated to these satellites could lead to the identification of the most probable satellite responsible for the corresponding event: this is investigated in detail in Section 4.4. Furthermore, three cases (*event 10*, *event 14* and *event 17*) are highlighted due to the fact that the prediction of the model does not seem to fit with the available data. In fact, for these first two cases, comparing the predicted duration with the estimated one, it can be noted that there is a very large difference: this means that it is highly probable that these satellites are not the responsible ones; while for *event 17*, the reported (01:22:44 UTC) and the predicted times (minimum angular distance at 01:32:31 UTC) do not coincide, therefore, also in this case, GAOFEN 2 should probably not be the real responsible.

Furthermore, an additional check between the reported and the predicted values can be performed in order to confirm the predicted responsible satellites:

- Event 16: RFI is reported in the time frame between 13:40:10 and 13:40:18 UTC; the simulated duration is from 13:40:11 to 13:40:16, which is consistent with the reported values.
- Event 18: the model predicts a minimum angular distance at 23:27:08 UTC, which is very close to the reported time of 23:27:07 UTC.
- Event 22: RFI reported at 23:14:46 UTC, while the model has a very similar results with maximum interference at 23:14:48.
- Event 23: KSAT identified a RFI between 14:22:18 and 14:22:28 UTC; the model correctly predicts the duration inside this time frame, between 14:22:16 and 14:22:20 UTC.
- Event 25: RFI maximum interference reported at 20:11:12 UTC, which is very similar to the minimum angular distance computed by the model at 20:11:11 UTC.
- Event 31: KSAT registered an RFI with COSMO SKYMED-1 at approximately 22:50:20 UTC; the model identifies the same responsible satellite with RFI start time at 22:50:19 UTC.
- Event 32: RFI reported at 22:44:20 UTC; the model predicts a maximum interference at 22:40:22 UTC.
- Event 33: RFI registered at around 22:38:35 UTC, similar to the model prediction of 22:38:37 UTC.
- Event 34: RFI reported at 09:06:43 UTC, which is the same time of minimum angular separation computed by the model.

- Event 37: the event started at 09:21:16 UTC; the model correctly identifies an RFI between 09:21:16 and 09:21:18 UTC.
- Event 38: RFI registered at 08:49 UTC; coherently the model predicts an event between 08:49:05 and 08:49:12 UTC.
- Event 39: RFI happened at 13:14:11 UTC; similarly the predicted duration is between 13:14:10 and 13:14:15 UTC.
- Event 40: Interference at 08:01:52 UTC, which is coincident with the computed time of minimum angular distance of 08:01:52 UTC.
- Event 42: RFI caused spike in signal at 22:56:07 UTC, same time at which the model predicts the minimum separation between the two satellites.
- Event 44: RFI with SUPERVIEW-1 03, with maximum interference at 13:48:33 UTC; coherently the model identifies the same spacecraft and the same time of minimum angular separation.
- Event 45: Around 12:52:55 UTC there is a strong RFI for around 4 seconds; the model predicts a RFI which start at 12:52:55 and last for 4 seconds up to 12:52:59 UTC.

Moreover, a further analysis has been conducted for each event in order to find the angular limit such that the estimated duration and the predicted one are close to each other: an iterative process has been performed changing the angle in order to match the duration values. The results, considering only the confirmed satellites, are presented in Table 4.5. In fact, the complete results shown in Table 4.3 and Table 4.4 are obtained running the model with the angle found in these computations.

Event	Predicted satellite
1	COSMO SKYMED-2
2	COSMO SKYMED-4
3	-
4	COSMO SKYMED-1
5	KOMPSAT-3
6	-
7	COSMO SKYMED-1
8	-
9	-
10	GAOFEN 2
11	-
12	-
13	-
14	JILIN-01-04
15	ICESAT-2 AQUA
16	SUPERVIEW-1 04
17	GAOFEN 1-02
18	COSMO SKYMED-4
19	SUPERVIEW-1 03 HANGJING 1A
20	SUPERVIEW-1 01
21	SUPERVIEW-1 01
22	COSMO SKYMED-4
23	SUPERVIEW-1 01
24	KOMPSAT-3

Event	Predicted satellite
25	GRUS-1A
26	SUPERVIEW-1 01
27	GRUS-1A
28	COSMO SKYMED-2 ICESAT-2
29	COSMO SKYMED-1 GAOFEN 1-02
30	SUPERVIEW-1 04 COSMO SKYMED-4 JILIN-01 GAOFEN 3F
31	COSMO SKYMED-1
32	COSMO SKYMED-2
33	COSMO SKYMED-1
34	KOMPSAT-3A
35	KOMPSAT-3
36	SUPERVIEW-1 03
37	KOMPSAT-3A
38	GRUS-1A
39	SUPERVIEW-1 04
40	KOMPSAT-3
41	COSMO SKYMED-2
42	GRUS-1E
43	GRUS-1B
44	SUPERVIEW-1 03
45	SUPERVIEW-1 03

Table 4.1: Satellites predicted for previous events

Event	Packets	Duration [s]
1	32715	7.4154
2	53000	12.0133
3	4141	0.9386
4	160288	36.3319
5	984	0.2230
6	9638	2.1846
7	14846	3.3651
8	8504	1.9276
9	151124	34.2548
10	220681	50.0210
11	144281	32.7037
12	24597	5.5753
13	312069	70.7356
14	402430	91.2175
15	7488	1.6973
16	19508	4.4218
17	15704	3.5596
18	142803	32.3687
19	18533	4.2008
20	23395	5.3029
21	33522	7.5983
22	131963	29.9116
23	18276	4.1426
24	10390	2.3551
25	20875	4.7317
26	21036	4.7683
27	14688	3.3294
28	16064	3.6412
29	152524	34.5721
30	14837	3.3631
31	42372	9.6043
32	46348	10.5055
33	124491	28.2178
34	22848	5.1789
35	15904	3.6049
36	18332	4.1553
37	8303	1.8820
38	31170	7.0652
39	20564	4.6612
40	17256	3.9114
41	719546	163.0971
42	11572	2.6223
43	10654	2.4149
44	18116	4.1063
45	16783	3.8041

Table 4.2: Previous events estimated duration

Event	Satellite	Start time	End time	Duration [s]	Position	Elevation [deg]*	Azimuth [deg]*	Packets lost	Minimum angular distance [deg]	Time*
1	COSMO SKYMED-2	2013-03-08T00:44:16	2013-03-08T00:44:34	18.492585058964597	Ascending	11,43914235	109,2464133	81584,93408	0,272071674	2013-03-08T00:44:25.37
2	COSMO SKYMED-4	2015-08-20T23:28:38	2015-08-20T23:28:55	17.171689788765555	Ascending	13,3804939	85,56841329	75757,45495	0,439940325	2015-08-20T23:28:46.65
4	COSMO SKYMED-1	2016-06-18T23:33:44	2016-06-18T23:34:21	36.424843216037814	Ascending	15,64587749	86,2121225	160697,8377	0,364160039	2016-06-18T23:34:04.19
5	KOMPSAT-3	2016-11-21T00:42:08	2016-11-21T00:42:10	1.056719146306074	Ascending	37,60560253	97,24995193	4661,996234	0,704706709	2016-11-21T00:42:08.99
7	COSMO SKYMED-1	2017-07-01T23:20:01	2017-07-01T23:20:06	5.203549030067286	Ascending	13,89473029	83,09354089	22956,83396	0,341010245	2017-07-01T23:20:03.57
10	GAOFEN 2	2018-02-25T01:44:08	2018-02-25T01:44:24	15.850667116083727	Descending	8,26177188	311,6092969	69929,41375	0,91108758	2018-02-25T01:44:16.36
14	JILIN-01-04	2018-04-25T03:26:51	2018-04-25T03:27:11	20.2940753812071	Descending	5,087062209	326,3017724	89532,68551	0,520936725	2018-04-25T03:27:01.48
15	ICESAT-2	2018-09-22T07:40:41	2018-09-22T07:40:43	1.6331127416777405	Ascending	11,06283348	279,4395461	7204,909154	0,119041301	2018-09-22T07:40:41.74
15	AQUA	2018-09-22T07:42:14	2018-09-22T07:42:16	2.449669112516611	Ascending	13,93407212	297,9001536	10807,36373	0,07566893	2018-09-22T07:42:14.83
16	SUPERVIEW-1 04	2019-01-04T13:40:11	2019-01-04T13:40:16	4.843280188316818	Descending	11,56366843	48,4968333	21367,4126	0,189954175	2019-01-04T13:40:13.59
17	GAOFEN 1-02	2019-01-15T01:32:28	2019-01-15T01:32:32	3.9786384271891455	Descending	7,14833619	309,7932795	17552,81659	0,05912645	2019-01-15T01:32:30.74
18	COSMO SKYMED-4	2019-02-04T23:26:51	2019-02-04T23:27:23	32.67176118463258	Ascending	17,8264462	83,48130764	144140,1229	0,355365144	2019-02-04T23:27:08.85
19	SUPERVIEW-1 03	2019-02-06T13:55:44	2019-02-06T13:55:48	4.2508759185264235	Descending	12,48343559	49,95077004	18753,86435	0,05248838	2019-02-06T13:55:45.75
19	HUANJING 1A	2019-02-06T13:57:13	2019-02-06T13:57:18	4.7231954650293595	Descending	10,72076447	67,71346569	20837,62705	0,159551467	2019-02-06T13:57:15.49
20	SUPERVIEW-1 01	2019-02-23T12:53:51	2019-02-23T12:53:56	5.60381054162502	Descending	9,045290167	41,05206434	24722,69357	0,098489977	2019-02-23T12:53:53.43
21	SUPERVIEW-1 01	2019-02-27T13:38:01	2019-02-27T13:38:09	7.925331556614117	Descending	11,43413263	45,77851348	34964,69804	0,262289947	2019-02-27T13:38:05.91
22	COSMO SKYMED-4	2019-03-02T23:14:31	2019-03-02T23:15:02	30.692893932309445	Ascending	15,32404895	81,45325999	135409,8262	0,094177547	2019-03-02T23:14:48.10
23	SUPERVIEW-1 01	2019-03-03T14:22:16	2019-03-03T14:22:20	4.250941962063353	Descending	14,24996861	50,30023313	18754,15571	0,373684261	2019-03-03T14:22:18.21
24	KOMPSAT-3	2019-11-19T08:16:50	2019-11-19T08:16:52	2.401634423712081	Ascending	11,54278104	305,1369459	10595,44599	0,036373754	2019-11-19T08:16:50.57
25	GRUS-1A	2020-02-14T20:11:09	2020-02-14T20:11:14	5.187584390474845	Ascending	13,13649468	47,25737012	22886,40172	0,213631204	2020-02-14T20:11:11.23
26	SUPERVIEW-1 01	2020-05-26T12:26:13	2020-05-26T12:26:18	4.803346229919677	Descending	7,782474613	37,93307652	21191,23337	0,457242791	2020-05-26T12:26:15.66
27	GRUS-1A	2020-06-06T21:53:34	2020-06-06T21:53:38	3.4102014666640654	Ascending	23,71762614	59,12804065	15045,00647	0,120694411	2020-06-06T21:53:35.93

* computed at minimum angular distance

Table 4.3: Results for previous events - Part 1

Event	Satellite	Start time	End time	Duration [s]	Position	Elevation [deg]*	Azimuth [deg]*	Packets lost	Minimum angular distance [deg]	Time*
28	COSMO SKYMED-2	2020-10-31T23:09:02	2020-10-31T23:09:12	9.798747835197474	Ascending	16.588336516886955	78.64445552421483	43229.7698611653	0.6350331070420786	2020-10-31T23:09:07.62
28	ICESAT-2	2020-10-31T23:09:03	2020-10-31T23:09:07	4.034778520375431	Ascending	16.32210083	78.76556149	17800.49347	0.044540638	2020-10-31T23:09:05.31
29	COSMO SKYMED-1	2020-11-13T23:02:20	2020-11-13T23:02:55	35.159887269938781	Ascending	12.86974874	78.82231698	155117.1497	0.036479535	2020-11-13T23:02:38.97
29	GAOFEN 1-02	2020-11-13T23:10:43	2020-11-13T23:10:45	1.729174783743841	Descending	18.82528807	286.8231091	7628.712281	0.015473968	2020-11-13T23:10:44.30
30	SUPERVIEW-1 04	2020-11-15T13:31:35	2020-11-15T13:31:38	3.586444297418925	Descending	11.25780145	45.99813248	15822.54837	0.23529758	2020-11-15T13:31:36.38
30	COSMO SKYMED-4	2020-11-15T13:33:53	2020-11-15T13:34:29	35.416137437012245	Descending	7.040395544	73.17005643	156247.6652	0.316154564	2020-11-15T13:34:10.15
30	JILIN-01 GAOFEN 3F	2020-11-15T13:33:05	2020-11-15T13:33:09	3.586444297418925	Descending	9.3257728l4	62.98722651	15822.54837	0.139312735	2020-11-15T13:33:06.94
31	COSMO SKYMED-1	2020-12-09T22:50:19	2020-12-09T22:50:28	9.094169948740567	Ascending	11.03901848	76.76318567	40121.3358	0.253342462	2020-12-09T22:50:23.92
32	COSMO SKYMED-2	2020-12-22T22:44:15	2020-12-22T22:44:29	13.449158110564515	Ascending	11.05388426	75.40084905	59334.52108	0.194975627	2020-12-22T22:44:22.04
33	COSMO SKYMED-1	2021-01-04T22:38:21	2021-01-04T22:38:50	29.139807881475533	Ascending	12.92644237	73.36106829	128557.9759	0.254692193	2021-01-04T22:38:36.99
34	KOMPSAT-3A	2021-01-30T09:06:41	2021-01-30T09:06:46	5.2836024024790333	Ascending	8.62874761	314.1440454	23310.0106	0.350428471	2021-01-30T09:06:43.30
35	KOMPSAT-3	2021-03-14T07:53:02	2021-03-14T07:53:06	3.90665777197002	Ascending	12.90521864	301.324013	17235.25488	0.034311789	2021-03-14T07:53:03.93
36	SUPERVIEW-1 03	2021-03-18T13:43:33	2021-03-18T13:43:38	4.402995331435302	Descending	11.67037943	47.69984133	19424.9794	0.064478346	2021-03-18T13:43:35.66
37	KOMPSAT-3A	2021-04-09T09:21:16	2021-04-09T09:21:18	1.729176784328705	Ascending	7.7672225523	315.5498401	7628.721108	0.3329572	2021-04-09T09:21:17.19
38	GRUS-1A	2021-04-15T08:49:05	2021-04-15T08:49:12	7.485103402160024	Descending	10.27149285	326.8402199	33022.51501	0.362759131	2021-04-15T08:49:08.44
39	SUPERVIEW-1 04	2021-05-04T13:14:10	2021-05-04T13:14:15	4.803272181148923	Descending	9.98155028 7	44.69085222	21190.90668	0.122299321	2021-05-04T13:14:12.45
40	KOMPSAT-3	2021-05-17T08:01:50	2021-05-17T08:01:54	3.842556370664549 4	Ascending	12.38705803	303.0775493	16952.45458	0.077355002	2021-05-17T08:01:52.03
41	COSMO SKYMED-2	2021-06-29T23:25:05	2021-06-29T23:27:49	164.26266438210305	Ascending	15.86939632	83.91653943	724688.2252	0.011426204	2021-06-29T23:26:58.57
42	GRUS-1E	2021-07-05T22:56:06	2021-07-05T22:56:09	2.441694462514067	Ascending	37.01649547	62.13024811	10772.18145	0.17711668	2021-07-05T22:56:07.70
43	GRUS-1B	2021-07-16T20:47:36	2021-07-16T20:47:39	2.441661106578677	Ascending	17.08071727	51.08028906	10772.03429	0.423330373	2021-07-16T20:47:37.55
44	SUPERVIEW-1 03	2021-09-06T13:48:32	2021-09-06T13:48:36	4.034749832449156	Descending	12.32497371	48.6699155	17800.36691	0.191133366	2021-09-06T13:48:33.77
45	SUPERVIEW-1 03	2021-09-10T12:52:55	2021-09-10T12:52:59	4.002721813855925	Descending	9.141902973	42.40665904	17659.06683	0.359354629	2021-09-10T12:52:57.15

* computed at minimum angular distance

Table 4.4: Results for previous events - Part 2

Event	Satellite	Angle [deg]
1	COSMO SKYMED-2	0.3
2	COSMO SKYMED-4	0.475
4	COSMO SKYMED-1	0.575
5	KOMPSAT-3	0.775
7	COSMO SKYMED-1	0.35
15	ICESAT-2	0.4
	AQUA	0.3
16	SUPERVIEW-1 04	0.7
18	COSMO SKYMED-4	0.6
19	SUPERVIEW-1 03	0.7
20	SUPERVIEW-1 01	0.675
21	SUPERVIEW-1 01	1.1
22	COSMO SKYMED-4	0.425
23	SUPERVIEW-1 01	0.8
24	KOMPSAT-3	0.35
25	GRUS-1A	0.725
26	SUPERVIEW-1 01	0.675
27	GRUS-1A	0.725

Event	Satellite	Angle [deg]
28	ICESAT-2	0.45
29	COSMO SKYMED-1	0.425
30	SUPERVIEW-1 04	0.55
31	COSMO SKYMED-1	0.275
32	COSMO SKYMED-2	0.25
33	COSMO SKYMED-1	0.425
34	KOMPSAT-3A	0.725
35	KOMPSAT-3	0.575
36	SUPERVIEW-1 03	0.65
37	KOMPSAT-3A	0.4
38	GRUS-1A	0.725
39	SUPERVIEW-1 04	0.625
40	KOMPSAT-3	0.6
41	COSMO SKYMED-2	1.9
42	GRUS-1E	0.75
43	GRUS-1B	0.6
44	SUPERVIEW-1 03	0.65
45	SUPERVIEW-1 03	0.625

Table 4.5: Angle estimation for correctly predicted previous events

Table 4.6 shows the list of satellites responsible for previous RFIs, along with the other spacecrafts which are part of the same family: inside the Database, this list is highlighted (as Previous RFI) in order to ease and fasten the computation of the prediction model; in fact, knowing this list, the user is able to select just these satellites to be analysed for possible RFIs, instead of all the satellites inside the Database.

Organization	Name	NORAD number
I	COSMO SKYMED-1	31598
I	COSMO SKYMED-2	32376
I	COSMO SKYMED-3	33412
I	COSMO SKYMED-4	37216
J	GRUS-1A	43890
J	GRUS-1C	47933
J	GRUS-1B	47934
J	GRUS-1E	47935
J	GRUS-1D	47936
KOR	KOMPSAT-3	38338
KOR	KOMPSAT-3A	40536
CHN	SUPERVIEW-1 01	41907
CHN	SUPERVIEW-1 02	41908
CHN	SUPERVIEW-1 03	43099
CHN	SUPERVIEW-1 04	43100
USA	ICESAT-2	43613
USA	AQUA	27424

Table 4.6: List of satellites responsible for past RFI

4.2. List of responsible satellites

In this section, the sets of satellites reported in Table 4.6 are presented in detail. In particular, the transmission frequency bands, the ground stations and the type of polar orbit are reported, if they are available, in order to investigate and highlight the possible source of the interference.

4.2.1. COSMO SKYMED family

COSMO SKYMED (Constellation of Small Satellites for Mediterranean basin Observation) First Generation is a 4-spacecraft constellation, conceived by ASI (Agenzia Spaziale Italiana) and funded by the Italian Ministry of Research and the Italian Ministry of Defense. Each of the four satellites is equipped with a X-band (working at 9.6 GHz) Synthetic Aperture Radar instrument and is capable of operating in all visibility conditions

at high resolution and in real time. The overall objective of this program is global Earth observation and relevant data exploitation for the needs of the military community as well as for the civil one.

Each COSMO SKYMED spacecraft is three-axis stabilized, consisting of the main body, two deployable solar arrays and a SAR antenna. The payload data are compressed, encrypted and downlinked in X-band (carrier frequency of 8.12 and 8.25 GHz) at 300 Mbit/s, while the TT&C function is provided in S-band. It has Svalbard GS in its ground network.

The spacecrafts are in a circular Sun-synchronous dawn-dusk orbit (Local Time of Ascending Node at 6:00), at a nominal altitude of 619.6 km, inclination of 97.86°, period of 97.1 min. All spacecraft of the constellation are positioned in the same orbital plane with a phasing of 90°. In Table 4.7, the launch data of each spacecraft are reported [8].

Mission	Launch date
COSMO SKYMED-1	June 8, 2007 on a Delta-2 launch vehicle from Vandenberg Space Force Base, USA
COSMO SKYMED-2	December 9, 2007 on a Delta-2 launch vehicle from Vandenberg Space Force Base, USA
COSMO SKYMED-3	October 25, 2008 on a Delta-2 launch vehicle from Vandenberg Space Force Base, USA
COSMO SKYMED-4	November 6, 2010 on a Delta-2 launch vehicle from Vandenberg Space Force Base, USA

Table 4.7: Launch dates for COSMO SKYMED constellation

4.2.2. GRUS family

GRUS is a constellation of five 80 kg Earth observation micro-satellites developed and operated by the Japanese company, AxelSpace. They are equipped with high-performance optical telescopes, which enable to take images with 2.5 m ground resolution and over 50 km swath. GRUS can obtain panchromatic and multi-spectral images.

They use a Sun-synchronous orbit at an altitude of 600 km. The first satellite, GRUS-1A, was launched on December 27, 2018 on a Soyuz-2 Fregat rocket from the Baikonur Cosmodrome in Kazakhstan, while the other four were launched on March 22, 2021 also on a Soyuz-2 Fregat [32]. The constellation has a unique KSAT ground station at Svalbard [18].

4.2.3. KOMPSAT-3 family

KOMPSAT-3 (Korea MUlti-Purpose SATellite-3) is an optical high-resolution Korean observation mission designed, developed and lead by the Korea Aerospace Research Institute. The spacecraft is 3-axis stabilized and features a body pointing capability of ±45° into any direction (cross-track or along-track). It had a launch mass of 980 kg. It employs an S-band transmitter for TT&C communications, while X-band is used to downlink the payload data at frequencies of 8185, 8205 and 8225 MHz.

The spacecraft was launched on May 17, 2012 at 16:39 UTC from the Tanegashima Space Center, Japan on the H-IIA launch system. It is on a Sun-synchronous near-circular orbit at an altitude of 685.1 km, inclination of 98.13°, period of 98.5 minutes and Local Time on Ascending Node equal to 13:30 hours [5].

KOMPSAT-3A (Korea MUlti-Purpose SATellite-3A) is Korea's first Earth observation visible and infrared satellite with two imaging systems on board. The main goal is to develop an Earth observation satellite to obtain infrared and high resolution optical images for Geographical Information Systems applications in environmental, agricultural and oceanographic sciences as well as natural disasters.

KOMPSAT-3A is a near replica of KOMPSAT-3, using an identical satellite bus and payload with the only difference being an added infrared capability via beamsplitter and relay optics. The satellite has a mass of just under 1100 kg measuring 2.0 m in diameter and standing 3.5 m tall. Also, KOMPSAT-3A makes use of an S-band systems for TT&C communications, while a high-speed X-band system (with speed up to 1 Gbit/s) is used to downlink the acquired imagery from a large solid-state memory module, using the same frequencies of KOMPSAT-3.

The spacecraft was launched on March 25, 2015 at 22:08:53 UTC on a Dnepr-1 vehicle from the Jasny Dombarovsky launch site in Russia. It orbits on a Sun-synchronous orbit at an altitude of 528 km, inclination of 97.5° and same Local Time on Ascending Node of KOMPSAT-3 [6].

4.2.4. SUPERVIEW-1 family

The SUPERVIEW-1 satellites, also known as GaoJing-1, are part of a commercial constellation of Chinese remote sensing satellites operated by the Beijing Space View Technology Co. Ltd., based on the CAST3000B light agile platform. Their objective is to provide imagery with 0.5 m panchromatic resolution and 2 m multispectral resolution on a swath of 12 km. The satellites are equipped with a pair of solar panel wings. The satellites have

a launch mass of 560 kg and a design life of 8 years.

The first pair, SUPERVIEW-1 01 and SUPERVIEW-1 02, was launched on December 28, 2016 at 3:23:56 UTC on a Long March 2D rocket from the Taiyuan Satellite Launch Center, while the second pair, SUPERVIEW-1 03 and SUPERVIEW-1 04, was launched on 9 January, 2018 also on a Long March 2D rocket from the Taiyuan Satellite Launch Center in China.

They are on a Sun-synchronous orbit with a Local Time on Descending Node of 10:30 hours, at an altitude of 530 km. The downlink transmission is in X-band in two bands, each at 450 Mbit/s [14].

4.2.5. ICESAT-2

ICESAT-2 (Ice, Cloud and land Elevation Satellite-2) is a NASA follow-up mission to ICESAT with the goal to continue measuring and monitoring the impacts of the changing environment. The ICESAT-2 observatory contains a single instrument, an improved laser altimeter called ATLAS (Advanced Topographic Laser Altimeter System). ATLAS is designed to measure ice-sheet topography, sea ice freeboard as well as cloud and atmospheric properties and global vegetation.

ICESAT-2 uses the LEOStar-3 platform, has a 1387 kg launch mass and employs a X-band 8151.50 MHz transmitter with a data rate of 220 Mbit/s for downlink to stations in Svalbard, Poker Flat, or Wallops Island, in Virginia [4].

The ICESAT-2 spacecraft was launched on 15 September 2018 at 13:02 UTC from Vandenberg Space Force Base on a Delta-II 7420-10 vehicle configuration. It is in a near polar LEO frozen orbit at an altitude of 496 km and inclination of 92° [3].

4.2.6. AQUA

The AQUA mission is a part of the NASA's international Earth Observing System. The focus of the AQUA mission is the multi-disciplinary study of the Earth's water cycle, including the interrelated processes (atmosphere, oceans and land surface) and their relationship to Earth system changes. The six different instruments on board provide information on cloud formation, precipitation and radiative properties, air-sea fluxes of energy, carbon and moisture and sea ice concentrations and extents.

It is in a near polar, Sun-synchronous orbit at an altitude of 705 km with inclination of 98.2° and Local Time on Ascending Node at 13:30. The spacecraft was launched on May

4, 2002 with a Delta-2 7920-10L vehicle from Vandenberg Space Force Base [2].

The direct downlink transmits the data from an on-board solid state recorder to polar ground stations in Alaska and Svalbard, through the X-band transmitter at a frequency of 8.16 GHz [1].

4.3. Prediction model results

The prediction model has been validated with the events reported during the course of this work, shown in Table A.4. The same procedure applied previously for the Past RFI model validation has been employed also for the Prediction model. The complete results for the Prediction model are shown in Table 4.10: the model has been run with a maximum angular separation of 2°. The complete results obtained by applying the Past RFI model are reported in Table 4.11.

Due to the fact that the Prediction model uses the constant attitude assumption, the results could be different with respect to the model with the real attitude. Therefore, after the report of each event, the quaternions have been recovered from the spacecraft telemetry and the model with the correct attitude has been simulated. In fact, this difference is present for *event 47*: the Prediction model has a minimum angular distance of 1.1216° at 12:39:27, while the model with the real attitude predicts a minimum separation equal to 0.1660° at time of 12:39:32. Hence all other values, like elevation and azimuth, are different.

Moreover, the check between the reported cases and the model prediction is performed:

- Event 47: this RFI has been detected at 12:39:30 UTC, which is consistent with the results of the model with the real attitude, which predicts a duration between 12:39:29 and 12:39:34 UTC.
- Event 48: KSAT reported a RFI with GRUS-1D with maximum interference at 20:04:17 UTC; the model correctly predicted the same satellite and the same time of minimum angular separation.
- Event 49: A possible RFI is reported at 17:03:01 UTC; the model predicts an RFI with COSMO SKYMED-4 between 17:03:07 and 17:04:46, which is not consistent. Moreover, the minimum angular separation is large, therefore this case has not been identified and it will be analysed in Section 4.4 and 4.5.
- Event 50: A drop in signal is reported to have lasted from approximately UTC 16:49:57 to 16:50:17. The model predicts an RFI with COSMO SKYMED-4 at

around the same time, however the predicted minimum angular distance is very large. Hence, immediately this seemed not to be a RFI due to this satellite. In fact, this event is not an RFI due to another adjacent satellite, but it has been confirmed as a tracking issue. In order to better analysed also this case, it is studied in Section 4.4 and 4.5.

- Event 51: the RFI is at 21:59:17 UTC, which is the exact time predicted by the model for the minimum angular distance, hence this RFI is correctly predicted.

Moreover, the estimated duration of the reported RFI is computed with Equation (4.1) and reported for each event in Table 4.8. Therefore, the same iterative process in order to find the angle such that the reported and predicted duration values are similar has been performed just for the events correctly predicted and the results are presented in Table 4.9.

Event	Packets	Duration [s]
46	816	0.1850
47	21580	4.8915
48	19536	4.4282
49	109065	24.7214
50	93512	21.1961
51	14558	3.2998

Table 4.8: New events estimated duration

Event	Satellite	Angle [deg]
46	GRUS-1E	0.4
47	SUPERVIEW-1 03	0.6
48	GRUS-1D	0.65
51	GRUS-1A	0.775

Table 4.9: Angle estimation for correctly predicted events

Event	Satellite	Start time	End time	Duration [s]	Position	Elevation [deg]*	Azimuth [deg]*	Packets lost	Minimum angular distance [deg]	Time*
46	GRUS-1E	2021-11-06T22:29:49	2021-11-06T22:29:57	8.018241242842153	Ascending	30.879698905447725	60.94134955180184	35374,59372	0.33876517290733776	2021-11-06T22:29:54
47	SUPERVIEW-1 03	2021-11-11T12:39:23	2021-11-11T12:39:27	3.9507047065624126	Descending	8.535318030228916	39.82020702186551	17429,57959	1.1215939534528667	2021-11-11T12:39:27
48	GRUS-1D	2021-11-20T20:04:09	2021-11-20T20:04:24	15.053909911765707	Ascending	13.113751490230198	45.836473417768424	66414,30843	0.07942334938781397	2021-11-20T20:04:17
49	COSMO SKYMED-4	2021-12-05T17:03:07	2021-12-05T17:04:46	99.35085386401778	Ascending	29.489829862725472	59.36063697054519	438312,5906	0.6101423822307639	2021-12-05T17:04:14
50	COSMO SKYMED-4	2021-12-31T16:47:06	2021-12-31T16:51:30	264.2254684618746	Ascending	19,12389446	39,46021636	1165700,596	1,398564104	2021-12-31T16:50:43
51	GRUS-1A	2022-01-10T21:59:13	2022-01-10T21:59:22	9.27474474763727	Ascending	26.34186836356534	58.8458939496381	40917,99153	0.14278755859024603	2022-01-10T21:59:17

* computed at minimum angular distance

Table 4.10: Results for new events - Constant attitude

Event	Satellite	Start time	End time	Duration [s]	Position	Elevation [deg]*	Azimuth [deg]*	Packets lost	Minimum angular distance [deg]	Time*
46	GRUS-1E	2021-11-06T22:29:53	2021-11-06T22:29:54	0.5603815879401881	Ascending	30,8381407	60,97036452	2472,271712	0,334658492	2021-11-06T22:29:53.39
47	SUPERVIEW-1 03	2021-11-11T12:39:29	2021-11-11T12:39:34	4.995442963107735	Descending	8,440495378	40,70240465	22038,71895	0,166024838	2021-11-11T12:39:31.74
48	GRUS-1D	2021-11-20T20:04:15	2021-11-20T20:04:19	4.034745830945606	Ascending	13,13541252	45,83645821	17800,34925	0,082868056	2021-11-20T20:04:17.07
49	COSMO SKYMED-4	2021-12-05T17:03:07	2021-12-05T17:04:46	98.86426287066388	Ascending	29.481864416538222	59.338591463550856	436165.86560587	0.610111344226902	2021-12-05T17:04:13.76
50	COSMO SKYMED-4	2021-12-31T16:47:06	2021-12-31T16:51:30	264.2254684618746	Ascending	19,12389446	39,46021636	1165700,596	1,398564104	2021-12-31T16:50:43.02
51	GRUS-1A	2022-01-10T21:59:15	2022-01-10T21:59:19	3.266278854125814	Ascending	26,35755923	58,83779397	14410,05377	0,113716906	2022-01-10T21:59:17.44

* computed at minimum angular distance

Table 4.11: Results for new events - Real attitude

4.3.1. Validation though GENEOS Flight Dynamics tool

An additional validation of X-band RFI Prediction Tool has been conducted comparing its output results with the ones computed with the GENEOS Flight Dynamics tool. The comparison has been performed over the passes of a selected week with a maximum angular separation of 2°. The results of the predicted interference events are presented in Table 4.12. The table shows very good accordance between the two tools: in fact, both predicts the same events, with the same responsible satellites. There is some small disagreement in the start and end times, but this is due to the difference in the GS position (the position of the Svalbard station inside the GENEOS tool is not coincident with the one used inside the XRPT).

	XRPT	GENEOS
Start time	2022-02-16T22:55:43	2022-02-16T22:55:36
End time	2022-02-16T22:57:54	2022-02-16T22:57:52
Satellite	COSMO SKYMED-4	COSMO SKYMED-4
Start time	2022-02-17T10:39:29	2022-02-17T10:39:14
End time	2022-02-17T10:39:3	2022-02-17T10:39:32
Satellite	GRUS-1A	GRUS-1A
Start time	2022-02-19T07:41:34	2022-02-19T07:41:34
End time	2022-02-19T07:41:54	2022-02-19T07:41:54
Satellite	GRUS-1A	GRUS-1A
Start time	2022-02-20T15:26:33	2022-02-20T15:26:33
End time	2022-02-20T15:27:59	2022-02-20T15:27:58
Satellite	COSMO SKYMED-3	COSMO SKYMED-3

Table 4.12: Comparison of the XRPT and GENEOS results

4.4. Patterns' identification

A detailed investigation of the results leads to the identification of some possible patterns associated with the RFI parameters and with the families of responsible satellites. The identified patterns are: time of the day at which the RFI happens, duration of the RFI, value of minimum angular separation, elevation and azimuth at minimum angular distance, position and duration.

The first identifiable pattern is the time of the day. From Figure 4.1, there is a clear distinction between the different sets regarding this parameter: RFIs of COSMO SKYMED satellites tend to happen between 22 up to midnight, the ones of KOMPSAT-3 and KOMPSAT-3A in the morning (7 to 9), the ones associated the GRUS family in the evening (20 to 22) and the events due to SUPERVIEW-1 spacecrafts around midday (12 to 14). It is not possible to consider a time distribution for ICESAT-2 and AQUA, due to the small number of RFI associated to them. However, there are some exceptions: one RFI (*event 38*), with GRUS-1A as the responsible satellite, happens in the morning: this case is confirmed thanks to the consistency between the reported and the predicted values. Another particular case is associated to *event 5*, which sees as predicted responsible KOMPSAT-3 and it is an event that happens at midnight, so outside the pattern of the corresponding KOMPSAT-3 family.

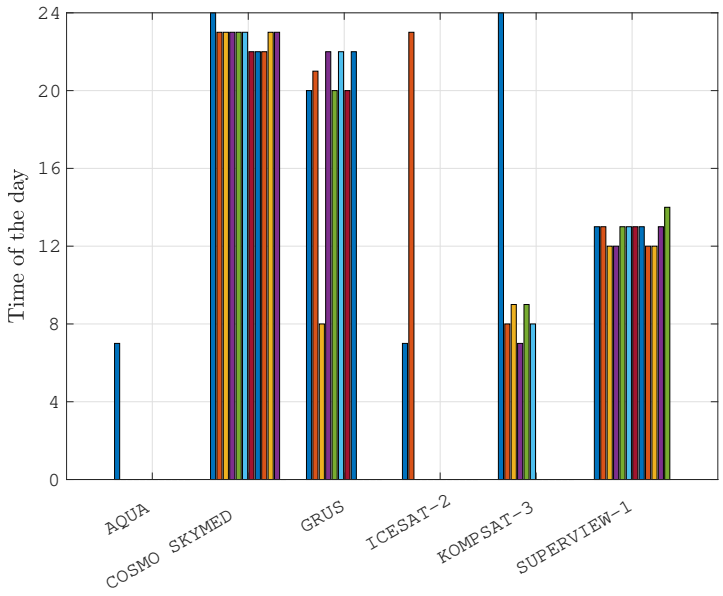

Figure 4.1: Time distribution

Another pattern to be considered is the value of the minimum angular distance: this should be small in order for the interference to occur. A classification per each satellite is presented in Figure 4.2 and it can be noted that all the values are quite low. A clear exception can be noticed: it is again associated with KOMPSAT-3 and computed for *event 5*.

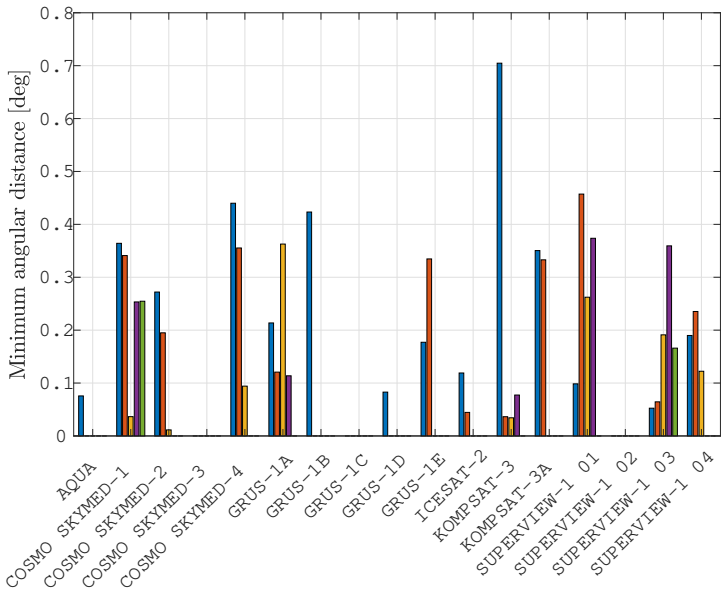

Figure 4.2: Minimum angular distance distribution

Then, the values of the elevation and azimuth of SMOS with respect to the Svalbard ground station at minimum angular distance are investigated. Also in this case, a pattern is identified: the RFIs happen inside ranges that are typical for each family. The overall values are presented in Figure 4.3, while the ranges of elevation and azimuth per each family are shown in Figure 4.4, without considering two events that will be discussed in the following.

In particular, two cases can be highlighted, especially looking at the azimuth distribution in Figure 4.3b. The first one is associated with GRUS-1A for the correctly predicted *event 38*, whereas the second is again linked with KOMPSAT-3 for *event 5*: it is also in this case outside of the typical range of the KOMPSAT-3 family. Therefore, following the reasoning about the time of the day, the minimum angular distance and the elevation and azimuth ranges, *event 5* is considered as a wrongly predicted case, it is highly probable that KOMPSAT-3 is not the satellite responsible for this event. Considering that the estimated duration of this event is very small and that no other satellite is predicted, it is probable that it was not caused by an adjacent satellite interference.

Moreover, as previously said in Section 1.4, the lowest elevation angles represent the worst link budget cases, hence represent also the cases when a RFI is more probable to happen. This can be confirmed in Figure 4.3a, where it can be noted that the majority of the events happen at low elevation angles, when SMOS is more susceptible to interference from other spacecrafts.

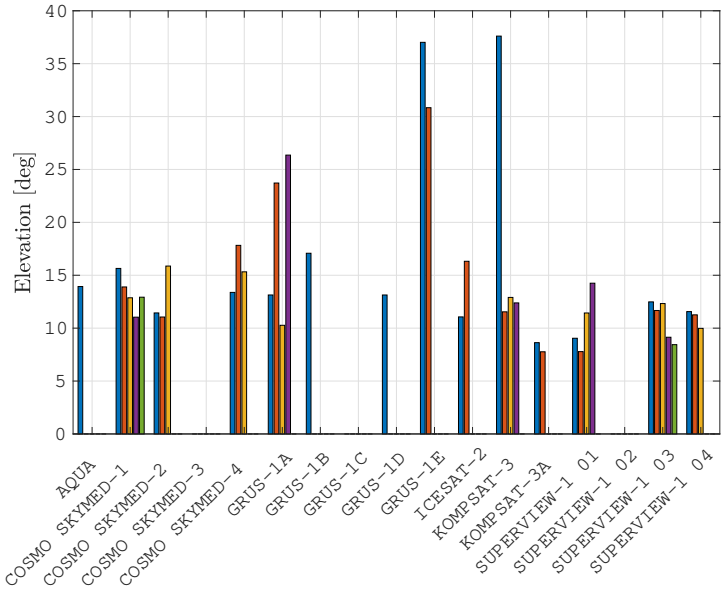

(a) Elevation distribution

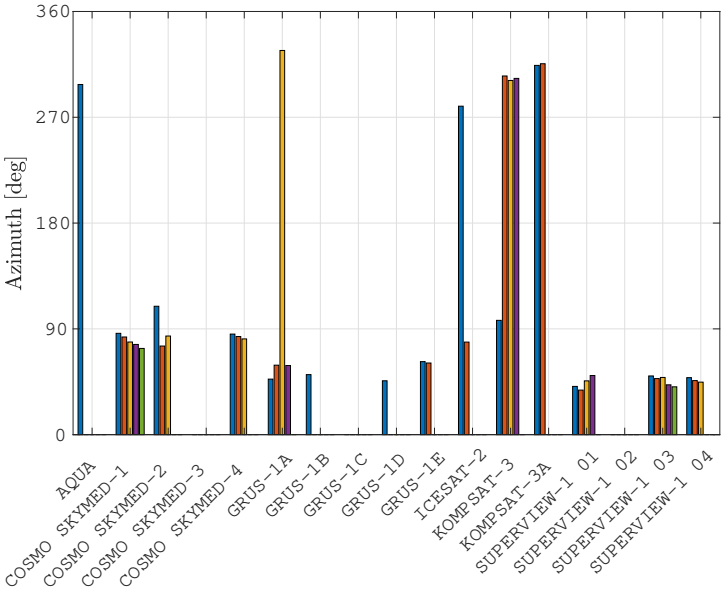

(b) Azimuth distribution

Figure 4.3: Elevation and azimuth distribution

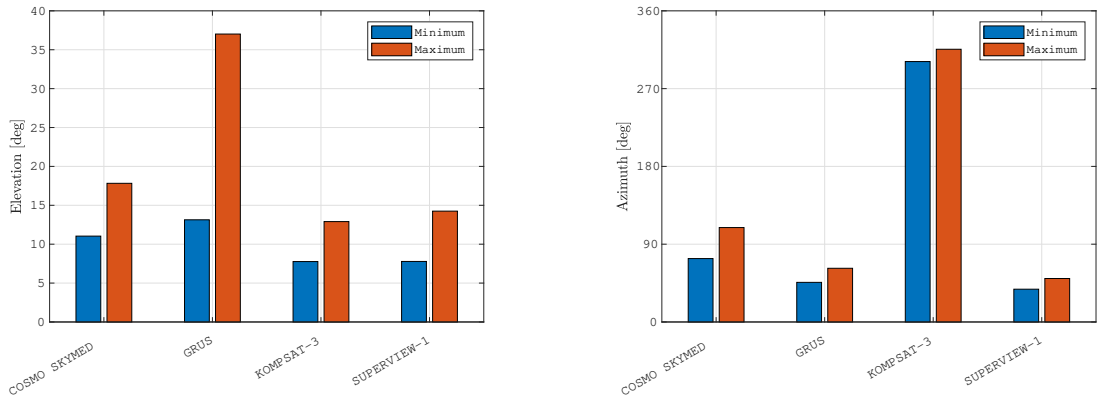

(a) Elevation ranges

(b) Azimuth ranges

Figure 4.4: Elevation and azimuth ranges per family

The patterns described until now can be used inside the Prediction model in order to compute the probability of a predicted RFI. In fact, these four parameters can be computed for each event and represent meaningful values to be compared. This will be investigated in Section 4.5.

Nevertheless, other parameters have been investigated. The estimated duration of the RFI is one of them and the values are presented in Figure 4.5: a clear trend is present for the events linked with the COSMO SKYMED family, which all have a higher duration, while the other events have a lower duration. However, this pattern cannot be employed in the Prediction model because its knowledge depends on the number of packets lost, which can only be recovered after that the RFI has happened.

Another one is the position of SMOS during the visibility window, distinguishing between the ascending phase (i.e. the minimum angular distance is reached before the elevation maximum value during the corresponding pass) and the descending phase (i.e. it is reached after the time of maximum elevation). The overall results per each satellite is presented in Figure 4.6. For the COSMO SKYMED family, all confirmed RFIs have an ascending result; the same is for GRUS and KOMPSAT-3 families, with the only exception of GRUS-1A, which presents a descending position during the confirmed *event 38*. Instead, for SUPERVIEW-1 satellites, the typical result is a descending position, with only one exception, associated with *event 23*.

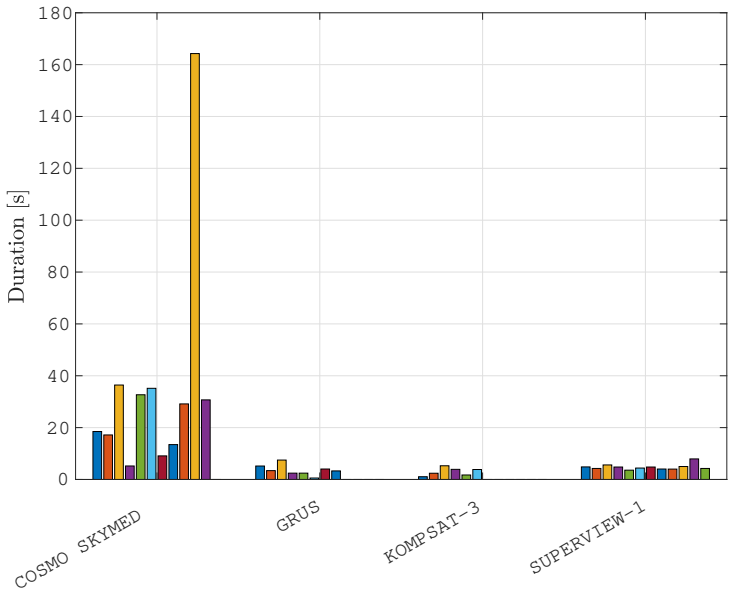

Figure 4.5: Duration distribution

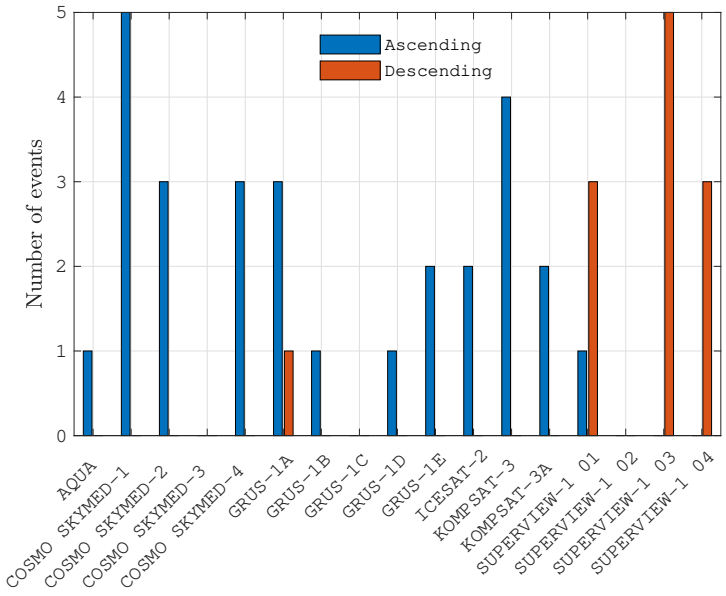

Figure 4.6: Position distribution

The analysis of the patterns can be employed to identify and confirm in another way the most probable responsible satellite for the events where two or more spacecrafts are predicted. This analysis is now presented:

- Event 19: for this event, SUPERVIEW-1 03 is identified as the most probable responsible, because the time of the day, the minimum angular distance, the elevation

and azimuth values and the position are all inside the typical patterns of this family.

- Event 28: this event represents an exception, because, considering only the time of the day, the most probable responsible satellite would have been COSMO SKYMED-2. However, the minimum angular distance is large and outside of the range of the corresponding family. Therefore, it is a clue that COSMO SKYMED-2 is not the real responsible satellite, in fact this is confirmed thanks to the reported time of the event, as explained in Section 3.4.
- Event 29: in this case, COSMO SKYMED-1 should be considered the real responsible satellite, in fact all the computed parameters are inside its family patterns.
- Event 30: SUPERVIEW-1 04 is the highest probable satellite because the predicted values are all inside the typical ranges of its set, while the other predicted satellites could not be the responsible due to the fact that the computed parameters are not coherent with the respective satellite's family patterns.

The same analysis has been performed over the two particular cases, previously reported in Section 4.3:

- Event 49: the predicted satellite is COSMO SKYMED-4, however, considering the time of the day, the minimum angular distance, the elevation and azimuth values at maximum interference, they are all outside the typical range for each parameter. Therefore, as previously explained, it should not be the real responsible satellite.
- Event 50: the same reasoning can be applied for this event: all parameters are outside of their ranges. In fact, this has been confirmed as a tracking issue, not as a RFI.

4.5. Statistical analysis

For each identified pattern to be used inside the Prediction model, the values are collected in the following tables, subdivided per each family of satellites. It is interesting to note that all the values follow a Gaussian distribution. These data are then used in order to compute the Mahalanobis distance of a new case and subsequently its corresponding p-value. If a new interference event is confirmed, its corresponding parameters will be automatically inserted by the software inside the family's overall data.

The *Time* parameter represents the time of the day in correspondence of the minimum angular distance of the corresponding event. It is computed in seconds as follows:

$$Time = Hour \cdot 3600 + Minute \cdot 60 + Seconds \tag{4.2}$$

with Hour, Minute and Seconds of the corresponding time of maximum interference.

Moreover, for the predicted events, the computed p-value is reported in Table 4.13. It can be noted that three events have a p-value larger than 0.001, hence confirming that they are real RFIs. *Event 47* is a confirmed interference, however, due to the constant attitude assumptions, the results are not coincident with the real ones, so the p-value computation is wrong: in fact, using the parameters predicted by the Past RFI model, the p-value is computed equal to 0.10168. While *event 49* and *event 50* are clearly outliers, confirming even more that these two events are not due to adjacent satellite interference.

Event	p-value [-]
46	0.635918958
47	0
48	0.36339459
49	0
50	0
51	0.402604529

Table 4.13: New events p-value

4.5.1. COSMO SKYMED family

The COSMO SKYMED family is responsible for 11 events, with COSMO SKYMED-1 associated to 5 RFIs, the highest number of conjunctions along with SUPERVIEW-1 01. Satellites 2 and 4 are associated with 3 events, while COSMO SKYMED-3 has never been responsible for any interference.

Satellite	Number of RFIs
COSMO SKYMED-1	5
COSMO SKYMED-2	3
COSMO SKYMED-3	0
COSMO SKYMED-4	3

Table 4.14: Number of RFIs per satellite - COSMO SKYMED family

Time [s]*	Minimum angular distance [deg]	Elevation [deg]*	Azimuth [deg]*
89065.37	0.272071674	11.43914235	109.2464133
84526.65	0.439940325	13.3804939	85.56841329
84844.19	0.364160039	15.64587749	86.21212250
84003.57	0.341010245	13.89473029	83.09354089
84428.85	0.355365144	17.8264462	83.48130764
82958.97	0.036479535	12.86974874	78.82231698
82223.92	0.253342462	11.03901848	76.76318567
81862.04	0.194975627	11.05388426	75.40084905
81516.99	0.254692193	12.92644237	73.36106829
84418.57	0.011426204	15.86939632	83.91653943
83688.10	0.094177547	15.32404895	81.45325999

* computed at minimum angular distance

Table 4.15: COSMO SKYMED family data

4.5.2. GRUS family

GRUS satellites have been confirmed for 8 RFIs, although in Table 4.17 the dataset consists of only 7 events because one event, associated to GRUS-1A, happens in the morning, hence it is discarded from the statistical analysis. GRUS-1A is responsible for the highest number of RFIs, this could be due to the fact that it was launched before the other 4 satellites in the constellation. Satellite E is responsible for 2 events, while B and D to one each; GRUS-1C has never been associated to any RFI.

Satellite	Number of RFIs
GRUS-1A	4
GRUS-1B	1
GRUS-1C	0
GRUS-1D	1
GRUS-1E	2

Table 4.16: Number of RFIs per satellite - GRUS family

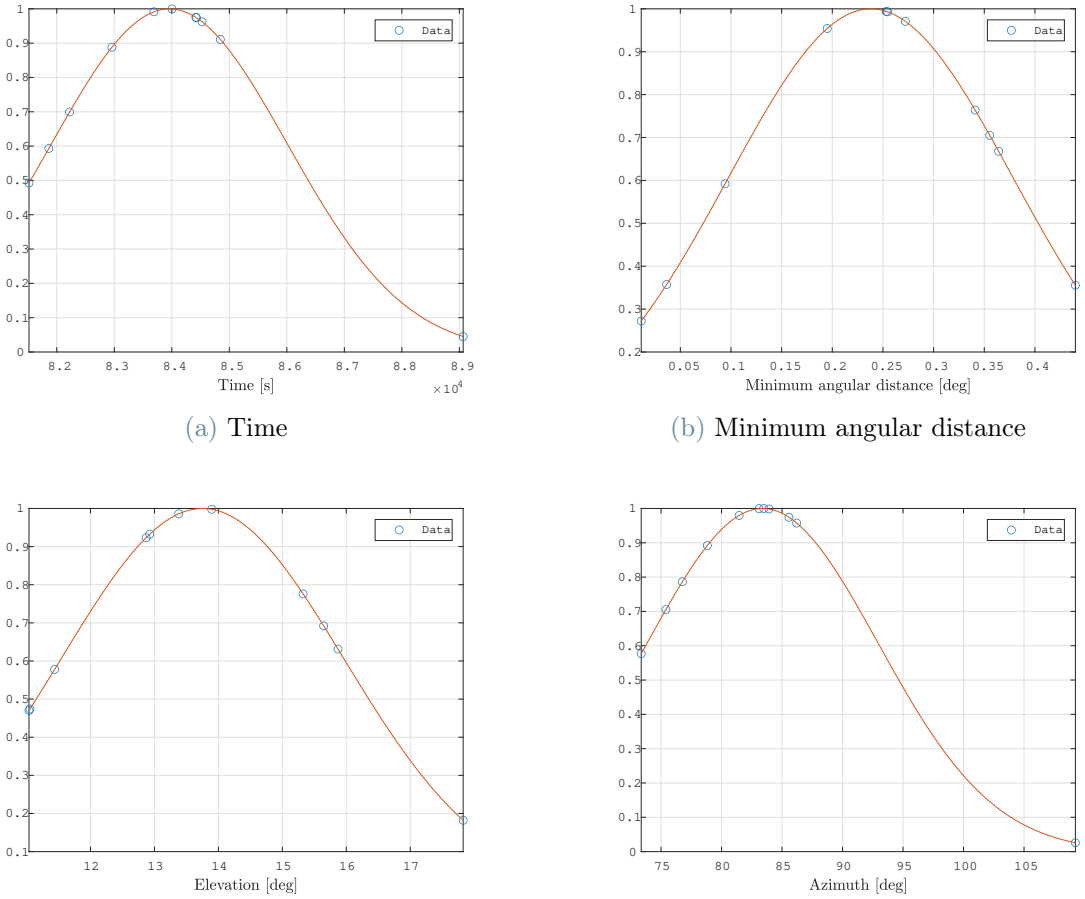

(a) Time

(b) Minimum angular distance

(c) Elevation

(d) Azimuth

Figure 4.7: Data distribution for each pattern for COSMO SKYMED family

Time [s]*	**Minimum angular distance [deg]**	**Elevation [deg]***	**Azimuth [deg]***
72671.23	0.213631204	13.13649468	47.25737012
78815.93	0.120694411	23.71762614	59.12804065
82567.70	0.177116680	37.01649547	62.13024811
74857.55	0.423330373	17.08071727	51.08028906
80993.39	0.334658492	30.83814070	60.97036452
72257.07	0.082868056	13.13541252	45.83645821
79157.44	0.113716906	26.35755923	58.83779397

* computed at minimum angular distance

Table 4.17: GRUS family data

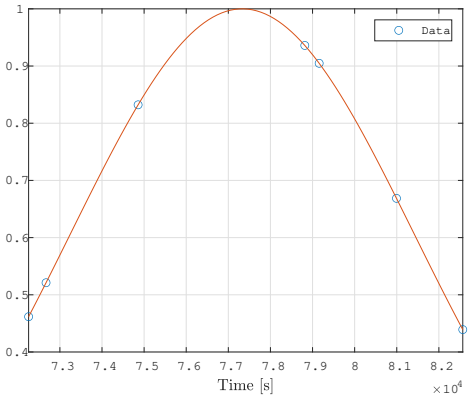

(a) Time

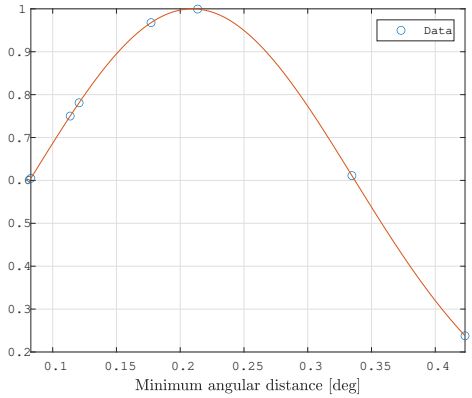

(b) Minimum angular distance

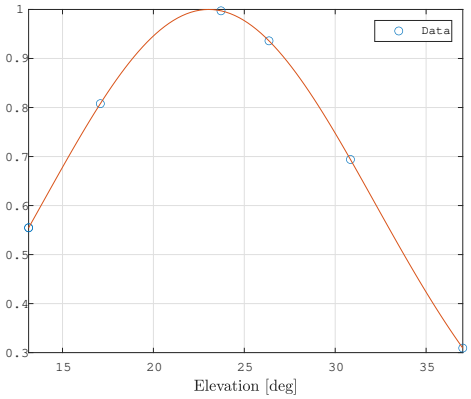

(c) Elevation

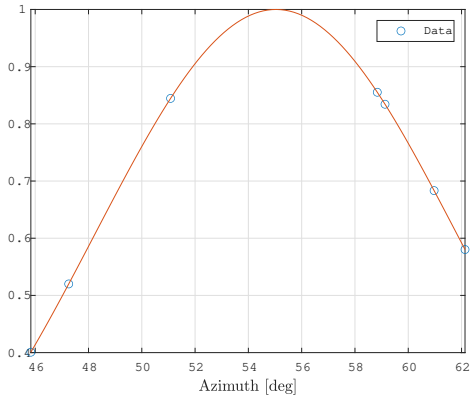

(d) Azimuth

Figure 4.8: Data distribution for each pattern for GRUS family

4.5.3. KOMPSAT-3 family

This set is associated to just 5 confirmed events, therefore the available data are very low and spread out. KOMPSAT-3 is responsible for 3 RFIs, while 3A for 2 events.

Satellite	Number of RFIs
KOMPSAT-3	3
KOMPSAT-3A	2

Table 4.18: Number of RFIs per satellite - KOMPSAT-3 family

Time [s]*	Minimum angular distance [deg]	Elevation [deg]*	Azimuth [deg]*
29810.57	0.036373754	11.54278104	305.1369459
32803.3	0.350428471	8.62874761	314.1440454
28383.93	0.034311789	12.90521864	301.324013
33677.19	0.3329572	7.767225523	315.5498401
28912.03	0.077355002	12.38705803	303.0775493

* computed at minimum angular distance

Table 4.19: KOMPSAT-3 family data

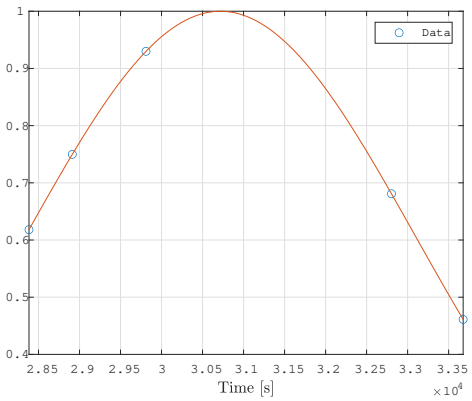

(a) Time

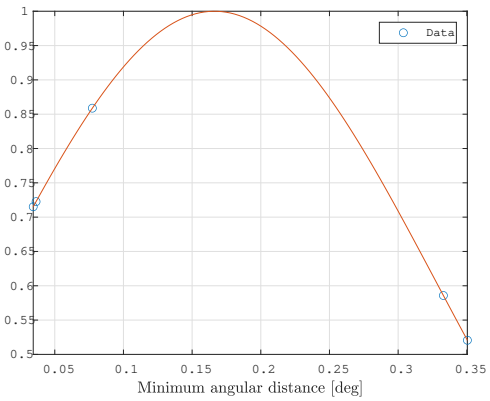

(b) Minimum angular distance

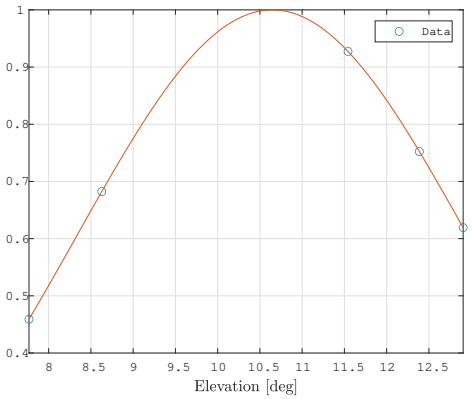

(c) Elevation

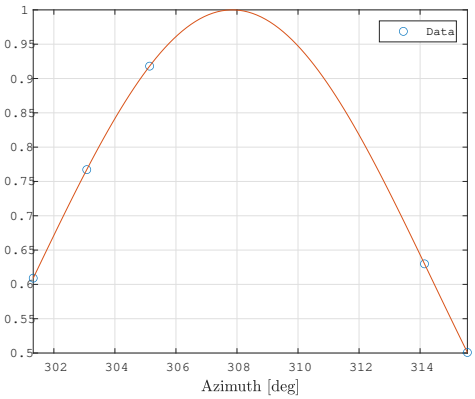

(d) Azimuth

Figure 4.9: Data distribution for each pattern for KOMPSAT-3 family

4.5.4. SUPERVIEW-1 family

SUPERVIEW-1 satellites are the responsible for the highest number of RFIs. Satellite 03 has the highest number of events along with COSMO SKYMED-1, while 02 has never been predicted to generate an interference. Given this larger dataset, the curves, shown in Figure 4.10, present a good Gaussian shape.

Satellite	Number of RFIs
SUPERVIEW-1 01	4
SUPERVIEW-1 02	0
SUPERVIEW-1 03	5
SUPERVIEW-1 04	3

Table 4.20: Number of RFIs per satellite - SUPERVIEW-1 family

Time [s]*	Minimum angular distance [deg]	Elevation [deg]*	Azimuth [deg]*
49213.59	0.189954175	11.56366843	48.4968333
50145.75	0.05248838	12.48343559	49.95077004
46433.43	0.098489977	9.045290167	41.05206434
44775.66	0.457242791	7.782474613	37.93307652
48696.38	0.23529758	11.25780145	45.99813248
49415.66	0.064478346	11.67037943	47.69984133
47652.45	0.122299321	9.981550287	44.69085222
49713.77	0.191133366	12.32497371	48.6699155
46377.15	0.359354629	9.141902973	42.40665904
45571.74	0.166024838	8.440495378	40.70240465
49085.91	0.262289947	11.43413263	45.77851348
51738.21	0.373684261	14.24996861	50.30023313

* computed at minimum angular distance

Table 4.21: SUPERVIEW-1 family data

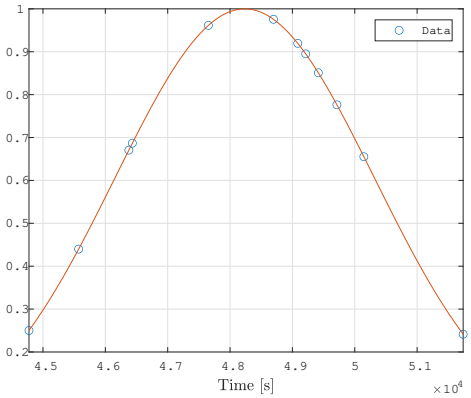

(a) Time

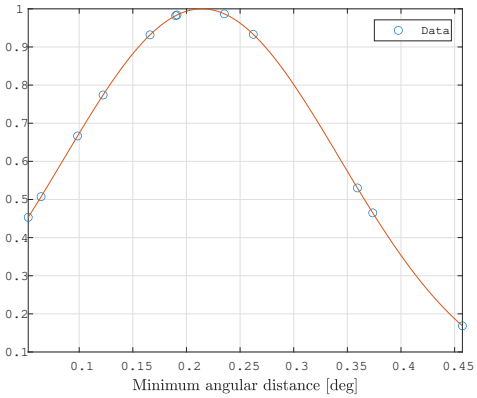

(b) Minimum angular distance

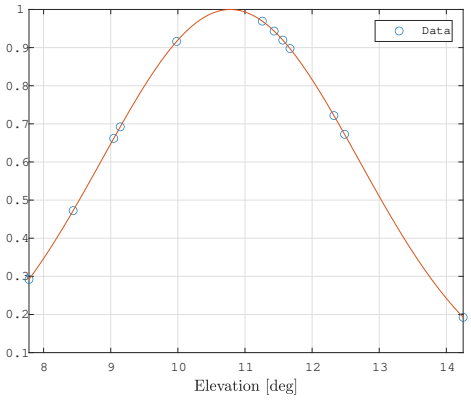

(c) Elevation

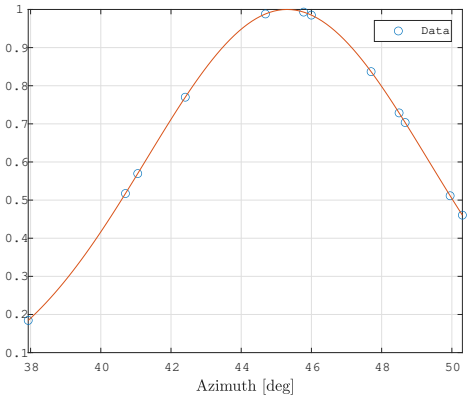

(d) Azimuth

Figure 4.10: Data distribution for each pattern for SUPERVIEW-1 family

4.5.5. All data

In Figure 4.11, all collected values are reported per each identified pattern. The values are normalized with respect to the mean of the corresponding pattern of each family. It can be noted that increasing the number of values, the curves take even more the Gaussian shape.

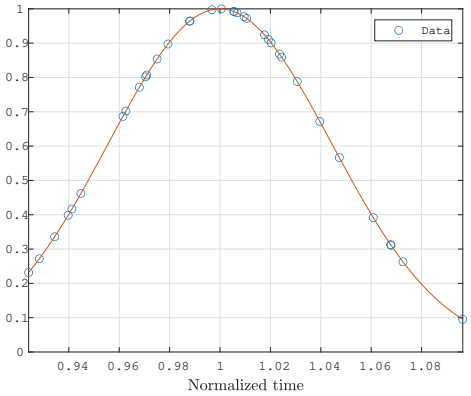

(a) Time

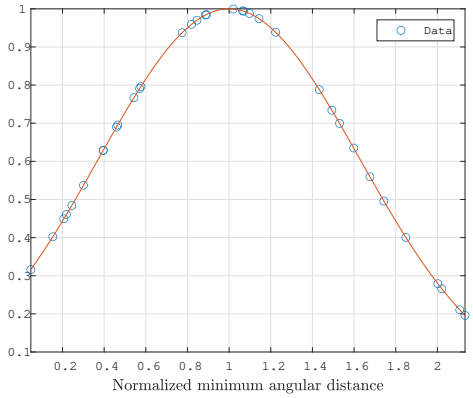

(b) Minimum angular distance

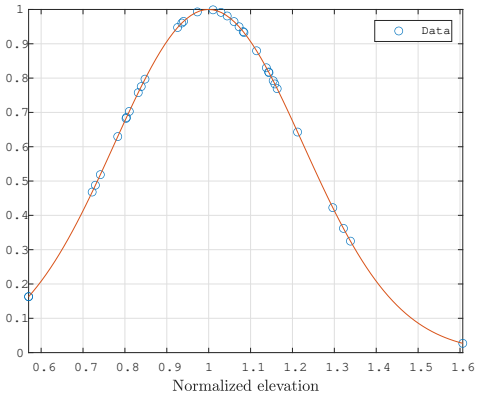

(c) Elevation

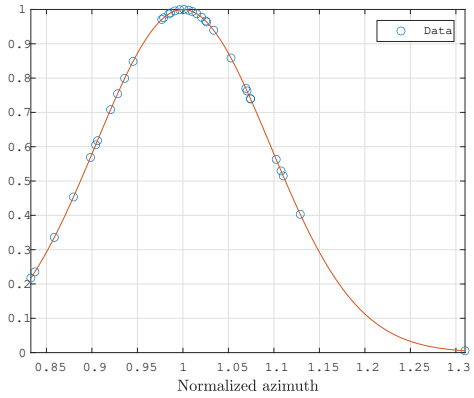

(d) Azimuth

Figure 4.11: Data distribution for each pattern for all data

4.6. Final version of the software

Different versions of the software have been delivered and validated in order to fulfill all the requirements. In fact, the software development is based on an agile approach: for each intermediate versions, the needs of the user and of the developer, along with the results of the testing phase, are discussed and the requirements are adapted accordingly for the next release. The list of already presented requirements along with the corresponding version in which they have been implemented is shown in Table C.1, Table C.2, Table C.3, Table C.4, Table C.5, Table C.6 and Table C.7.

XRPT 1.0 represents the final version of the software: it is currently used by the FOS as part of the weekly planning and its results are used for operational purpose. The user interface of this version is shown in Figure 4.12, with its features description presented in the following.

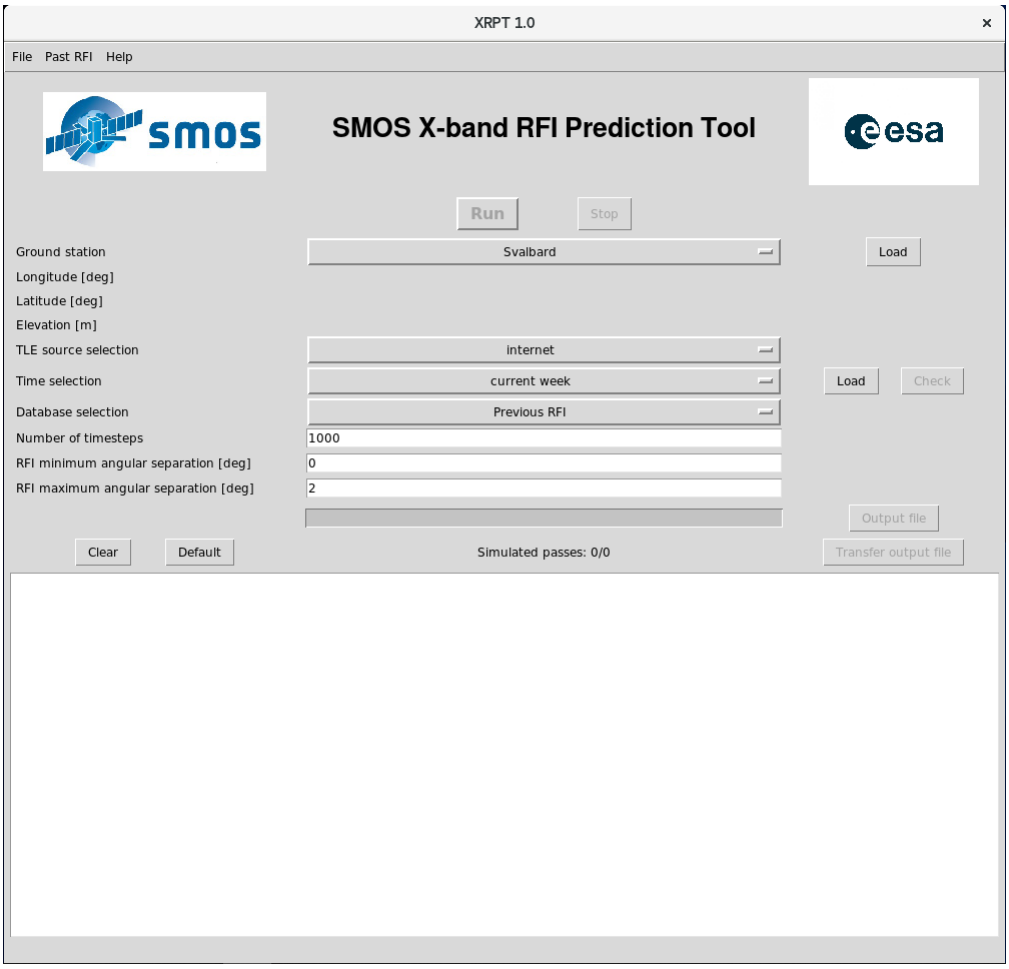

Figure 4.12: XRPT 1.0 user interface

File menu

- **Database**
  In order to connect with the *Database.xlsx* file, which contains the list of satellites to be investigated, divided in: Previous RFI (list of satellite responsible for past RFIs), Commercial (list of commercial satellite with transmission frequency inside the frequency band of SMOS) and Military (list of military satellites in polar orbit).

- **Configuration file**
  In order to retrieve the Configuration file containing the *SpaceTrack* account username and password and the FTP server address, username, password and directory.

- **Exit**
  In order to exit from the software. Another window will appear to confirm the exit (**Yes button**) or to keep the window running (**No button**).

Past RFI menu

- **Past RFI**
  In order to connect with the *Past_ RFI.xlsx*, which contains the list of all previous confirmed RFIs, with their corresponding parameters.
- **Store predicted RFI**
  In order to store the RFIs predicted in the current simulation. Another window will appear in order to confirm the storage (**Yes button**) or to cancel it and exit from the window (**No button**).
- **Confirm predicted RFI**
  In order to save the predicted RFIs confirmed in operation. Another window will appear with all the RFIs previously stored: if a RFI is confirmed, the **Yes checkbox** beside should be pressed: this RFI will be saved in the *Past RFI file* and the *Database file* and *Data file* will be updated. At the end, press the **Save button** in order to save the confirmed RFIs and to cancel the stored ones. The *Data.xlsx* file contains the required data in order to perform the computation of the Mahalanobis distance and therefore of the probability of a RFI.

Help menu

- **Help**
  In order to connect with the Help file.

Run button
Button in order to run the software. This becomes active only after pressing the *Check button.*

Stop button
Button in order to stop the simulation. This becomes active only when running the simulation.

Ground station
Two items can be selected: **Svalbard** and **ESAC**.
The **Load button** displays the **Latitude [deg]**, **Longitude [deg]** and **Elevation [m]** of the selected ground station.

TLE source
Three items can be selected: **SMOS FTP server**, **internet** or **local file** and Algorithm 3.1 is used.

- **SMOS FTP server**: the SMOS TLEs are retrieved from the *smos_ tle.txt file*

in the FTP server. This parameter should be selected with a *current week* time selection in order to keep the simulation as much accurate as possible.

- **internet**: all TLEs are retrieved either from *CelesTrak* or *n2yo.com* or *SpaceTrack*. The recovered TLEs will be the nearest possible to the selected time period.
- **local file**: SMOS TLEs are retrieved from a local repository of SMOS TLE, *tle_file.txt*, which contains the list of all previous SMOS TLEs and it is automatically updated by the software with the newest available TLEs. The recovered TLEs will be the nearest possible to the selected time period.

Time
Three items can be selected in order to identify the time period to be checked for possible RFI:

- **current week**, checking current week retrieving the current week's passes;
- **week number**, checking the selected week;
- **time period**, checking a selected time period.

The **Load button** displays the user selection:
for **week number**, a couple of integer numbers (week number and year number) must be provided (e.g. ww = 20 and yyyy = 2021 representing the 20th week of 2021).
for **time period**, two times must be provided in this format: start time in CCSDS format and end time in CCSDS format (e.g. 2021-10-10T00:00:00 and 2021-10-11T00:00:00). Moreover, the user is able to select the name of the output file.

The **Check button** checks and confirms the user selection.

Database
The list of satellites to be investigated can here be selected:

- **Previous RFI** represents the list of satellite responsible for past RFIs.
- **Commercial** represents the list of commercial satellite with transmission frequency inside the frequency band of SMOS.
- **Military** represents the list of military satellites in polar orbit.
- **All** represents the sum of all previous lists.

Number of timesteps
Integer number representing the steps in the orbit propagation. The number must be

larger or equal than 2. The higher the number of timesteps, the higher will be the accuracy of the simulation. 1000 is taken as the default value.

RFI minimum angular separation
Value in degree representing the minimum angular separation to be considered inside the software. Must be larger or equal than 0. Must be lower than RFI maximum angular separation.

RFI maximum angular separation
Value in degree representing the maximum angular separation to be considered inside the software. Must be larger or equal than 0. Must be larger than RFI minimum angular separation. 2° is considered as the default value in order to take into account the constant attitude assumption.

Progress bar
Bar in order to display the status of the software: it steps forward for each simulated pass.

The number of **Simulated passes** is indicated under the *Progress bar* as follows:
Number of simulated passes/Total number of passes to be analysed.

End window
At the end of the simulation, a new window will appear in order to highlight to the user the end of the current simulation. An **Ok button** is present in order to confirm the end of the simulation and to make the *Output file button* and *Transfer output file button* active.

Clear button
Button in order to clear the output display.

Default button
Button in order to reinsert the default values of the variables.

Output file button
Button in order to retrieve the final html output file.

Transfer output file button
Button in order to transfer the final html output file to the FTP server. It is active only with a *current week* or *week number* time selection, because it transfers the html output file to the corresponding directory inside the FTP server.

Another window will appear with two buttons:
Yes button
Button in order to confirm the transfer of the html output file to the corresponding

directory inside the FTP server. A confirmation entry will appear when the file has been transferred.

No button

Button in order to cancel the transfer of the html output file to the FTP server and to close the window.

Output display

It displays the results of the simulation and provides the user with the information about the status of the software:
[INFO] reports useful information about any commands executed inside the software;
[WARNING] reports any error encountered inside the software stopping the simulation.

The description of how to run a simulation is presented in the following.

From the user interface, first select the Ground station and press the Load button beside: the latitude, longitude and elevation of the selected GS will appear. It is not necessary to press the Load button because the software will automatically recognize the selection of the GS.

Then, select the TLE source and the Time period. After selecting the time, press the Load button: in case of *week number* or *time period* selection, insert the selection of respectively the week and year numbers or of the start time, end time and name of the output file on the next entries. Then, press the Check button in order to check the user selection: if an error is present or it is not possible to retrieve the corresponding file from the FTP server, this will be highlighted in the corresponding entry and in the output display with a [WARNING]. After, select the Database, the Number of timesteps, the RFI minimum and maximum angular separation.

In order to start the simulation, press the Run button, which becomes active only after pressing the Check button: if no errors are present, the simulation will start, otherwise the error will be highlighted in the corresponding entry and in the output display with a [WARNING]. Instead, the Stop button is located beside the Run button in order to exit from the simulation and retrieve the results of the passes simulated until the press of the Stop button. While in order to exit from the GUI, the Exit is located in the File menu: a new window will appear in order to confirm the exit (Yes button) or to keep the GUI running (No button).

A window will appear at the end of the simulation or if the simulation has been stopped: press the Ok button to activate the Output file and the Transfer output file buttons. The output of the simulation will appear in the bottom part of the GUI. Moreover, the Output

file button opens the html output file; the Transfer output file button is active only in case of *current week* or *week number* time selection: after pressing it, another window will appear with two buttons: Yes button in order to confirm the transfer of the html output file to the corresponding directory inside the FTP server or No button in order to cancel the transfer of the html output file to the FTP server and close the window.

In order to run a new simulation, the Clear button clears the output display, while the Default button reinserts the default values of the variables, so another simulation can be launched.

After running a simulation, the user is able to store the RFIs predicted in the current simulation: this is possible through the Store predicted RFI button inside the Past RFI menu. A new window will appear in order to confirm the transfer (Yes button) or to cancel the transfer, discard the predicted RFIs and exit from the window (No button). If no action is taken after the end of the simulation, the predicted RFIs are discarded.

Moreover, the user is able to view the RFIs predicted in other simulations which have been previously stored and to save the ones which have been confirmed in operation: this is possible through the Confirm predicted RFI button inside the Past RFI menu. Another window will appear with all the RFIs previously stored; if a RFI is confirmed, press the Yes checkbox beside: this RFI will be saved in the *Past RFI file* and the *Database file* and the *Data file* will be updated. At the end, press the Save button in order to save the confirmed RFIs and to cancel the stored ones. The *Past RFI file* can be accessed through the corresponding button inside the Past RFI menu.

Two output files are generated: a *.html* file and a *.csv* file representing the output of the simulation, also containing the list of the selected variables for the simulation. These files are called *yyyy_wxx_rfi.html* and *yyyy_wxx_rfi.csv* if the software is run for a selected week or *selected_name.html* and *selected_name.csv* if a selected time period is chosen. All these files can be retrieved from the corresponding folder *OUTPUT* created inside the *XRPT_1.0* folder. Moreover, inside the *XRPT_1.0* folder, two other folders are present: *DOCS* folder containing all the required files to run the software and the *CODE* folder containing the Python file and the SPICE kernels.

5 | Conclusions and future developments

In this final chapter, a summary of this thesis is described in order to highlight that the objectives to be achieved during this work have been met. First, a model able to identify the satellite responsible of a Radio Frequency Interference has been implemented and validated. Potentially conflicting commercial and military satellites have been collected inside the Database. Then, different sources have been analyzed in order to retrieve the TLEs: these can be recovered from internet, in particular from *CelesTrak*, *n2yo.com* or *SpaceTrack*. Moreover, to meet the software requirements, other two sources have been implemented for retrieving SMOS TLEs. Then, the main model has been developed: this is based on the orbital propagation of the TLE according to the time range of interest. Then, the satellites' state is converted into position with respect to the selected ground station and the declination and azimuth are computed. If the satellite is in view of the GS, SMOS attitude is calculated in order to check if the ground station and the other satellite are both in the field of view of the X-band antenna. If this is verified, the angular distance between SMOS and the satellite, as seen from the ground, is computed: if this angle is inside the selected angular range, a possible interference condition could happen.

This model has been validated on the reported events of past interference. Given that these cases have already happened, the spacecraft telemetry is available and the real quaternions can be recovered. Therefore, a model with the real attitude has been employed and most of the previous events are associated to a responsible satellite. For some cases, there is no predicted guilty satellite, for others two or more spacecrafts are predicted. In fact, for all events, in order to confirm the real responsible satellite, the reported and the predicted times have been compared leading to the identification of the correct satellite: the model shows very good accuracy between computed and real times. At the end, a list of satellites responsible for these past events is made and is used inside the software to fasten the computation.

Subsequently, the prediction model has been implemented and validated. Given that

the quaternions cannot be recovered for future times, the model exploits the feature that SMOS has a constant flight attitude. However, the real and the assumed constant attitude can differ and this could lead to different predicted parameters for the same event.

Moreover, an analysis for the identification of potential patterns on the parameters of all confirmed events has been made: this has led to the identification of four parameters (time of the day at which the RFI happens, minimum angular distance, elevation and azimuth values at maximum interference), which shows meaningful patterns related to each family of responsible satellites. Therefore, these patterns are used inside the prediction model in order to compute the probability of a new event: this is based on the computation of the Mahalanobis distance of this predicted event with respect to the available dataset of previous RFIs and then on computation of the corresponding probability value. A threshold on the p-value is assumed in order to distinguish between *High* probability and *Low* probability events. The prediction model shows very good accordance between predicted and reported events.

On this basis, the X-band RFI Prediction Tool has been completely developed: the final version achieves all the software requirements.

5.1. Possible future developments

A possible future development of this thesis work is the use of Machine Learning in order to predict RFI conjunctions and assign a corresponding probability value. This method could not only be applied to SMOS but to many other satellites. In fact, the dataset from which the model has to be trained must be much larger than the number of events used inside this work. The patterns identified during this thesis could be used inside the Neural Networks, but also new patterns could be found by the trained model in order to compute the probability of an RFI. These actions may provide a very useful tool in managing the prediction and consequently the mitigation of RFIs, given the increasing number of satellites launched.

Bibliography

[1] Aqua Mission Brochure, -. URL https://atrain.nasa.gov/publications/Aqua.pdf.

[2] Aqua Mission, -. URL https://directory.eoportal.org/web/eoportal/satellite-missions/a/aqua.

[3] ICE-Sat-2, -. URL https://directory.eoportal.org/web/eoportal/satellite-missions/i/icesat-2.

[4] ICE-Sat-2 Mission Brochure, -. URL https://science.gsfc.nasa.gov/sci/content/uploadFiles/highlight_files/ICESat-2_missionBrochure_508.pdf.

[5] KOMPSAT-3 (KOrea Multi-Purpose SATellite-3), -. URL https://directory.eoportal.org/web/eoportal/satellite-missions/k/kompsat-3.

[6] KOMPSAT-3A (KOrea Multi-Purpose SATellite-3A), -. URL https://directory.eoportal.org/web/eoportal/satellite-missions/k/kompsat-3A.

[7] Space Network List, -. URL https://www.itu.int/ITU-R/go/space/snl/en.

[8] COSMO Sky-Med. URL https://directory.eoportal.org/web/eoportal/satellite-missions/c-missions/cosmo-skymed.

[9] Database of Frequency Allocations. URL http://www.classic.grss-ieee.org/frequency_allocations.html.

[10] Frequency Allocations. URL https://life.itu.int/radioclub/rr/art05.htm.

[11] N2YO.COM REST API v1. URL https://www.n2yo.com/api/.

[12] SMOS (Soil Moisture and Ocean Salinity) Mission. URL https://directory.eoportal.org/web/eoportal/satellite-missions/s/smos.

[13] SpaceTrack Python module. URL https://pypi.org/project/spacetrack/.

[14] GaoJing / SuperView Earth Observation Constellation. URL https://eoportal.org/web/eoportal/satellite-missions/g/gaojing.

[15] Kongsberg Satellite Services. URL `https://www.svalbardblues.com/svalbard/bedrifter/kongsberg-satellite-services/`.

[16] USE OF THE FREQUENCY BAND 8025-8400 MHZ BY EESS. Technical report, Electronic Communications Committee (ECC), Ljubljana, 1 2008.

[17] The International Terrestrial Reference System (ITRS), 2013. URL `https://www.iers.org/IERS/EN/Science/ITRS/ITRS.html`.

[18] Axelspace selects SKY Perfect JSAT & KSAT Ground Station Service for GRUS, the first commercial Japanese optical EO satellite, 2018.

[19] JPSS Ground System ConOps. Technical report, NASA Goddard Space Flight Center, 7 2019.

[20] How to Calculate Mahalanobis Distance in Python, 2020. URL `https://www.statology.org/mahalanobis-distance-python/`.

[21] "High Accuracy" Orientation and Body-fixed Frames for the Moon and Earth, 2020. URL `https://naif.jpl.nasa.gov/pub/naif/toolkit_docs/Tutorials/pdf/individual_docs/23_lunar-earth_pck-fk.pdf`.

[22] Anritsu. Resolving Interference Issues at Satellite Ground Stations, 2020.

[23] S. Cakaj. The Downlink Adjacent Interference for Low Earth Orbiting Search and Rescue Satellites. *Int. J. Communications, Network and System Sciences*, 3:107–115, 2010.

[24] S. Cakaj, B. Kamo, V. Kolici, and O. Shurdi. The range and horizon plane simulation for ground stations of low earth orbiting (leo) satellites. *IJCNS*, 4:585–589, 01 2011. doi: 10.4236/ijcns.2011.49070.

[25] H. D. Curtis. *Orbital Mechanics for Engineering Students*. Butterworth-Heinemann, 2010.

[26] B. Donnelly. Improving your signal and mitigating downlink adjacent satellite interference effects in ground satellite terminals, 12 2017.

[27] Dr. T.S. Kelso. Models for Propagation of NORAD Element Sets. Technical report, 12 1993.

[28] Dr. T.S. Kelso. Frequently Asked Questions: Two-Line Element Set Format, 2019. URL `https://www.celestrak.com/columns/v04n03/`.

[29] Dr. T.S. Kelso. NORAD Two-Line Element Set Format, 2019. URL https://www.celestrak.com/NORAD/documentation/tle-fmt.php.

[30] Dr. T.S. Kelso. A New Way to Obtain GP Data (aka TLEs), 2020. URL https://celestrak.com/NORAD/documentation/gp-data-formats.php.

[31] J. L. V. Garcıa. Introduction to SPICE. COSPAR Workshop on Planetary Science, 7 2007.

[32] G. D. Krebs. GRUS 1A, 1B, 1C, 1D, 1E Satellite. URL https://space.skyrocket.de/doc_sdat/grus-1.htm.

[33] N. Mohanta. How many satellites are orbiting the Earth in 2021?, 2021. URL https://www.geospatialworld.net/blogs/how-many-satellites-are-orbiting-the-earth-in-2021/.

[34] T. M. Nguyen. Radio interference modeling and prediction for satellite operation applications, 8 2015.

[35] S. Prabhakaran. Mahalanobis Distance, 2019. URL https://www.machinelearningplus.com/statistics/mahalanobis-distance/.

[36] Prof. Camilla Colombo. Orbital Mechanics Course Notes, Chapter 6: Orbit Perturbations, 2019.

[37] Prof. Franco Bernelli Zazzera. Spacecraft Attitude Dynamics and Control Course Notes, Part 1: Attitude dynamics and kinematics, 2020.

[38] E. B. Salas. Number of active satellites from 1957 to 2021, 2022. URL https://www.statista.com/statistics/897719/number-of-active-satellites-by-year/.

[39] R. E. Taylor. RADIO FREQUENCY INTERFERENCE PREDICTION PROGRAM FOR EARTH-ORBITING SATELLITES. Technical report, NASA Goddard Space Flight Center, 10 1967.

A | Events and Requirements

Event	Pass	Missing packets	Remarks
1	20130308T004234_20130308T005549	32715	-
2	20150820T232634_20150820T233944	53000	-
3	20150902T100214_20150902T101013	4141	-
4	20160618T233131_20160618T234442	160288	-
5	20161121T003728_20161121T005043	984	-
6	20161217T020405_20161217T021726	9638	-
7	20170701T231747_20170701T233057	14846	-
8	20180119T035120_20180119T040428	8504	-
9	20180213T005936_20180213T011253	151124	-
10	20180225T013208_20180225T014527	220681	-
11	20180302T132409_20180302T133338	144281	-
12	20180315T163754_20180315T165028	24597	-
13	20180413T024145_20180413T025505	312069	-
14	20180425T031419_20180425T032734	402430	-
15	20180922T073751_20180922T074812	7488	-
16	20190104T133346_20190104T134501	19508	RFI in timeframe: 13:40:10-13:40:18 UTC
17	20190115T011953_20190115T013414	15704	RFI has occurred around 01:22:44 UTC
18	20190204T232354_20190204T233816	142803	RFI around 23:27:07 UTC
19	20190206T134923_20190206T140120	18533	RFI at 13:55:46 UTC
20	20190223T124714_20190223T125730	23395	-
21	20190227T133150_20190227T134303	33522	-

Table A.1: Previous events - Part 1

Event	Pass	Missing packets	Remarks
22	20190302T231156_20190302T232614	131963	RFI at 23:14:46 UTC
23	20190303T141616_20190303T142831	18276	RFI around 14:22:18-14:22:28 UTC
24	20191119T081135_20191119T082340	10390	-
25	20200214T200843_20200214T202311	20875	RFI at 20:11:12 UTC
26	20200526T121927_20200526T122933	21036	-
27	20200606T214947_20200606T220413	14688	-
28	20201031T230556_20201031T232025	16064	RFI at 23:09:05 UTC
29	20201113T225954_20201113T231432	152524	RFI between 23:02:22 and 23:02:57 UTC
30	20201115T132511_20201115T133625	14837	RFI during acquisition at 13:31:35 UTC
31	20201209T224813_20201209T230236	42372	KSAT register an RFI with COSMO Skymed-1 at approximately 22:50:20 UTC
32	20201222T224214_20201222T225634	46348	RFI at 22:44:20 UTC
33	20210104T223610_20210104T225020	124491	RFI starts around 22:38:35 UTC
34	20210130T090224_20210130T091337	22848	RFI at 09:06:43 UTC
35	20210314T074725_20210314T075953	15904	-
36	20210318T133716_20210318T134831	18332	-
37	20210409T091722_20210409T092821	8303	RFI at 09:21:16 UTC
38	20210415T084320_20210415T085435	31170	RFI at 08:49 UTC
39	20210504T130740_20210504T131551	20564	RFI at 13:14:11 UTC
40	20210517T075623_20210517T080839	17256	RFI at 08:01:52 UTC
41	20210629T232404_20210629T233826	719546	-
42	20210705T225100_20210705T230320	11572	Predicted RFI causing spike in signal at 22:56:07 UTC
43	20210716T204423_20210716T205650	10654	-

Table A.2: Previous events - Part 2

Event	Pass	Missing packets	Remarks
44	20210906T134214_20210906T135339	18116	RFI with Superview-1 03, with maximum interference at 13:48:33 UTC
45	20210910T124612_20210910T125628	16783	Around 12:52:55 UTC there is a strong RFI for around 4 seconds

Table A.3: Previous events - Part 3

Event	Pass	Missing packets	Remarks
46	20211106T222520_20211106T223931	816	-
47	20211111T123243_20211111T124238	21580	RFI detected 12:39:30 UTC
48	20211120T200148_20211120T201617	19536	RFI with GRUS-1D with maximum interference at 20:04:17 UTC
49	20211205T165822_20211205T171129	109065	Possible RFI at 17:03:01 UTC
50	20211231T164628_20211231T165930	93512	Drop in signal lasted from approximately UTC 16:49:57 to 16:50:17
51	20220110T215645_20220111T220704	14558	RFI at 21:59:17 UTC

Table A.4: New events

ID	Description	Expected version
GENERAL REQUIREMENTS		
XRPT-GEN-001	The XRPT SW shall not depend on any commercial license and shall be written in an Open-Source programming language	0.1
XRPT-GEN-002	The SW shall be a standalone installation with no client/server architecture	0.1
XRPT-GEN-003	The XRPT SW shall run in different operative systems or platforms either LINUX or WINDOWS	0.1
XRPT-GEN-005	For each SW release, the contractor shall produce a SW release note detailing the list of requirements implemented and the list of Software problems fixed. The SW release note, SRN, shall clearly detail the SW installation process	0.1
MMI REQUIREMENTS		
XRPT-MMI-001	The SW shall have a graphical user interface, MMI, which allows the user to practically implement all the user requirements	0.1
XRPT-MMI-002	The MMI shall show the user the current state of the SW and to highlight any possible errors to the user	0.1
XRPT-MMI-003	The MMI shall be launched either from command line or directly from an icon desktop	0.1
XRPT-MMI-004	The MMI shall contain a Help menu or a link to a pdf SW user manual	0.1
XRPT-MMI-005	The user shall be able through the MMI to configure the SW configuration file	0.1

Table A.5: Requirements - Part 1

ID	Description	Expected version
CONFIGURATION FILE REQUIREMENTS		
XRPT-CON-001	The user shall be able to configure the general characteristics of the SW using a dedicated configuration file	0.1
XRPT-CON-002	The configuration file shall contain a list of variables and their actual values	0.1
XRPT-CON-003	No hardcoded variables shall be defined inside the code	0.1
XRPT-CON-004	The configuration file shall contain a list of variables and their actual values: a. The name of the X-Band ground station (by default Svalbard) b. The latitude, longitude and elevation of the ground station (by default the ones for Svalbard station, units should be degrees and meters respectively) c. TLE source selection, either SMOS FTP server, internet or local file d. SMOS FTP address, IP, username, password and directory e. SMOS FOS Webpage, IP, username, password and directory f. Minimum RFI distance computation in degrees g. Maximum RFI distance computation in degrees	0.1
ORBIT SOURCE FILES REQUIREMENTS		
XRPT-ORB-001	The SW shall use as source of orbit file computation Two Line Elements files	0.2
XRPT-ORB-002	The SW shall be able to remotely retrieve from internet SMOS TLE files	0.2
XRPT-ORB-003	The SW shall optionally be able to retrieve latest SMOS TLE file included on the SMOS FTP server, file *smos_tle.txt*, directory */exchange-data/anonymous/smos/FOS/Mission-Planning*	0.2

Table A.6: Requirements - Part 2

ID	Description	Expected version
XRPT-ORB-004	The SW shall locally store and update a repository of SMOS TLE files which may allow the user to compute orbit positions along the whole SMOS mission	0.2
XRPT-ORB-005	If the SW is not able to find a suitable set of TLE files shall clearly highlight the error to the user and to abort any possible computation	0.2
ACCESS REQUIREMENTS		
XRPT-ACC-001	The XRPT shall be able to access the SMOS FTP server	0.2
PLANNING READING REQUIREMENTS		
XRPT-PLR-001	The user shall be able to specify a SMOS planning week by defining its year and calendar week	0.2
XRPT-PLR-002	Upon user specification of a certain SMOS planning week, the SW shall be able to remotely transfer from the SMOS FTP server, directory */exchange-data/anonymous/smos/FOS/ Mission_ Planning/yyyy_ W_ xx* the corresponding file	0.2
XRPT-PLR-003	The SW shall be able to read *yyyy_ wxx_ passes.html* SMOS planning files and to extract the list of Svalbard passes defined inside the file (AOS and LOS times for each pass)	0.2
XRPT-PLR-004	If the SW is not able to find or to remotely transfer the required mission planning file it shall clearly highlight the error to the user and to stop any further computation	0.2
XRPT-PLR-005	For each X-Band Svalbard pass, the SW shall be able to compute the list of possible satellite conflicting the pass and generating an RFI	0.2

Table A.7: Requirements - Part 3

ID	Description	Expected version
XRPT-PLR-006	For each possible conflicting satellite, the SW shall be able to compute the start and end time of the satellite RFI and the name of the satellite	0.2
XRPT-PLR-007	For each possible conflicting satellite, the SW shall be able to compute the amount of telemetry packets and time lost during the pass	0.2
XRPT-PLR-008	For each possible conflicting satellite, the SW shall be able to compute the minimum angular distance in degrees between SMOS and the conflicting satellite	0.2
STANDALONE COMPUTATION REQUIREMENTS		
XRPT-STA-001	The SW shall allow the user to specify a calendar time range where to compute possible RFI conflicts over Svalbard	0.3
XRPT-STA-002	The allowed user time range should be maximum two weeks from start to the end time	0.3
XRPT-STA-003	The SW shall check that the format and time range for the start and end times are correct and to clearly spot those format/range problems to the user for their further correction	0.3
XRPT-STA-004	For the corresponding correct time range introduced by the user, the SW shall be able to compute the list of all possible Svalbard X-Band passes in that period	0.3
XRPT-STA-005	The SW shall be able to compute X-Band passes with a precision of at least 5 seconds (AOS and LOS times)	0.3
XRPT-STA-006	For each computed X-Band pass, the SW shall be able to compute the data included in requirements XRPT-PLR-005, XRPT-PLR-006, XRPT-PLR-007 and XRPT-PLR-008	0.3

Table A.8: Requirements - Part 4

ID	Description	Expected version
XRPT-STA-007	Output results shall be displayed either on the screen or into an output file (output file requirements on section 9 are fully applicable)	0.3
OUTPUT FILE REQUIREMENTS		
XRPT-OUT-001	The SW shall be able to generate an output file containing the results of the RFI computation	0.4
XRPT-OUT-002	For a certain planning computation using as source file *yyyy_wxx_passes.html*, the result output default file shall be an XML file with filename *yyyy_wxx_rfi.html*. For a standalone computation the user shall be able to freely define the name of the output file	0.4
XRPT-OUT-003	Optionally the user shall be able to generate as output file a CSV type file. For this type of file and in case more than one conflicting satellite is found for a single satellite, the file shall contain for the same pass as many lines as conflicting satellites are found	0.3
XRPT-OUT-004	The SW shall be able to automatically transfer, prior final user confirmation, the *yyyy_wxx_rfi.html* output file to the SMOS FOS Web page and the SMOS FTP server directory */exchangedata/anonymous/smos/FOS/Mission_Planning/yyyy_W_xx*	0.4

Table A.9: Requirements - Part 5

ID	Description	Expected version
XRPT-OUT-005	The output file shall content the following information and formats (in case no RFI is detected for a certain pass all the fields exception of Pass number, AOS pass, LOS pass and RFI-FLAG shall be empty) a. Pass number: A continues number starting at one and counting the number of Svalbard passes inside the file. b. AOS pass time: CCSDS format. c. LOS pass time: CCSDS format. d. RFI-FLAG: YES or NO. YES in case at least one conflicting satellite has been detected inside that pass. e. Satellite ID: If RFI-FLAG reads YES, the name or names of the conflicting satellites. f. RFI Start Time: Start time for the RFI expressed in CCSDS format (second precision). g. RFI End Time: End Time for the RFI expressed in CCSDS format (second precision). h. RFI time: Expected duration time for the RFI expressed in seconds and computed as RFI End Time minus RFI Start Time. i. Elevation: SMOS elevation over station horizon expressed in degrees (this should be at the maximum of expected the RFI time). j. Azimuth: SMOS azimuth over station horizon expressed in degrees (this should be at the maximum of expected the RFI time). k. TM packets: Amount of expected TM packets lost during the RFI. l. Min distance: Minimum angular distance expressed in degrees during the RFI period. m. Min distance time: Absolute time for the minimum angular distance between SMOS and the conflicting satellite. n. Probability: High or low probability of a RFI happening based the Mahalanobis distance and corresponding p-value of the predicted RFI with respect to the data available of past confirmed RFIs.	0.4

Table A.10: Requirements - Part 6

ID	Description	Expected version
STATISTICAL REQUIREMENTS		
XRPT-STA-001	The SW shall be able to internally store the list of all predicted RFIs	0.3
XRPT-STA-002	The SW shall allow the user to manually retrieve, view and edit the RFIs historical records	0.5
XRPT-STA-003	The user shall be able to edit the historical records and to flag which past RFIs were confirmed in operations	0.5
XRPT-STA-004	The SW shall allow the user to produce some general statistics based on the RFIs historical records, in particular: a. A general report with all predicted RFIs. b. A bar chart splitting the number of RFIs per satellite.	0.5

Table A.11: Requirements - Part 7

B | Database

Organization	Name	NORAD number
AFS	ZACUBE-2	43907
ALG	ALSAT 1B	41785
ARS	SAUDISAT 2	28371
ARS	SAUDISAT 3	31118
ARS	SAUDISAT 4	40016
ARS	SAUDISAT 5A	43831
ARS	SAUDISAT 5B	43833
BLR	BKA 2	38708
BUL	SPARTAN	48964
CAN	RADARSAT-2	32382
CAN	CANX-2	32790
CAN	CANX-4	40055
CAN	CANX-5	40056
CAN	CANX-7	41788
CHN	BEIJING 1	28890
CHN	ZIYUAN 1-02C	38038
CHN	ZIYUAN 3-1	38046
CHN	ZIYUAN 3-2	41556
CHN	ZHANGHENG 1	43196
CHN	JILIN 1	40961
CHN	JILIN-01-03	41914
CHN	JILIN-01-04	43022
CHN	JILIN-01-05	43023
CHN	JILIN-01-06	43024
CHN	JILIN-01-07	43159
CHN	JILIN-01-08	43160
CHN	JILIN-01-09	43943
CHN	JILIN-01-10	43944
CHN	JILIN-01 GAOFEN 2A	44777
CHN	JILIN-01 GAOFEN 2B	44836
CHN	JILIN-01 GAOFEN 2D	49256
CHN	JILIN-01 KUANFU 01	45016
CHN	JILIN-01 GAOFEN 3B	46454
CHN	JILIN-01 GAOFEN 3C	46455
CHN	JILIN-01 GAOFEN 3D	46456
CHN	JILIN-01 GAOFEN 3E	46457
CHN	JILIN-01 GAOFEN 3F	46458
CHN	JILIN-01 GAOFEN 3G	46459
CHN	JILIN-01 GAOFEN 3H	46460
CHN	JILIN-01 GAOFEN 3I	46461

Organization	Name	NORAD number
CHN	GAOFEN 1	39150
CHN	GAOFEN 2	40118
CHN	GAOFEN 8	40701
CHN	GAOFEN 9-01	40894
CHN	GAOFEN 3	41727
CHN	GAOFEN 1-02	43259
CHN	GAOFEN 1-03	43260
CHN	GAOFEN 1-04	43262
CHN	GAOFEN 5-01	43461
CHN	GAOFEN 6	43484
CHN	GAOFEN 11-1	43585
CHN	GAOFEN 10R	44622
CHN	GAOFEN 7	44703
CHN	GAOFEN 12-1	44819
CHN	GAOFEN 9-02	45625
CHN	GAOFEN 9-03	45794
CHN	GAOFEN DUOMO	45856
CHN	GAOFEN 9-04	46025
CHN	GAOFEN 11-2	46396
CHN	GAOFEN 13	46610
CHN	GAOFEN 14	47231
CHN	GAOFEN 12-2	48079
CHN	GAOFEN 5-02	49122
CHN	JILIN-01 GAOFEN 3J	46462
CHN	TIANWANG 1A	40928
CHN	JIADING 1	43713
CHN	HAIYANG 1B	31113
CHN	HAIYANG 2A	37781
CHN	HAIYANG 1C	43609
CHN	HAIYANG 2B	43655
CHN	HAIYANG 1D	45721
CHN	CBERS 4	40336
CHN	CBERS 4A	44883
CHN	HUANJING 1A	33320
CHN	HUANJING 1B	33321
CHN	HUANJING 1C	38997
CHN	HAISI 1	47297
CHN	ZHUHAI-1 OHS-01	43439
CHN	ZHUHAI-1 OVS-02	43440
CHN	ZHUHAI-1 OHS-02	43441

Table B.1: List of commercial satellites inside the database - Part 1

Organization	Name	NORAD number
CHN	ZHUHAI-1 OHS-03	43442
CHN	ZHUHAI-1 OHS-04	43443
CHN	ZHUHAI-1 03A	44534
CHN	ZHUHAI-1 03B	44536
CHN	ZHUHAI-1 03C	44537
CHN	ZHUHAI-1 03D	44538
CHN	ZHUHAI-1 03E	44539
CHN	TIANYAN 02	44887
CHN	FENGYUN 3A	32958
CHN	FENGYUN 3B	37214
CHN	FENGYUN 3C	39260
CHN	FENGYUN 3D	43010
CHN	FENGYUN 3E	49008
CHN	YUNHAI 1	41857
CHN	YUNHAI 1-02	44547
CHN	XINGYUN SHIYAN-1	41913
CHN	XINGYUN-2 01	45602
CHN	XINGYUN-2 02	45603
CHN	HONGYUN 1	43871
CHN	GAOFEN 3-02	49495
CHN	SHIYAN 11	49501
CHN	SHIYAN 1	28220
CHN	SHIYAN 3	33433
CHN	SHIYAN 4	37931
CHN	SHIYAN 7	39208
CHN	SHIYAN 5	39455
CHN	SHIYAN 6 01	43711
CHN	SHIYAN 6 02	45859
CHN	SHIYAN 6 03	48157
CHN	SHIYAN 13	51102
CHN	JILIN-01 GAOFEN 2F	49338
CHN	TIANHUI 2-02A	49071
CHN	TIANHUI 2-02B	49072
CHN	TIANHUI 1	36985
CHN	TIANHUI 1-02	38256
CHN	TIANHUI 1-03	40988
CHN	TIANHUI 2-01A	44207
CHN	TIANHUI 2-01B	44209
CHN	TIANHUI 1-04	49049
CHN	ZHANGHENG	43194
CHN	ZIYUAN 1-02E	50465
CHN	ZIYUAN 1-02D	44528
CHN	SHIJIAN-6 01A	28413
CHN	SHIJIAN-6 01B	28414
CHN	SHIJIAN-6 02A	29505
CHN	SHIJIAN-6 02B	29506
CHN	SHIJIAN-6 03A	33408
CHN	SHIJIAN-6 03B	33409

Organization	Name	NORAD number
CHN	SHIJIAN-6 04A	37179
CHN	SHIJIAN-6 04B	37180
CHN	SHIJIAN-15	39120
CHN	SHIJIAN-6 05A	49961
CHN	SHIJIAN-6 05B	49962
CHN	SUPERVIEW-1 01	41907
CHN	SUPERVIEW-1 02	41908
CHN	SUPERVIEW-1 03	43099
CHN	SUPERVIEW-1 04	43100
D	TERRASAR-X	31698
E	PAZ	43215
E	DEIMOS-2	40013
E	AISTECHSAT-2	43768
E	AISTECHSAT-3	44103
EGY	MIRSSAT-1	44047
F	PLEIADES 1A	38012
F	PLEIADES 1B	39019
F/ESA	SENTINEL-5P	42969
F/ESA	SENTINEL-2A	40697
F/ESA	SENTINEL-2B	42063
F/ESA	SENTINEL-3A	41335
F/ESA	SENTINEL-3B	43437
F/ESA	OPS-SAT	44878
F	EYESAT-NANO	44877
F/ESA	SENTINEL-1A	39634
F	PLEIADES NEO 3	48268
F	PLEIADES NEO 4	49070
F	SPOT 6	38755
F	SPOT 7	40053
FIN	ICEYE-X1	43114
FIN	ICEYE-X2	43800
FIN	ICEYE-X5	44389
FIN	ICEYE-X4	44390
FIN	ICEYE-X7	46496
FIN	ICEYE-X6	46497
FIN	ICEYE-X9	47506
FIN	ICEYE-X8	47510
FIN	ICEYE-X12	48914
FIN	ICEYE-X13	48916
FIN	ICEYE-X15	48917
FIN	ICEYE-X11	48918
FIN	ICEYE-X14	51070
G	DMC3-FM1	40715
G	DMC3-FM2	40716
G	DMC3-FM3	40717
G	TECHDEMOSAT-1	40076
G	CARBONITE 2	43115
G	NOVASAR 1	43619

Table B.2: List of commercial satellites inside the database - Part 2

Organization	Name	NORAD number
I	EAGLET	43790
I	PRISMA	44072
I	COSMO SKYMED-1	31598
I	COSMO SKYMED-2	32376
I	COSMO SKYMED-3	33412
I	COSMO SKYMED-4	37216
I	COSMO SKYMED SG-1	44873
I	COSMO SKYMED SG-2	51444
IND	IRS-1C	23751
IND	OCEANSAT-2	35931
IND	SCATSAT 1	41790
IND	RISAT-1	38248
IND	SARAL	39086
IND	HYSIS	43719
IND	RESOURCESAT-2	37387
IND	RESOURCESAT-2A	41877
IND	IRS-P5 (CARTOSAT-1)	28649
IND	CARTOSAT-2	29710
IND	CARTOSAT-2A	32783
IND	CARTOSAT-2B	36795
IND	CARTOSAT-2C	41599
IND	CARTOSAT-2D	41948
IND	CARTOSAT-2E	42767
IND	CARTOSAT-2F	43111
IND	CARTOSAT-3	44804
INS	LAPAN-A3	41603
ISR	VENUS	42901
J	GOSAT	33492
J	ALOS-2	39766
J	ASNARO-2	43152
J	ASNARO	40298
J	GOSAT 2	43672
J	CE-SAT 2B	46818
J	HODOYOSHI-3	40015
J	HODOYOSHI-4	40011
J	QPS-SAR-2	47485
J	GCOM-W1	38337
J	GCOM-C	43065
J	STRIX-ALPHA	47253
J	GRUS-1A	43890
J	GRUS-1C	47933
J	GRUS-1B	47934
J	GRUS-1E	47935
J	GRUS-1D	47936
KAZ	KAZSTSAT	43783
KAZ	KAZEOSAT 1	39731
KAZ	KAZEOSAT 2	40010
KOR	KOMPSAT-2	29268
KOR	KOMPSAT-3	38338
KOR	KOMPSAT-3A	40536
KOR	KOMPSAT-5	39227
KOR	CAS500-1	47932
KOR	STSAT-3	39422
LUX	KSF1-B	48926
LUX	KSF1-A	48930
LUX	KSF1-C	48942
LUX	KSF1-D	48950
MRC	MOHAMMED VI-A	43005
MRC	MOHAMMED VI-B	43717
NOR	NORSAT 1	42826
NOR	NORSAT 2	42828
NOR	NORSAT 3	48272
PAK	PRSS 1	43530
PAK	PAKTES 1A	43529
PRU	PERUSAT 1	41770
RUS	METEOR-3M	27001
RUS	KANOPUS-V	42825
RUS	CHALLENGE ONE	47956
SVN	NEMO-HD	46277
THA	THEOS	33396
UAE	DUBAISAT-2	39419
UAE	KHALIFASAT	43676
UAE	FALCON EYE 2	47226
USA	OCO 2	40059
USA	SMAP	40376
USA	GLOBAL-1	43730
USA	BLACKSKY GLOBAL 2	43812
USA	SEAHAWK	43820
USA	TERRA (EOS AM)	25994
USA	PATHFINDER 1	41787
USA	SIRION PATHFINDER-2	43759
USA	M2 PATHFINDER	45727
USA	TROPICS PATHFINDER	48901
USA	AQUA (EOS-PM)	27424
USA	ICESAT-2	43613
USA	AURA	28376
USA	LANDSAT 7	25682
USA	UMBRA-2001	48906
USA	LANDSAT 8	39084
USA	LANDSAT 9	49260
USA	LEMUR-2-JOBANPUTRA	41991
USA	LEMUR-2-SPIRE-MINIONS	41992
USA	LEMUR-2-SATCHMO	41993
USA	LEMUR-2-SMITA-SHARAD	41994
USA	LEMUR-2-RDEATON	41995
USA	LEMUR-2-TACHIKOMA	41996
USA	LEMUR-2-NOGUECORREIG	41997
USA	LEMUR-2-MIA-GRACE	41998
USA	LEMUR-2-SHAINAJOHL	42771
USA	LEMUR-2-XUENITERENCE	42772
USA	LEMUR-2-LUCYBRYCE	42773
USA	LEMUR-2-KUNGFOO	42774
USA	LEMUR-2-LYNSEY-SYMO	42779
USA	LEMUR-2-LISASAURUS	42780

Table B.3: List of commercial satellites inside the database - Part 3

Organization	Name	NORAD number
USA	LEMUR-2-SAM-AMELIA	42781
USA	LEMUR-2-MCPEAKE	42782
USA	LEMUR-2-GREENBERG	42837
USA	LEMUR-2-ANDIS	42838
USA	LEMUR-2-MONSON	42839
USA	LEMUR-2-FURIAUS	42840
USA	LEMUR-2-PETERG	42841
USA	LEMUR-2-DEMBITZ	42842
USA	LEMUR-2-ZACHARY	42845
USA	LEMUR-2-ARTFISCHER	42881
USA	LEMUR-2-MCCAFFERTY	43123
USA	LEMUR-2-PETERWEBSTER	43124
USA	LEMUR-2-BROWNCOW	43125
USA	LEMUR-2-DAVEWILSON	43126
USA	LEMUR-2-JIN-LUEN	43182
USA	LEMUR-2-URAMCHANSOL	43183
USA	LEMUR-2-KADI	43184
USA	LEMUR-2-THENICKMOLO	43185
USA	LEMUR-2-ORZULAK	43731
USA	LEMUR-2-KOBYSZCZE	43732
USA	LEMUR-2-DULY	43745
USA	LEMUR-2-VLADIMIR	43746
USA	LEMUR-2-CHRISTINAHOLT	43882
USA	LEMUR-2-TINYKEV	43883
USA	LEMUR-2-REMY-COLTON	43884
USA	LEMUR-2-GUSTAVO	43885
USA	LEMUR-2-ZO	43886
USA	LEMUR-2-NATALIEMURRAY	43887
USA	LEMUR-2-SARAHBETTYBOO	43888
USA	LEMUR-2-DAISY-HARPER	43889
USA	LEMUR-2-JOHANLORAN	44084
USA	LEMUR-2-BEAUDACIOUS	44085
USA	LEMUR-2-ELHAM	44086
USA	LEMUR-2-VICTOR-ANDREW	44087
USA	LEMUR-2-LILLYJO	44396
USA	LEMUR-2-WANLI	44402
USA	LEMUR-2-MORAG	44403
USA	LEMUR-2-DUSTINTHEWIND	44405
USA	LEMUR-2-ALEX-MADDY	44407
USA	LEMUR-2-EJATTA	44409
USA	LEMUR-2-GREGROBINSON	44411
USA	LEMUR-2-YNDRD	44413
USA	LEMUR-2-ETHANOAKES	46298
USA	LEMUR-2-OSCARLATOR	46299
USA	LEMUR-2-SCHMIDTFALL	46315
USA	LEMUR-2-DJUPROERA	46316
USA	LEMUR-2-SQUAREJAWS	46317
USA	LEMUR-2-URSA-AVION	46318
USA	LEMUR-2-SLICERS	46500
USA	LEMUR-2-DAYWZAGOODDAY	46501
USA	LEMUR-2-SUSURRUS	46502
USA	LEMUR-2-NICHOL	46503
USA	LEMUR-2-NEVA	47450
USA	LEMUR-2-SAOIRSEDH5GUO	47453
USA	LEMUR-2-NALLYWACKER	47457
USA	LEMUR-2-MANGO1	47493
USA	LEMUR-2-RUAIRI-EILIDH	47511
USA	LEMUR-2-JENNIFERSONG	47525
USA	LEMUR-2-CHANTAL	47529
USA	LEMUR-2-NOOBNOOB	47538
USA	LEMUR-2-AMANDA-SVANTE	48269
USA	LEMUR-2-SPECIAL-K	48273
USA	LEMUR-2-JACKSON	48885
USA	LEMUR-2-ANNABANANA	48923
USA	LEMUR-2-JOHN-TREIRES	48925
USA	LEMUR-2-AC-CUBED	48927
USA	LEMUR-2-MERIMA	48929
USA	LEMUR-2-CARLSANTAMARI	48959
USA	LEMUR-2-RAMONAMAE	51021
USA	LEMUR-2-KING-JULIEN	51022
USA	LEMUR-2-ROHOVITHSA	51036
USA	LEMUR-2-DJIRANG	51058
USA	LEMUR-2-MIRIWARI	51054
VEN	VRSS-1	38782
VEN	VRSS-2	42954

Table B.4: List of commercial satellites inside the database - Part 4

Organization	Name	NORAD number
CHN	YAOGAN 32 2A	49383
CHN	YAOGAN 32 2B	49384
USA	USA 314	48247
CHN	LKW-3	43146
USA	USA 281	43145
I	OPTSAT 3000	42900
RUS	COSMOS 2519	42798
J	IGS RADAR-5	42072
TUR	GOKTURK-1A	41875
CHN	YAOGAN 30	41473
RUS	COSMOS 2515 (BARS-M 2)	41394
CHN	YAOGAN 29	41038
CHN	YAOGAN 28	41026
CHN	YAOGAN 27	40878
RUS	COSMOS 2506	40699
J	IGS OPTICAL 5	40538
RUS	COSMOS 2503	40420
J	IGS 9A	40381
CHN	SJ-11-08	40286
USA	USA 245	39232
RUS	COSMOS 2486	39177
CAN	SAPPHIRE	39088
J	IGS 8A	39061
CHN	YAOGAN 15	38354
CHN	YAOGAN 14	38257
F	ELISA E12	38010
F	ELISA W23	38009
F	ELISA E24	38008
F	ELISA W11	38007
J	IGS 7A	37954
CHN	YAOGAN 13	37941
CHN	YAOGAN 12	37875
J	IGS 6A	37813
USA	USA 225	37364
USA	USA 224	37348
USA	SBSS (USA 216)	37168
CHN	YAOGAN 10	36834
F	HELIOS 2B	36124
J	IGS 2A	36104
USA	DMSP 5D-3 F18 (USA 210)	35951
USA	USA 205	34903
RUS	COSMOS 2441	33272
D	SAR LUPE 5	33244
D	SAR LUPE 4	32750
D	SAR LUPE 3	32283
D	SAR LUPE 1	29658
ISR	EROS B	29079
USA	USA 186	28888
F	ESSAIM-4	28497
F	ESSAIM-3	28946
F	ESSAIM-2	28495
F	ESSAIM-1	28494
F	HELIOS-2A	28492
USA	MTI	26102
USA	JAWSAT	26061

Table B.5: List of military satellites inside the database

C | Requirements' fulfillment

ID	Description	Implemented Version
GENERAL REQUIREMENTS		
XRPT-GEN-001	The XRPT SW shall not depend on any commercial license and shall be written in an Open-Source programming language	0.1
XRPT-GEN-002	The SW shall be a standalone installation with no client/server architecture	0.1
XRPT-GEN-003	The XRPT SW shall run in different operative systems or platforms either LINUX or WINDOWS	0.1
XRPT-GEN-005	For each SW release, the contractor shall produce a SW release note detailing the list of requirements implemented and the list of Software problems fixed. The SW release note, SRN, shall clearly detail the SW installation process	0.1
MMI REQUIREMENTS		
XRPT-MMI-001	The SW shall have a graphical user interface, MMI, which allows the user to practically implement all the user requirements	0.1
XRPT-MMI-002	The MMI shall show the user the current state of the SW and to highlight any possible errors to the user	0.15
XRPT-MMI-003	The MMI shall be launched either from command line or directly from an icon desktop	0.1
XRPT-MMI-004	The MMI shall contain a Help menu or a link to a pdf SW user manual	0.1
XRPT-MMI-005	The user shall be able through the MMI to configure the SW configuration file	0.15

Table C.1: Implemented requirements - Part 1

ID	Description	Implemented Version
CONFIGURATION FILE REQUIREMENTS		
XRPT-CON-001	The user shall be able to configure the general characteristics of the SW using a dedicated configuration file	0.1
XRPT-CON-002	The configuration file shall contain a list of variables and their actual values	0.1
XRPT-CON-003	No hardcoded variables shall be defined inside the code	0.1
XRPT-CON-004	The configuration file shall contain a list of variables and their actual values: a. The name of the X-Band ground station (by default Svalbard) b. The latitude, longitude and elevation of the ground station (by default the ones for Svalbard station, units should be degrees and meters respectively) c. TLE source selection, either SMOS FTP server, internet or local file d. SMOS FTP address, IP, username, password and directory e. SMOS FOS Webpage, IP, username, password and directory f. Minimum RFI distance computation in degrees g. Maximum RFI distance computation in degrees	0.1
ORBIT SOURCE FILES REQUIREMENTS		
XRPT-ORB-001	The SW shall use as source of orbit file computation Two Line Elements files	0.1
XRPT-ORB-002	The SW shall be able to remotely retrieve from internet SMOS TLE files	0.1
XRPT-ORB-003	The SW shall optionally be able to retrieve latest SMOS TLE file included on the SMOS FTP server, file *smos_tle.txt*, directory */exchangedata/anonymous/smos/FOS/Mission-Planning*	0.1

Table C.2: Implemented requirements - Part 2

ID	Description	Implemented version
XRPT-ORB-004	The SW shall locally store and update a repository of SMOS TLE files which may allow the user to compute orbit positions along the whole SMOS mission	0.2
XRPT-ORB-005	If the SW is not able to find a suitable set of TLE files shall clearly highlight the error to the user and to abort any possible computation	0.1
ACCESS REQUIREMENTS		
XRPT-ACC-001	The XRPT shall be able to access the SMOS FTP server	0.15
PLANNING READING REQUIREMENTS		
XRPT-PLR-001	The user shall be able to specify a SMOS planning week by defining its year and calendar week	0.15
XRPT-PLR-002	Upon user specification of a certain SMOS planning week, the SW shall be able to remotely transfer from the SMOS FTP server, directory */exchange-data/anonymous/smos/FOS/ Mission_ Planning/yyyy_ W_ xx* the corresponding file	0.15
XRPT-PLR-003	The SW shall be able to read *yyyy_ wxx_ passes.html* SMOS planning files and to extract the list of Svalbard passes defined inside the file (AOS and LOS times for each pass)	0.15
XRPT-PLR-004	If the SW is not able to find or to remotely transfer the required mission planning file it shall clearly highlight the error to the user and to stop any further computation	0.15
XRPT-PLR-005	For each X-Band Svalbard pass, the SW shall be able to compute the list of possible satellite conflicting the pass and generating an RFI	0.1

Table C.3: Implemented requirements - Part 3

ID	Description	Implemented version
XRPT-PLR-006	For each possible conflicting satellite, the SW shall be able to compute the start and end time of the satellite RFI and the name of the satellite	0.1
XRPT-PLR-007	For each possible conflicting satellite, the SW shall be able to compute the amount of telemetry packets and time lost during the pass	0.1
XRPT-PLR-008	For each possible conflicting satellite, the SW shall be able to compute the minimum angular distance in degrees between SMOS and the conflicting satellite	0.1
STANDALONE COMPUTATION REQUIREMENTS		
XRPT-STA-001	The SW shall allow the user to specify a calendar time range where to compute possible RFI conflicts over Svalbard	0.15
XRPT-STA-002	The allowed user time range should be maximum two weeks from start to the end time	0.1
XRPT-STA-003	The SW shall check that the format and time range for the start and end times are correct and to clearly spot those format/range problems to the user for their further correction	0.1
XRPT-STA-004	For the corresponding correct time range introduced by the user, the SW shall be able to compute the list of all possible Svalbard X-Band passes in that period	0.25
XRPT-STA-005	The SW shall be able to compute X-Band passes with a precision of at least 5 seconds (AOS and LOS times)	0.2
XRPT-STA-006	For each computed X-Band pass, the SW shall be able to compute the data included in requirements XRPT-PLR-005, XRPT-PLR-006, XRPT-PLR-007 and XRPT-PLR-008	0.25

Table C.4: Implemented requirements - Part 4

ID	Description	Implemented version
XRPT-STA-007	Output results shall be displayed either on the screen or into an output file (output file requirements on section 9 are fully applicable)	0.2
OUTPUT FILE REQUIREMENTS		
XRPT-OUT-001	The SW shall be able to generate an output file containing the results of the RFI computation	0.1
XRPT-OUT-002	For a certain planning computation using as source file *yyyy_wxx_passes.html*, the result output default file shall be an XML file with filename *yyyy_wxx_rfi.html*. For a standalone computation the user shall be able to freely define the name of the output file	0.15
XRPT-OUT-003	Optionally the user shall be able to generate as output file a CSV type file. For this type of file and in case more than one conflicting satellite is found for a single satellite, the file shall contain for the same pass as many lines as conflicting satellites are found	0.15
XRPT-OUT-004	The SW shall be able to automatically transfer, prior final user confirmation, the *yyyy_wxx_rfi.html* output file to the SMOS FOS Web page and the SMOS FTP server directory */exchangedata/anonymous/smos/FOS/Mission_Planning/yyyy_W_xx*	0.2

Table C.5: Implemented requirements - Part 5

ID	Description	Implemented version
XRPT-OUT-005	The output file shall content the following information and formats (in case no RFI is detected for a certain pass all the fields exception of Pass number, AOS pass, LOS pass and RFI-FLAG shall be empty) a. Pass number: A continues number starting at one and counting the number of Svalbard passes inside the file. b. AOS pass time: CCSDS format. c. LOS pass time: CCSDS format. d. RFI-FLAG: YES or NO. YES in case at least one conflicting satellite has been detected inside that pass. e. Satellite ID: If RFI-FLAG reads YES, the name or names of the conflicting satellites. f. RFI Start Time: Start time for the RFI expressed in CCSDS format (second precision). g. RFI End Time: End Time for the RFI expressed in CCSDS format (second precision). h. RFI time: Expected duration time for the RFI expressed in seconds and computed as RFI End Time minus RFI Start Time. i. Elevation: SMOS elevation over station horizon expressed in degrees (this should be at the maximum of expected the RFI time). j. Azimuth: SMOS azimuth over station horizon expressed in degrees (this should be at the maximum of expected the RFI time). k. TM packets: Amount of expected TM packets lost during the RFI. l. Min distance: Minimum angular distance expressed in degrees during the RFI period. m. Min distance time: Absolute time for the minimum angular distance between SMOS and the conflicting satellite. n. Probability: High or low probability of a RFI happening based the Mahalanobis distance and corresponding p-value of the predicted RFI with respect to the data available of past confirmed RFIs.	0.1

Table C.6: Implemented requirements - Part 6

ID	Description	Implemented version
STATISTICAL REQUIREMENTS		
XRPT-STA-001	The SW shall be able to internally store the list of all predicted RFIs	0.3
XRPT-STA-002	The SW shall allow the user to manually retrieve, view and edit the RFIs historical records	0.3
XRPT-STA-003	The user shall be able to edit the historical records and to flag which past RFIs were confirmed in operations	0.3
XRPT-STA-004	The SW shall allow the user to produce some general statistics based on the RFIs historical records, in particular: a. A general report with all predicted RFIs. b. A bar chart splitting the number of RFIs per satellite.	0.3

Table C.7: Implemented requirements - Part 7

List of Figures

List of Tables

List of Symbols

Variable	Description	SI unit
$2LE$	Two-Line Element set	-
$3LE$	Three-Line Element set	-
$8PSK$	8 Phase-Shift Keying	-
Σ	Variance-Covariance Matrix	-
Ω	Right ascension of the ascending node	deg
θ	True anomaly	deg
μ	Gravitational parameter	m^3/s^2
μ	Mean	-
ρ_0	Atmospheric density	kg/m^3
ω	Argument of perigee	deg
A	Azimuth	deg
A	Cross-sectional area	m^2
A	Direction cosine matrix	-
a	Altitude	deg
a	Semi major axis	km
AOS	Acquisition of Signal	-
API	Application Programming Interface	-
ASI	Adjacent Satellite Interference	-
ASI	Agenzia Spaziale Italiana	-
$ATLAS$	Advanced Topographic Laser Altimeter System	-
B	Ballistic coefficient	m^2/kg
B^*	Adjusted ballistic coefficient	$(Earth\ radii)^{-1}$
C_D	Drag Coefficient	-
$CATNR$	Catalog Number	-
CCD	Charged Coupled Device	-
$CCSDS$	Consultative Committee for Space Data Systems	-
CDF	Cumulative Distribution Function	-

Variable	Description	SI unit
CEC	Calibration Engineering Centre	-
CGS	Common Ground System	-
CK	Pointing Kernels	-
$CNES$	Centre National d'études Spatiales	-
$COSMO$	Constellation of Small Satellites for Mediterranean basin Observation	-
CSV	Comma-Separated Values	-
D_M	Mahalanobis Distance	-
$DPGS$	Data Processing Ground Segment	-
e	Eccentricity	-
e	Euler axis	-
$EIRP$	Equivalent IRradiated Power	-
EK	Events Kernels	-
ESA	European Space Agency	-
$ESAC$	European Space Astronomy Center	-
$ESTRACK$	European Space Tracking	-
ET	Ephemeris Time	-
$FCDAS$	Fairbanks Command and Data Acquisition Station	-
FK	Reference Frame specifications Kernels	-
FOS	Flight Operation Segment	-
FTP	File Transfer Protocol	-
GEO	Geostationary orbit	-
GPZ	GEO Protected Zone	-
GS	Ground Station	-
GUI	Graphical User Interface	-
h	Angular momentum vector	km^2/s
$HTML$	Hyper Text Markup Language	-
i	Inclination	deg
IAU	International Astronomical Union	-
$ICESat-2$	Ice, Cloud and land Elevation Satellite-2	-
$IERS$	International Earth Rotation Service	-
IK	Instrument Kernels	-
$INTDES$	International Designator	-
IP	Internet Protocol	-

Variable	Description	SI unit
$ITRF$	International Terrestrial Reference Frame	-
$ITRS$	International Terrestrial Reference System	-
ITU	International Telecommunication Union	-
J_2	Second gravitational harmonic for Earth	-
J_3	Third gravitational harmonic for Earth	-
J_4	Fourth gravitational harmonic for Earth	-
$J2000$	Epoch at January 1, 2000	-
JPL	Jet Propulsion Laboratory	-
$JPSS$	Joint Polar Satellite System	-
$JSON$	JavaScript Object Notation	-
$KOMPSAT$	Korea MUlti-Purpose SATellite	-
$KSAT$	Kongsberg Satellite Services	-
KVN	Key-Value Notation	-
LEO	Low-Earth Orbit	-
$LICEF$	LIght-weight Cost EFfective	-
LOS	Loss of Signal	-
LSK	Leapseconds Kernels	-
LUT	Local User Terminal	-
$LVLH$	Local Vertical Local Horizontal	-
m	Mass	kg
$MIRAS$	Microwave Imaging Radiometer using Aperture Synthesis	-
MPS	Mission Planning and Scheduling	-
N	Line of Nodes vector	-
$NAIF$	Navigation and Ancillary Information Facility	-
$NORAD$	North American Aerospace Defense	-
NSC	Norwegian Space Centre	-
p_value	Probability value	-
PCK	Planetary Constants Kernels	-
$PROTEUS$	Plateforme Reconfigurable pour l'Observation, les Télécommunications et les Usages Scientifiques	-
q	Quaternion	-
R	Radius	km
R_E	Equatorial Radius	km
R_P	Polar Radius	km

Variable	Description	SI unit
r	Position vector	km
r_{apogee}	Apogee radius	km
$r_{perigee}$	Perigee radius	km
RF	Radio Frequency	-
RFI	Radio Frequency Interference	-
SAR	Synthetic Aperture Radar	-
$SARSAT$	Search and Rescue Satellite Aided Tracking	-
$SATCAT$	SATellite CATalog	-
$SCLK$	Spacecraft Clock correlation datas Kernels	-
$SCLK$	Spacecraft Clock Time	-
SGP	Simplified General Perturbations	-
$SIRG$	Satellite Interference Reduction Group	-
$SMOS$	Soil Moisture and Ocean Salinity	-
SNL	Space Network List	-
$SPICE$	Spacecraft Planets Instrument C-matrix Events	-
SPK	Spacecraft and Planetary ephemeris Kernels	-
SRN	Software Release Note	-
SSO	Sun-Synchronous Orbit	-
$STADAN$	Space Tracking and Data Acquisition Network	-
SW	Software	-
TAI	International Atomic Time	-
TDB	Barycentric Dynamical Time	-
$TDRS$	Tracking and Data Relay Satellite System	-
TDT	Terrestrial Dynamical Time	-
TLE	Two-Line Elements	-
TM	TeleMetry	-
$TT\&C$	Telemetry, Tracking & Command	-
URL	Uniform Resource Locator	-
$USSPACECOM$	United States Space Command	-
$UT1$	Universal Time 1	-
UTC	Coordinated Universal Time	-
v	Velocity vector	km/s
XML	eXtensible Markup Language	-
$XRPT$	X-band RFI Prediction Tool	-

Acknowledgements

First, I would like to thank my ESA Internship tutor, Jorge Fauste, for his availability and patience throughout all my project work. It was an amazing experience.

Secondly, I want to thank Professor Pierluigi Di Lizia, for being my thesis advisor and letting me use my internship project as the topic for this work. In each of ours meeting, he had always given me helpful and valuable advice on how to improve my work and my software.

I want to thank with all my heart my parents, Agostino and Rita, because they have always supported me during all my university career and they have always encouraged my choices. Thank you very much!

I would like to thank also all my relatives, in particular my dear aunt Vally.

I want to thank all the new friends that I have met at PoliMi, in particular I want to acknowledge Alexia, Giulia, Ivan, Francesco and Anita. You have been an amazing support since we met.

Finally, I would like to thank all my dear friends in Treviso, Matteo, Camilla D., Camilla S., Nicolò, Andrea and Carlo, for always been there for me even if we were far apart.